Synthesis, Characterization and Spectroscopic Properties of Chiral Perylene 3,4-dicarboxylic-9,10-((*R*)-(+)-1-phenylethyl)-carboximide for Solar Cell Applications

Hamidu Ahmed

Submitted to the
Institute of Graduate Studies and Research
in partial fulfillment of the requirements for the Degree of

Master of Science
in
Chemistry

Eastern Mediterranean University
February 2013
Gazimağusa, North Cyprus

Approval of the Institute of Graduate Studies and Research

Prof. Dr. Elvan Yılmaz
Director

I certify that this thesis satisfies the requirements as a thesis for the degree of Master of Science in Chemistry.

Prof. Dr. Mustafa Halilsoy
Chair, Department of Chemistry

We certify that we have read this thesis and that in our opinion it is fully adequate in scope and quality as a thesis for the degree of Master of Science in Chemistry.

Prof. Dr. Huriye İcil
Supervisor

Examining Committee

1. Prof. Dr. Huriye İcil
2. Assoc. Prof. Dr. Hamit Caner
3. Asst. Prof. Dr. Nur P. Aydınlık

ABSTRACT

Perylene chromophoric derivatives are versatile compounds for many applications in various fields. Excellent optical properties such as high extinction coefficients and strong fluorescence combined with ease in electron accepting ability are most notable advantages of perylene derivatives.

Herein, the project focused on the synthesis of different kinds of perylene dyes, a chiral perylene diimide, a chiral perylene monoimide, and a perylene dicarboxylic acid chiral monoimide, named, N,N′-bis((*R*)-(+)-1-phenylethyl)-3,4,9,10-perylenebis(dicarboximide) (PDI), N-((*R*)-(+)-1-phenylethyl)-3,4,9,10-perylenetetracarboxylic-3,4-anhydride-9,10-imide (PMI), chiral perylene-3,4-dicarboxylic -9,10-((*R*)-1-phenylethyl)carboximide (CPMI), respectively. The final perylene derivative CPMI was synthesized in three consecutive reactions. CPMI was especially designed to be applicable in photovoltaic cells such as dye sensitized solar cells.

The synthesized perylene derivatives are characterized in detail by investigating their optical, photophysical, and thermal properties using the techniques FTIR, UV-vis, Fluorescence, DSC, TGA and elemental analysis. They exhibited interesting optical properties, high solubilities, high molar absorption coefficients, and thermal stabilities.

Keywords: perylene diimide, perylene monoimide, carboxylic acid monoimde, chiral, extinction coefficient.

ÖZ

Perilen kromoforik türevleri pek çok alanda uygulama olanağına sahip çok yönlü bileşiklerdir. Yüksek molar absorplama sabitleri ve elektron kabul etme kolaylığı ile birlikte güçlü fluoresansa sahip olma gibi özellikler perilen türevlerinin dikkat çeken çok önemli üstünlüklerindendir.

Çeşitli perilen boyaların sentezlenmesine odaklanılan bu çalışmada, yeni bir kiral perilen diimid (N,N′-bis((*R*)-(+)-1-phenylethyl)-3,4,9,10-perylenebis(dicarboximide) (PDI)),, kiral bir perilen monoimid (N-((*R*)-(+)-1-phenylethyl)-3,4,9,10-perylenetetracarboxylic-3,4-anhydride-9,10-imide (PMI)) ve bir kiral perilen dikarboksi asit monoimid (perylene-3,4-dicarboxylic -9,10-((*R*)-1-phenylethyl)carboximide (CPMI)). Son sentezlenen perilen türevi olan CPMI üç adımla sentezlenmiştir. Boya duyarlı güneş pilleri gibi fotovoltaik sistemlerde uygulanabilmesi amacıyla tasarlanmıştır.

Sentezlenmiş olan perilen türevlerinin optik, fotofiziksel ve termal özellikleri FTIR, UV-vis, Floresans, DSC, TGA ve elementel analiz teknikleri kullanılarak karakterize edilmiştir. Bu maddeler oldukça ilginç optik özelliklerin yanında, yüksek çözünebilirlik, molar soğurma katsayıları ve termal kararlılık göstermektedirler.

Anahtar kelimeler: perilen diimid, perilen monoimid, karboksilik asit monoimid, kiralite, soğurma katsayısı.

to my family

ACKNOWLEDGMENTS

Bismillahi Rahmani Rahim

I would like to say a big thank you to my supervisor Prof. Dr. Huriye Icil for allowing me to work in her group and for giving me the opportunity and resources to work on this interesting topic, I also wish to point out her great knowledge and experience not only in organic chemistry but also, in general life, her ability for teaching, telling motivating stories and of great sense to give rise of someone's interest in chemistry, particularly organic chemistry aspect. With her invaluable supervision, all my efforts could have been short-sighted.

I am grateful to Jagadeesh Babu Bodapati for his helps. I am also grateful to everyone in the research group, Duygu Uzun, Ilke Yucekan, Hurmus Refiker, Suleyman Asir, Mayram Bahari, Abimbola Aleshinloye, Mayram Pakseresht, Pawand Jalal, Ramona Pasandideh, Rizgar Zubair, Shaban Rajab for their assistance and friendship.

To my late Honorable father…… Alh. Ahmadu .M.Boderel;

To my lovely mother.…… Hajja Hauwa Ahmadu;

To my brothers and my sisters, uncles, Aunts, Cousins, grandfather, my in-law and all my relatives;

To my brothers (in Islam) in Eastern Mediterranean University.

To all of them, I'd like to dedicate this work on behalf of them, and I ask ALLAH to consider this action as right deeds and accept it from me.

To crown it all, my grate gratitude goes to Zirar Mohammed Taher, Murat Bahro, Mohammed Aliyu Uva, Jafari (Grace) Josephn, Zoher libya, Abdulkarim and Timothy Iyendo (jayendo) and his wife to be Shammila thanks for you all for the support.

TABLE OF CONTENTS

LIST OF TABLES

LIST OF FIGURES

LIST OF ILLUSTRATIONS

LIST OF SYMBOLS/ABBREVIATIONS

$\overset{o}{A}$	:	Armstrong
A	:	Absorption
Anal.	:	Analytical
AU	:	Arbitrary unit
Avg.	:	Average
c	:	Concentration
calcd.	:	Calculated
δ	:	Chemical shift
CPMI	:	Chiral perylene dicarboxylic acid monoimide
DMF	:	N,N′-dimethylformamide
DMSO	:	Dimethyl sulfoxide
DSC	:	Differential scanning calorimetry
DSSC	:	Dye sensitized solar cell
ε	:	Extinction coefficient
ε_{max}	:	Maximum Extinction coefficient/Molar absorptivity
$\varepsilon_A(\bar{\nu})$	:	Extinction coefficient of acceptor
eV	:	Electron volt
E_g	:	Band gap energy
E_s	:	Singlet energy (Excited state energy of 0-0 electronic)

f	:	Oscillator strength
Fig.	:	Figure
FT-IR	:	Fourier transform infrared spectroscopy
h	:	Hour
hν	:	Irradiation
^{1}H NMR	:	Proton nuclear magnetic resonance spectroscopy
HOMO	:	Highest occupied molecular orbital
IR	:	Infrared spectrum/spectroscopy
J	:	Coupling constant
kcal	:	Kilocalorie
k_f	:	Fluorescence rate constant
l	:	Path length
LED	:	Light emitting diode
LUMO	:	Lowest unoccupied molecular orbital
M	:	Molar concentration
max	:	Maximum
MHz	:	Megahertz
min	:	Minute
mmol	:	Millimole
mol	:	Mole
mp	:	Melting point
NMP	:	*N*-methyl-2-pyrrolidinone

NMR	:	Nuclear magnetic resonance spectroscopy
Φ_f	:	Fluorescence quantum yield
PDA	:	Perlyene 3,4,9,10-tetracarboxylic dianhydride
PDI	:	Perlylene diimide
PMI	:	Perlylene monoimide
ppm	:	Parts per million
τ_0	:	Theoretical radiative lifetime
TGA	:	Thermogravimetric analysis
UV	:	Ultraviolet
UV-vis	:	Ultraviolet visible light
$\bar{\nu}$	:	Wavenumber
$\Delta\bar{\nu}_{1/2}$	:	Half-width (of the selected absorption)
$\bar{\nu}_{max}$	:	Maximum wavenumber/Mean frequency
V	:	Volt
vs.	:	Versus
λ	:	Wavelength
λ_{exc}	:	Excitation wavelength
λ_{em}	:	Emission wavelength
λ_{max}	:	Maximum wavelength

Chapter 1

INTRODUCTION

1.1 Perylene Dyes; Versatile Building Blocks of Supramolecular Systems

Perylene dyes are established on the perylene framework. Perylene structure is made up of two naphthalene units connected by carbon-carbon bonds at the 1 and 8 positions on both molecules (Figure 1.1).

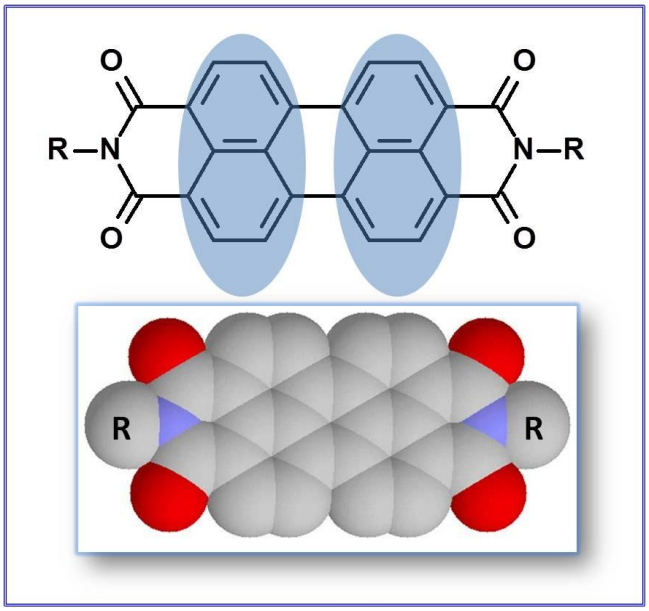

Figure 1.1: General structure of a perylene dye, the two naphthalene units are shown in blue color.

The conjugated perylene chromophoric system is an excellent advantage for versatile applications in many fields. Numerous derivatives of perylene chromophore were reported in literature (Asir et al. 2010 and Icil et al. 2001), certainly due to the ease in functionality through the imide and core substitutions. Depending on the structure developed, the perylene dyes exhibit several outstanding optical and electrochemical

properties *via* covalent and noncovalent interactions. For example, self-assembly, π–π stacking, hydrogen bonding, and folding, *etc* cause attractive electronic and optical properties for perylene dyes, thereby in developing organic-based optical and electronic device architectures. Therefore, perylene dyes are considered as building blocks of supramolecular systems.

The mechanism of supramolecular perylene assemblies rely on self-assembly which is said to be one of the most important general approaches to the development of well defined supramolecular structures. Supramolecular assembly could be made up of a state of matter that is just in between pigment particles and dissolved dyes. A logical approach to obtain supramolecular perylene diimide assemblies is the modification of the perylene chromophore in such a way that self-assembly becomes possible with appropriate intermolecular interactions. It is considered that a great balance is required between molecular stacking interactions and solubility for processing the self-assembling of perylene diimide molecules into ordered structures (Lan.Y.Y et al 2008, wurthner 2004).

Generally, perylene chromophoric dyes suffer from poor solubility owing to their rigidity and it was reported widely that the solubility could be improved by attaching various long alkyl chains or bulky substituents at the imide positions (Icil and et al. 2008).

To sum up, perylene dyes are superior in their class of compounds having chemical and photochemical stabilities, high molar absorptivity and fluorescence quantum yield. Currently, perylene dyes are focus of study in preparing highly advanced materials for optoelectronic and photovoltaic devices, thermographic processes,

energy transfer cascades, light-emitting diodes, molecular sensors, and near-infrared-absorbing systems (Hassan M.L. et al 2012).

1.2 Chiral Perylene Dyes

Chiral perylene dyes (Figure 1.2) are reported as excellent and promising materials for preparation of chiral molecular switches (Asir et al. 2010). This is due to the fact that chiral perylene dyes possess high photochemical and electrochemical stabilities with attractive optical and redox properties. Chirality of conjugated perylene chromophoric dyes, generally, is a challenging task and could offer optimized optical properties and emit circularly polarized light (Asir S. et al 2010).

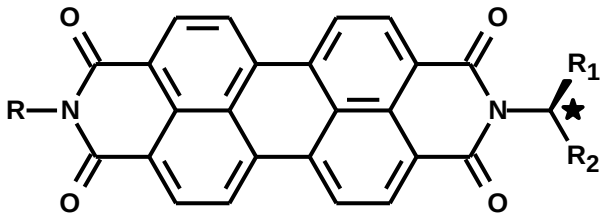

Figure 1.2: General structure of a chiral perylene dye.

The research reports in literature confirm that engineering efficient organic dye-based optical and plastic device architectures can be successfully achieved by employing chiral perylene derivatives (Asir S. et al 2010). Because of the combination of conjugated perylene chromophoric structure with chirality (chiral substituents), optical response is much more sensitive and hence the conformational changes may lead to many interesting photophysical properties such as high absorbance and excimer light emission. It is also important to note that introducing chirality to supramolecular assemblies is quite difficult. This issue can be easily solved by means of perylene chromophoric dyes which are building blocks for designing various supramolecular structures. Chirality can be easily introduced to perylene dyes resulting in chiral supramolecular structures. One of the great advantages of such structural designs is that they can offer solid-state chiral optics (for example, solid-state CD) which are manadatory for novel photonics design (Andrea et al 2010).

1.3 Solar Cells

A solar cell is a device which converts sunlight into electrical energy. A simple example is a calculator that is used in everyday life. It is made up of photovoltaic modules. Most of the commercial solar cells are conventional silicon solar cells where processed silicon semiconductor is employed in their design. In general photovoltaic cell is also used as an alternative to solar cell. The typical solar cell is shown in the following diagram (Figure 1.3) (Cornell C. 2004).

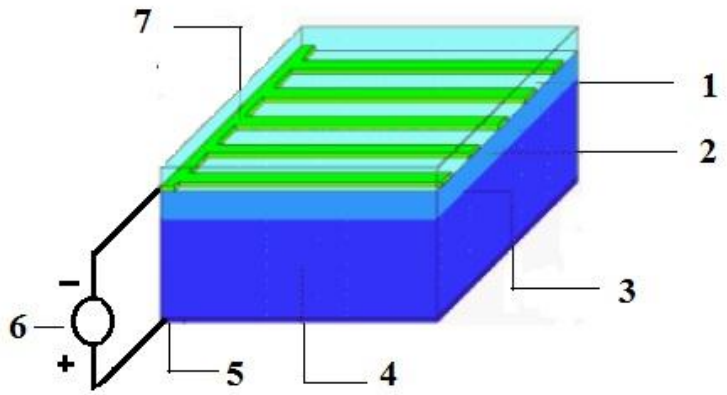

Figure 1.3: Model of a crystalline solar cell material

1. anti-reflection, 2. *n*-semiconductor layer, 3. p-n-junction, 4. *p*-semiconductor layer, 5. rear metal contact, 6. consumer, 7. contact.

The working principle of a solar cell is a simple mechanism of circulation of electrons which causes current and therefore power. A material which can absorb sunlight is involved and absorption of light with proper frequency causes that material to free an electron. The freed electron place is generally called as a hole. Connecting to suitable electrodes with an external circuit, circulation of electrons (current) could be achieved (Cornell C.2004).

However, efficient conventional silicon solar cells that exist in market are very expensive in general. This is due to the fact that silicon needs to be processed before employing it in solar cells. The processing needs very high amount of energetic series of steps. Therefore, as an effective alternative to conventional photovoltaics, organic-based solar cells are emerged as competitive alternative (Cornell C.2004).

1.3.1 Dye Sensitized Solar Cells

Dye-sensitized solar cells (DSSCs) are merged as one of the best organic-based solar cells that can compete silicon-based solar cells. They are especially cheap and open for continuous development as the employing materials are organic-based. The new version of DSSCs are also called as Gratzel cells. Versatile compounds are produced every passing day that suit to DSSCs for improving the efficiencies. Efficiencies up to 10% are already reported in literature.

The principle mechanism of DSSCs is generally similar to that of photovoltaic cells. The main difference lies in employing of electrolyte in between the electron donating and accepting materials and binding of dye molecules to nanoTiO_2.

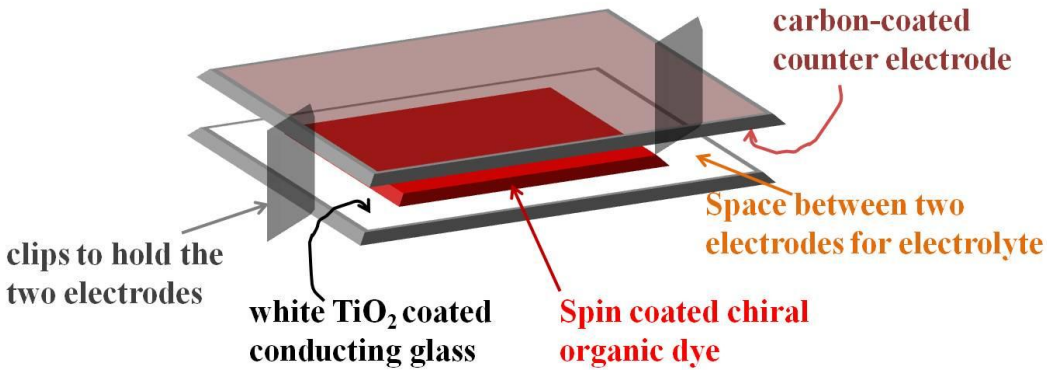

Figure 1.4: A simple laboratory made dye sensitized solar cell model.

1.3.2 Perylene Dyes in Dye Sensitized Solar Cells

The outstanding stabilities, high molar absorption coefficients and excellent electron accepting nature of perylene derivatives offered them to be used in DSSCs and plenty of various perylene dye sensitizers were reported in literature for the fabrication of DSSCs (Chiba and et al. 2006). The device efficiencies are in the range of 1 – 8%, but, extensive research on perylene chromophoric dyes for DSSCs may soon result in high efficiencies (Chiba and et al. 2006).

One of the best advantages relating to perylene chromophoric dyes lies in the starting material, perylene dianhydride which can itself be binded to the nanoporous TiO_2. Therefore optimized properties of perylene dyes are in research stage and laboratory made DSSCs involving perylene dyes are fruitful with high conversion efficiencies (Zafer C. et al 2007) (Li C. et al 2008).

In the present research work, we focused on synthesis and characterization of novel chiral perylene derivatives (a chiral perylene diimide (PDI), a chiral perylene monoimide (PMI) and a chiral perylene dicarboxylic acid carboximide (CPMI)) for solar cell applications (Figures 1.5–1.8). Especially, chiral perylene dicarboxylic acid carboximide can be a potential dye sensitizer in the application of dye sensitized solar cells (Figure 1.8). The synthesized perylene derivatives are characterized and interpreted in detail using FTIR, UV-vis, fluorescence, Elemental, DSC, and TGA.

Further study is based on perylene dye-TiO_2 system which will be investigated for solar cell fabrication.

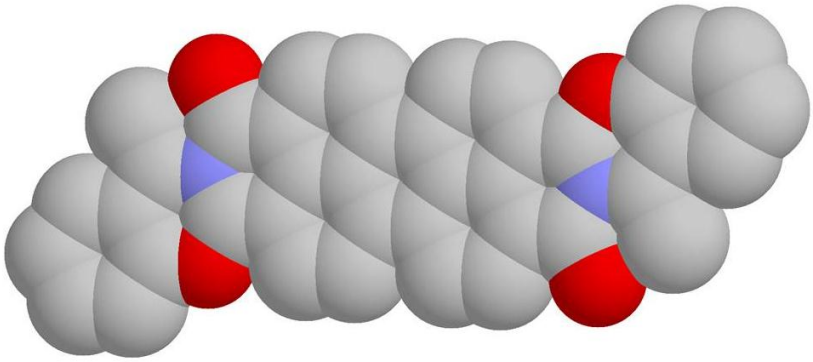

Figure 1.5: 3D Structure of chiral perylene diimide (PDI) synthesized.

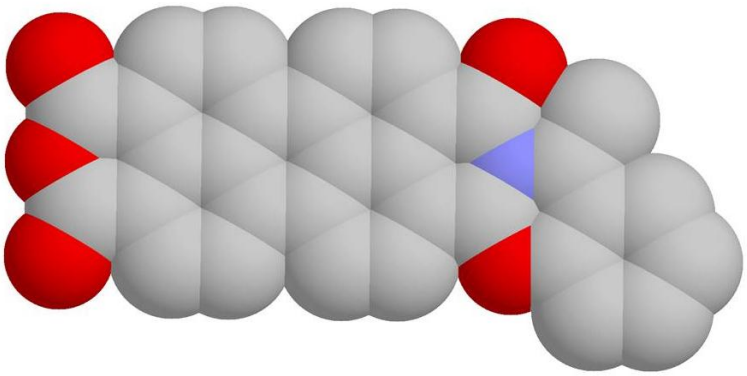

Figure 1.6: 3D Structure of chiral perylene monoimide (PMI) synthesized.

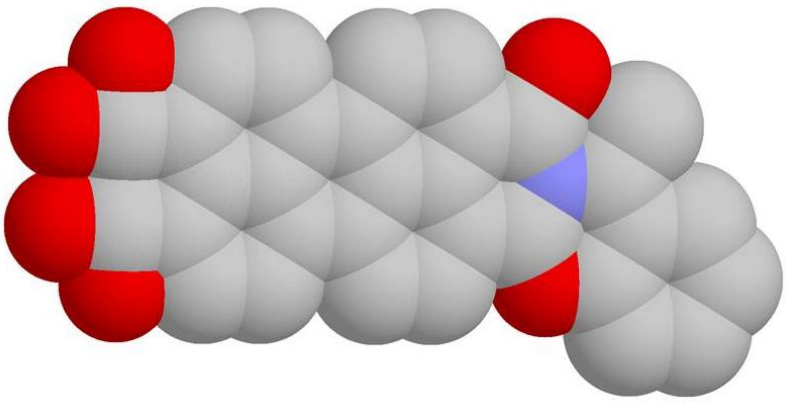

Figure 1.7: 3D Structure of chiral perylene dicarboxylic acid carboximide (CPMI) synthesized.

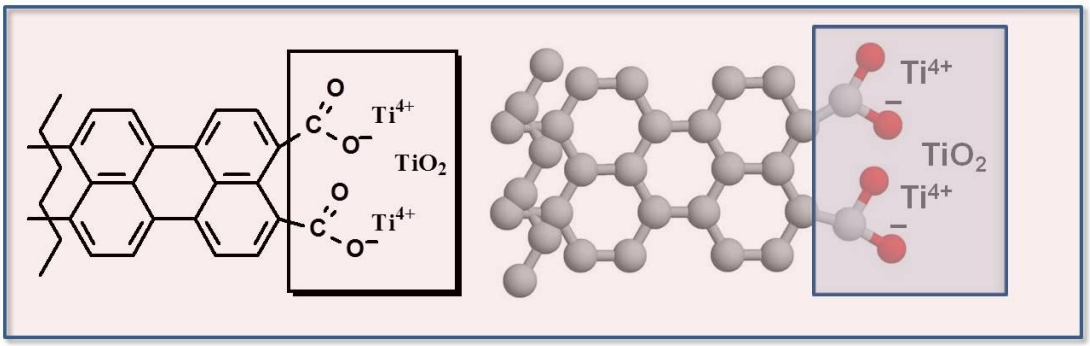

Figure 1.8: Probable TiO_2 binding of synthesized chiral perylene dicarboxylic acid carboximide (CPMI).

Chapter 2

THEORETICAL

2.1 Properties of Perylene Dyes

The introductory topics of perylene dyes already stressed the most important general properties such as high thermal stability, electrochemical stability, and photochemical stability. Further, the electron accepting nature and high fluorescence quantum yields were noted as excellent optical properties. These properties are explored in detail as follows.

(a) High molar absorptivity in the visible region.

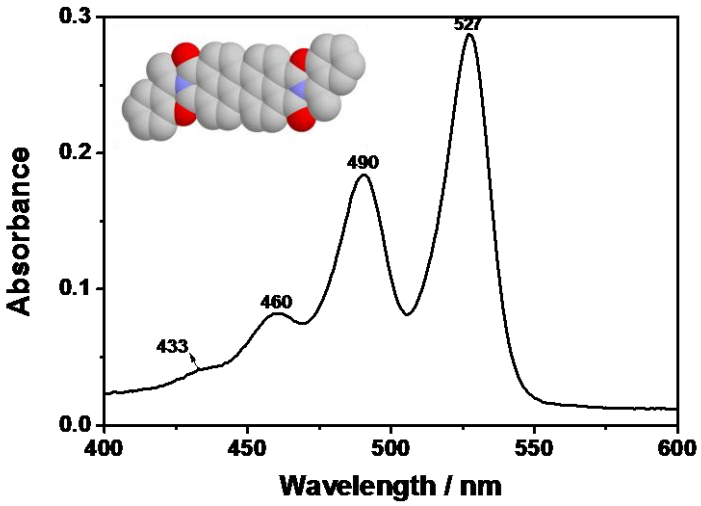

Figure 2.1: UV-vis spectrum of chiral PDI in chloroform.

As sown in Figure 2.1, the UV-vis spectrum of PDI is broad in the region 400 – 600 nm and the molar absorptivity is very high with ε_{max} = 80000 $M^{-1}cm^{-1}$ for the 0→0 absorption peak at λ_{max} = 527 nm. The high molar extinction coefficients are one of the crucial mandatory factors considering dye sensitized solar cells.

(b) High fluorescence quantum yield near unity (Φ_f = 1).

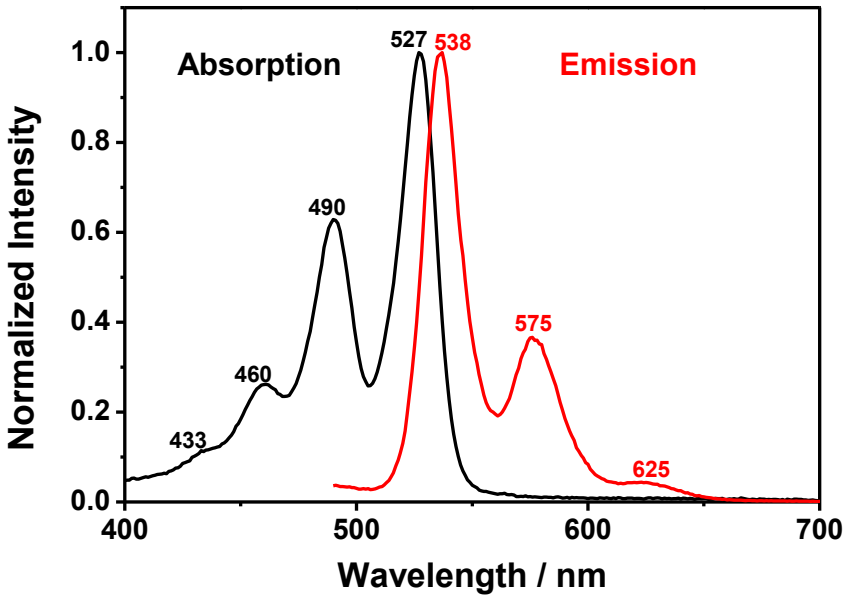

Figure 2.2: Normalized UV-vis and fluorescence spectra of chiral PDI in chloroform.

The low Stoke's shift value (11 nm) from Figure 2.2 confirms that the loss of energy of an excited PDI molecule is majorly occur via radiative path way (by releasing a photon), which is called the fluorescence of the molecule. As the PDI derivative is chiral, the compound possessed high fluorescence and lower Stoke's shift suggests the emission of all absorbed light resulting in high fluorescence quantum yield.

Moreover, the strong sense of fluorescence of perylene dyes is very attractive property considering the organic-based electronic device architectures. Plenty of reports in literature discussed the application of various perylene dyes in photonic devices, organic light emitting diodes, sensors, etc.

(c) Excellent electron acceptors and *n*-type semiconductors.

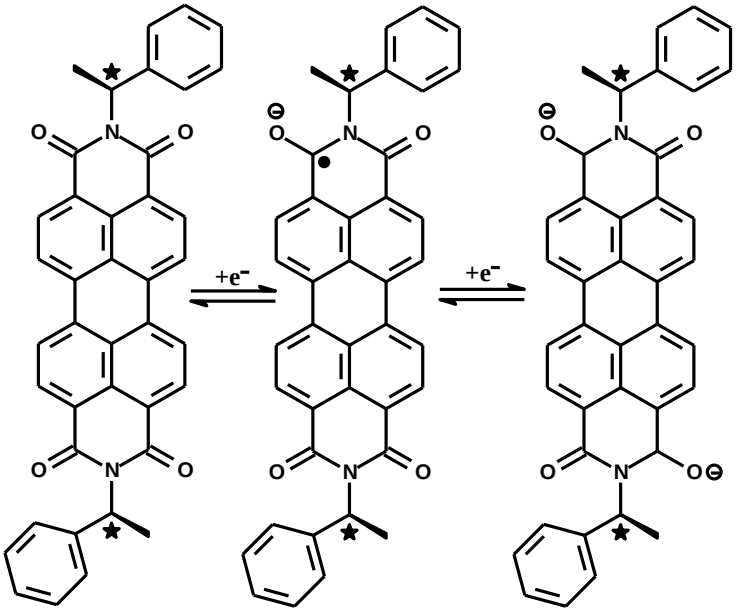

Figure 2.3: Stuructural representation of electron accepting nature of chiral PDI.

The perylene dyes easily accepts electron as the carbonyl groups are electrophilic. The formation of dianion suggests the ease of accepting electron and therefore perylene derivatives are excellent electron acceptors. This nature combining with outstanding stabilities cause them for use in solar cell fabrication as *n*-type semiconductors.

(d) High electrochemical stability and reversibility

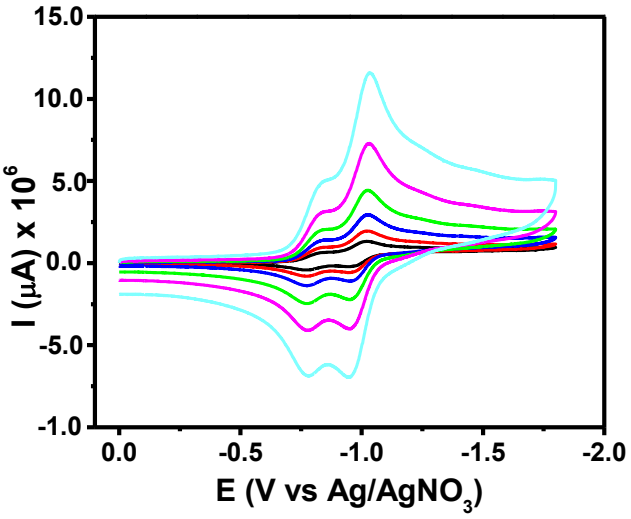

Figure 2.4: Representative cyclic voltammograms (CVs) of a perylene dye (Bodapati, et al., reproduced with the permission).

The CVs at different scan rates from Figure 2.4 clearly demonstrates the high electrochemical stability (as the ratio of peak currents is equal to unity and reproducible redox peaks at repeated cycles).

(e) Perylene dyes are thermally stable and in general the decomposition initializes at about an average of 400 ^{o}C and above. Many research papers have been widely discussed the high thermal stabilities exhibited by perylene dyes. More interstingly, it was reported that even long alkoxy chains attached at the imide positions had no negative impact on thermal stability of perylene derivatives which is mainly attributed to the rigidity of the conjugated aromatic perylene chropore structure (Bodapati, et al. 2008).

(f) High photochemical stabilities are also one of the general advantages of perylene dyes. They are also photoconductive and are widely employed in various electronic devices.

2.1.1 Photophysics and Excited state Dynamics

Numerous perylene dyes reported in literature suggests the ease in designing and synthesis of perylene dyes with a broad variety of substituents. The figure below shows the possible substitution at different places of the perylene chromophore (Figure 2.5).

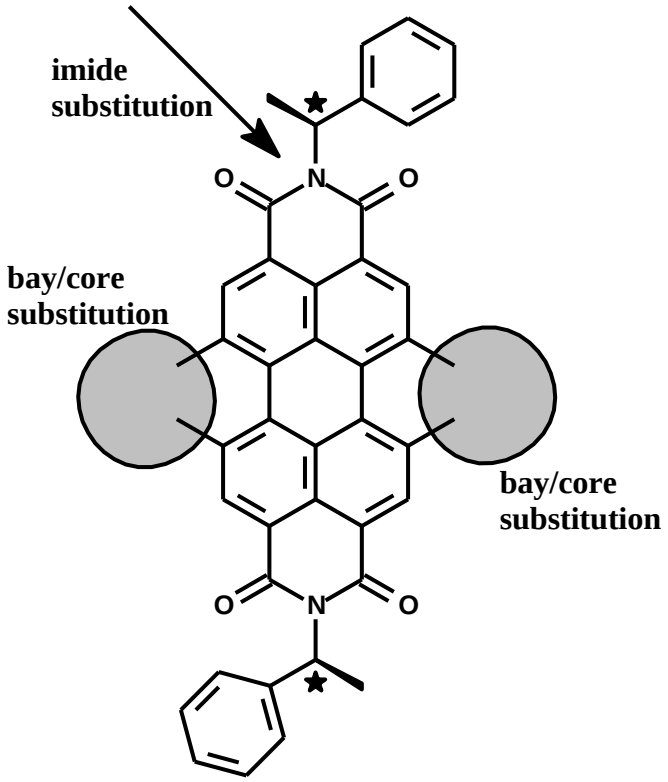

Figure 2.5: Possible substitutions of a perylene chromophore.

Depending on the purpose, the perylene derivatives can be specially designed either by imide substitution or by core substitution with the required choice of groups. Therefore fine tuning of structures is possible resulting in a wide variety of interesting optical, photophysical and electrochemical properties. Therefore, it is a bit complex to list out all kinds of photophysical properties. Depending on the

substitution, perylene derivatives exhibit charge transfer, aggregation, excimers, exciplexes, stacking, electron transfer, and energy transfer, etc.

To name a very few important excited state behaviors of perylene dyes, excimers, exciplexes, photoinduced electron transfer, resonance energy transfer, and fluorescence processes take priority.

In general, when a photon of suitable frequency strikes a perylene dye it causes absorption of light (electromagnetic radiation) and passes to singlet excited state. The absorption spectrum showed in Figure 2.1 confirms (as the singlet energy is around 54 kcal/mol) the transition to a singlet excited electronic state. Figure 2.2 suggests that the excited perylene molecule returns to the ground state rapidly by releasing a photon. Before returning to the ground state, there is a great possibility for a perylene molecule to make interactions with the ground state molecules, solvent molecules, monomeric molecules, etc., which causes to form excimers (excited state dimer), exciplexes (excited state complexes), photoinduced electron transfer, fluorescence resonance energy transfer, etc. Intramolecular/intermolecular hydrogen bonding, self-assembly, $\pi - \pi$ stacking interactions may cause also to deliver different kinds of photophysical properties. The energies of lowest unoccupied molecular orbital (LUMO) and highest occupied molecular orbital (HOMO) may vary accordingly and causes to have a variety of electronic properties.

In summary, the excited state dynamics and resulting photophysics of a perylene dye is solely depending to the type of substituent attached at a particular position and its behavior in particular solvent and in solid-state.

2.2 Applicability of Perylene Dyes

The starting material for thousands of perylene derivatives is a cheap and simple perylene dianhydride (PDA). PDA is in general insoluble in many common organic and aqueous solvents available. In fact, perylene derivatives also suffer from poor solubility. This was easily solved using the tailoring of PDA by introducing bulky groups or long alkyl chains as substituents. The high solubility brought up processability, whereas, rigid structure made it stable and the combination create them as excellent industrial materials. Interesting optical and electrochemical properties added them suitable for electronic and photonic applications. This led perylene dyes to involve everywhere and the potential applications were categorized briefly as follows.

2.2.1 Solid-state Absorbance and Fluorescence

Excellent optimized optical and electronic properties in solution were very widely discussed and reported in literature relating to perylene derivatives. A very few works can be found in literature concerning solid-state emission of perylene dyes. It is quite a difficult task to find optimum conditions for designing a perylene chrmophoric dye which emits light in solid-state due to probable self quenching and molecular assembly in solid-state. On the other hand, solid-state absorbance can be easily achieved with appropriate frequency of electromagnetic radiation.

Solid-state fluorescence of a perylene dye is an excellent opportunity to introduce them in many efficient photonic and electronic devices with a very little amount of energy investment.

2.2.2 Chiroptical Switches

Chiral perylene dyes can be employed in construction of molecular switches such as chiroptical switches as they are electrochromic materials and are bistable when they undergo redox reactions. As shown in Figure 2.3, the neutral chiral perylene diimide undergoes one electron reduction resulting in an anion of chiral PDI. The monoanions of chiral perylene derivatives show bathochromic shifts in general and absorb light in the near infrared (NIR) region unlike neutral chiral perylene dyes (which absorb in visible region as shown in Figure 2.1). Hence the monoanion of chiral PDI show distinct optical and electrochemical properties comparing to neutral chiral PDI molecule. As both molecules are different, stable, interconvertable and exhibit variations in their optical properties, chiral perylene dyes can be used as efficient material for chiroptical switches (Figure 2.6). Using circular dichroism (CD) technique, the optical activities of the both molecules can be investigated.

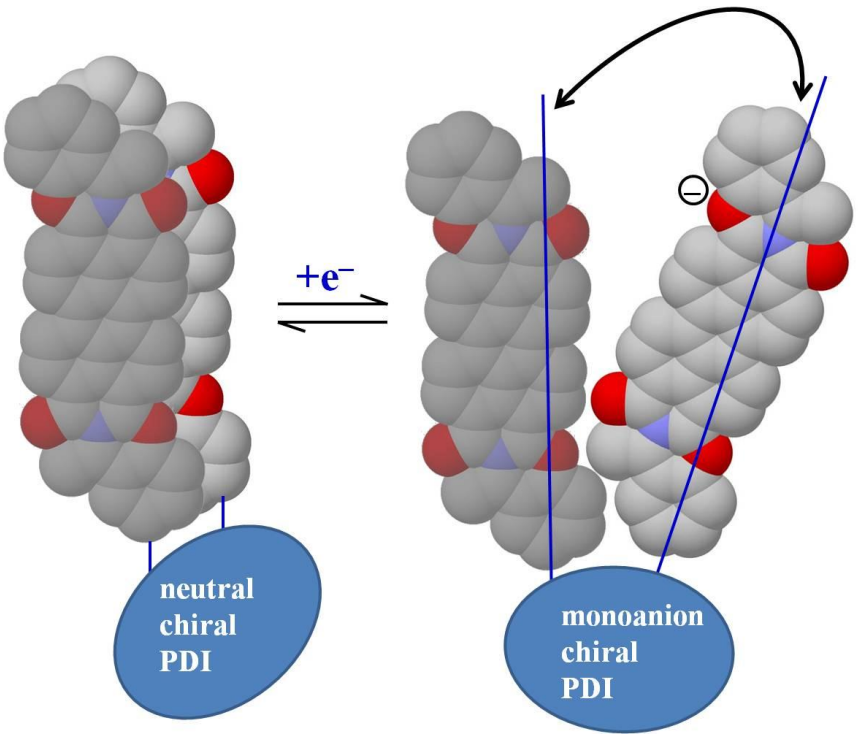

Figure 2.6: A representative diagram of a redox triggered chiroptical molecular switch involving chiral perylene dye.

2.2.3 Molecular Device Architectures

A molecular device or machine based on molecules is very interesting and could reduce energy consumption and global warming. The best example of a molecular machine is the human being made up of ordered millions and billions of nanostructural molecules.

The exciting optoelectronic properties of chiral perylene dyes could definitely offer designing of a complete molecular machine. An imaginative display board made up of chiral perylene dyes is shown in Figure 2.7.

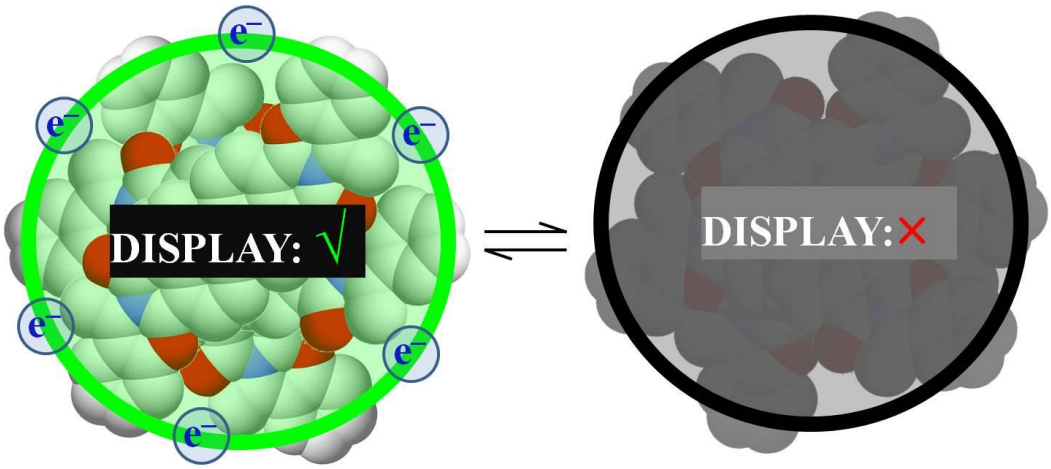

Figure 2.7: An imaginative fluorescent chiral perylene molecular made display board.

It can be pointed that light emission, quenching of light emission, conductivity, no conductivity, and color change, etc., such properties of nanochiral perylene molecules can be stimulated and governed by various parameters. Therefore, they can be applied as sensors and finally can be shaped into molecular machines and devices.

2.2.4 Renewable Energy Systems

In order to address the increasing global demand for energy (electrical energy), developing of renewable energy systems are essential. As discussed, conventional silicon solar cells are very expensive and environmentally hazardous; photovoltaics based on organic dyes became very crucial.

Chiral perylene dyes can be easily employed in photovoltaics as they can absorb sunlight energy (because of high molar absorptivities) and emit as much as light is absorbed. Moreover, they are photoconductive and transfer electrons, accept electrons and therefore act as *n*-type semiconductors. The lifetime of renewable energy systems can be long as these dyes are chemically, thermally stable. These can be easily employed with another suitable donor compounds and therefore fits several types of photovoltaics such as organic solar cells, dye sensitized solar cells, bulk heterojunction solar cells, etc.

2.3 Molecular Design and Theoretical Aspects of Perylene Dyes in the Construction of Solar Cells

The molecular designing of perylene dyes play key role to find applications for them in potential solar cell device architectures.

(a) The compounds must be highly soluble so that they can be easily processable. This could be possible by introducing bulky or long alkyl substituents.

(b) They should possess high thermal stabilities.

(c) They should absorb as much sunlight as possible (up to NIR region). This can be achieved with proper conjugation of dyes.

(d) They should exhibit interesting optical properties. This can be investigated by core substitution of perylene chromophore with various substituents.

(e) They should have low band gaps to fit to other *p*-type materials. This can be achieved by the introduction of some substituents which can offer band gap tunability.

(f) In solid-state the compounds must have similar effective properties.

(g) The compounds could be in the nanoform to increase the performance of various interesting properties and to bind to suitable other materials.

Chapter 3

EXPERIMENTAL

3.1 Materials

Perylene-3,4,9,10-tetracarboxylic dianhydride, isoquinoline, zinc acetate, (*R*)−(+)−1−phenylethylamine were obtained from Aldrich. There was no further purification for all the chemicals purchased. The common organic solvents were of raw grade and were distilled according to the standard literature procedures. For spectroscopic analyses, pure spectroscopic grade solvents were used directly but dissolved oxygen contents were bubbled off with inert gas (Armarego and Perrin, 1980).

3.2 Instruments

Infrared Spectra

The IR Spectra were recorded on a JASCO FT-IR spectrophotometer by preparing circular KBr discs.

Elemental Analyses

Elemental analyses were obtained from a Carlo-Erba-1106 C, H, and N analyzer.

Ultraviolet (UV-vis) Absorption Spectra

The UV-vis absorption spectra in solutions were recorded using a Varian Cary-100 spectrophotometer and spectra of solid-state were obtained in thin films using a perking-Elmer UV/VIS/NIR lambda 19 spectrophotometer, equipped with solid-state accessories.

Emission Spectra and Excitation Spectra

The Emission and excitation spectra of the synthesized compounds were studied using Varian-Cary Eclipse fluorescence spectrophotometer. For the emission spectra of all the synthesized perylene derivatives were excited at λ_{exc} = 485 nm. The excitation spectra were recorded at an emission wavelength of λ_{exc} = 620 nm.

Nuclear Magnetic Resonance (NMR) Spectra

^{1}H NMR and ^{13}C NMR spectra were recorded on a Bruker/XWIN spectrometer in $CDCl_3$ on 400 MHz and 100 MHz analyzer. The internal standard used for NMR spectra recording is the well known tetramethyl silane which is transparent to electromagnetic field.

Thermo Gravimetric Analysis (TGA)

The TGA thermograms were recorded from a Perkin Elmer, TGA, Model, Pyris 1. The samples were heated at a heating rate of 10 ^{o}C/min in oxygen atmosphere.

3.3 Methods of Syntheses

The objective of this project is to design and synthesize new perylene derivatives for dye-sensitized solar cells. Especially, the project focused on materials which can easily bind to TiO_2 system via dye sensitization of nano-crystalline titanium dioxide. The overall scheme of the design is shown in Scheme 3.1.

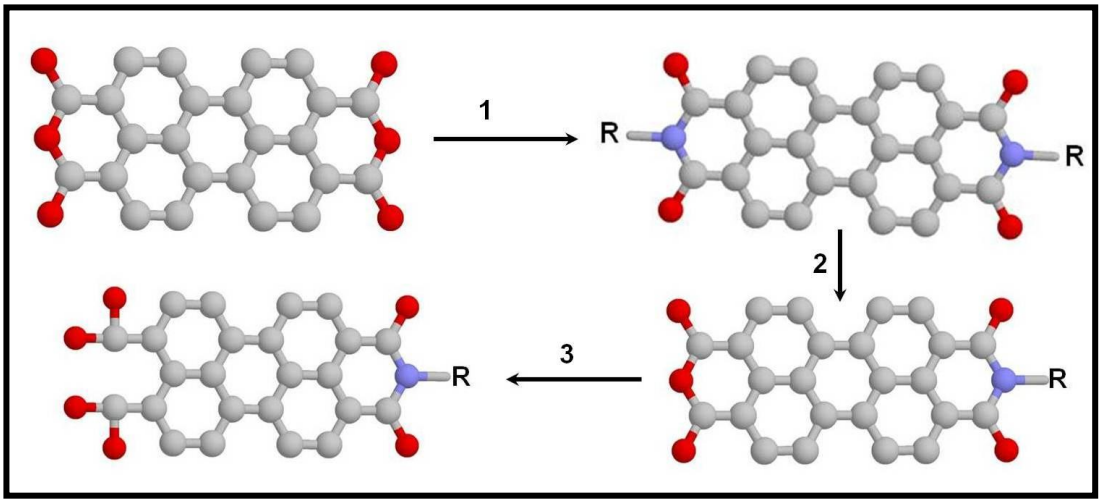

Scheme 3.1: Synthetic route of chiral perylene dicarboxylic acid carboximide (CPMI).

According to Scheme 3.1, the starting material perylene dianhydride (PDA) was converted to a chiral perylene diimide (PDI) in the first step. In the second step, PDI was converted to perylene monoimide (PMI) and finally to converted to chiral perylene dicarboxylic acid carboximide (CPMI) in the third step.

In the first step, the starting material perylene dianhydride (PDA) was converted to a chiral perylene diimide (PDI) in presence of isoquinoline and *m*-cresol as shown in Scheme 3.2.

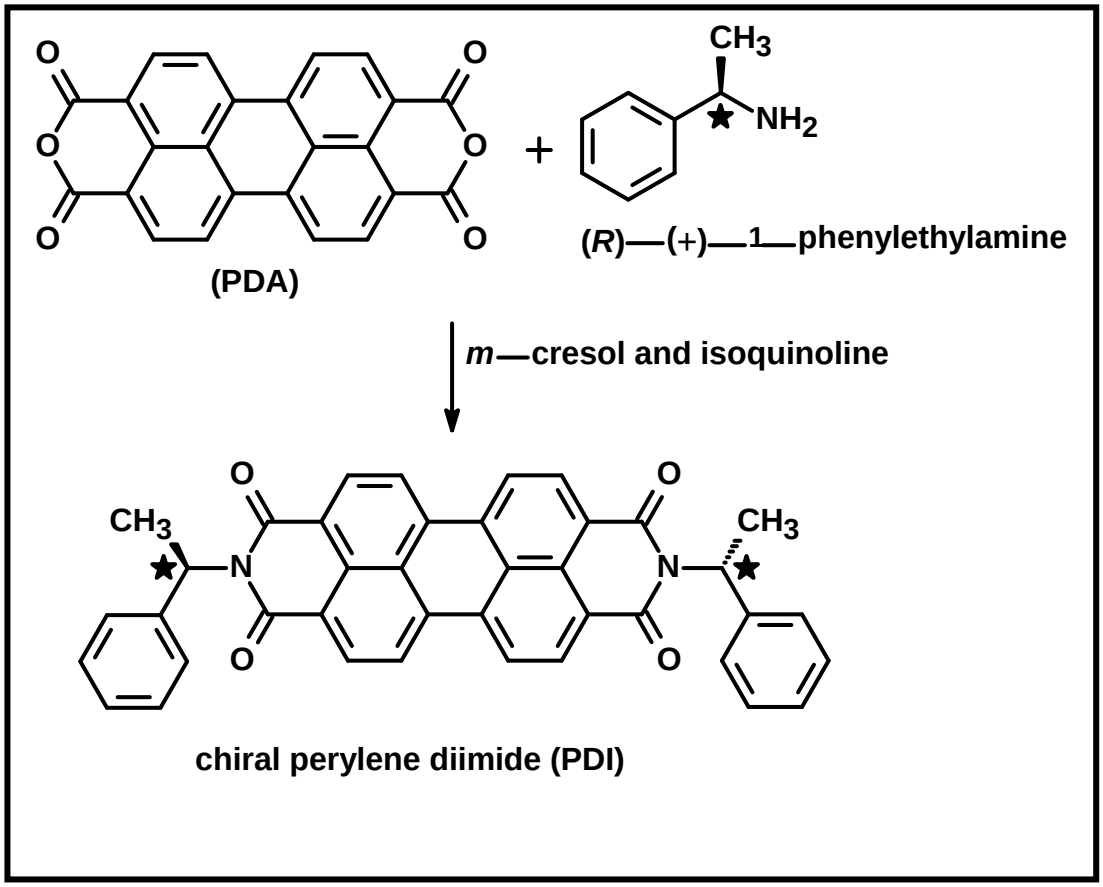

Scheme 3.2: Synthesis of N,N′-bis((*R*)-(+)-1-phenylethyl)-3,4,9,10-perylenebis(dicarboximide) (PDI) (Pucci, et al. 2010).

In the second step, the synthesized chiral perylene diimide (PDI) was converted to chiral perylene monoimide (PMI) in presence of KOH, isopropanol and water as shown in Scheme 3.3.

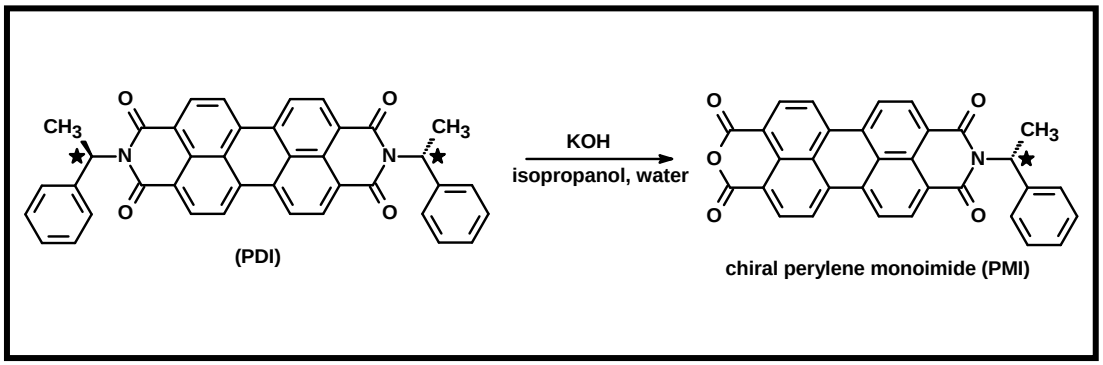

Scheme 3.3: Synthesis of N-((*R*)-(+)-1-phenylethyl)-3,4,9,10-perylenetetracarboxylic-3,4-anhydride-9,10-imide (PMI).

In the third step, the synthesized chiral perylene monoimide (PMI) was converted to chiral perylene dicarboxylic acid carboximide (CPMI) in presence of KOH and isopropanol as shown in Scheme 3.4.

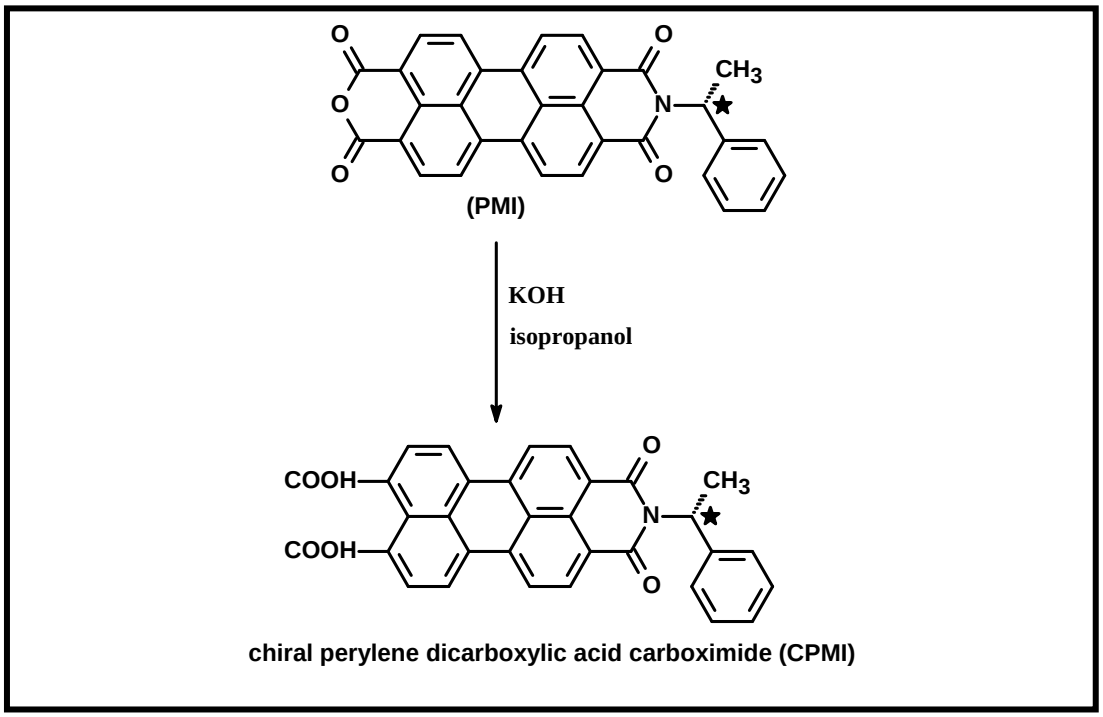

Scheme 3.4 Synthesis of chiral perylene-3,4-dicarboxylic -9,10-((*R*)-1-phenylethyl)carboximide (CPMI).

3.4 Synthesis of N,N′-bis((*R*)-(+)-1-phenylethyl)-3,4,9,10-perylenebis(dicarboximide) (PDI)

(Pucci, et al. 2010)

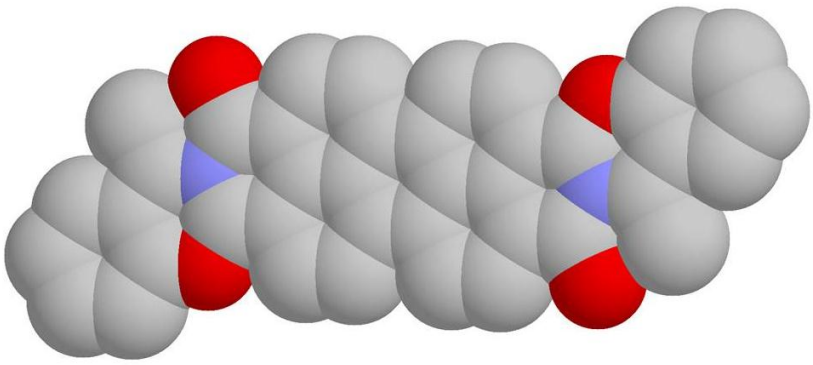

The chiral perylene diimide (PDI) was synthesized and characterized according to the previously reported procedure of Pucci, et al. (Pucci, et al. 2010).

3.5 Synthesis of N-((*R*)-(+)-1-phenylethyl)-3,4,9,10-perylenetetracarboxylic-3,4-anhydride-9,10-imide (PMI)

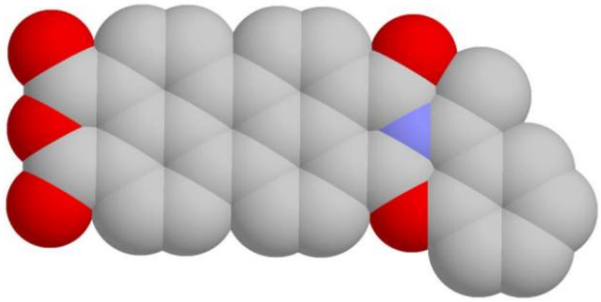

A suspension of N,N′-bis((*R*)-(+)-1-phenylethyl)-3,4,9,10-perylenebis(dicarboximide) (PDI) (300 mg, 0.5 mmol) and KOH (1.41 g, 0.214 mol) in isopropanol (20 mL) and water (3 mL) were stirred for 30 min at room temperature in a 2-necked round bottom flask equipped with a thermometer, condenser and magnetic stir bar. The reaction mixture was then stirred at reflux for 24 h for completion of reaction and poured into dilute HCl solution (100 mL). The precipitate was filtered off and washed with water. The obtained crude product was re-suspended in 5% KOH (100 mL) and stirred for 30 min, filtered. The product was then washed with dilute HCl and treated in Soxhlet apparatus with chloroform to yield the brownish monoimide solid. The resultant product was dried at 100 ^{o}C under vacuum overnight.

Yield: 89% (200 mg); **Color:** brown; **mp:** >300 ^{o}C.

FT-IR (KBr, cm^{-1}): ν = 3450, 3062, 2974, 1769, 1732, 1699, 1656, 1594, 1317, 810, 739, 698.

UV-Vis ($CHCl_3$) λ_{max}, nm (ε_{max}, M^{-1}cm^{-1}): 457 (15200), 486 (36500), 522 (58000).

Anal. calcd for ($C_{32}H_{17}NO_5$), (495.49): C, 77.57; H, 3.46; N, 2.83. **Found:** C, 76.17; H, 3.64; N, 2.89.

3.6 Synthesis of Chiral Perylene-3,4-dicarboxylic -9,10-((*R*)-1-phenylethyl)carboximide (CPMI)

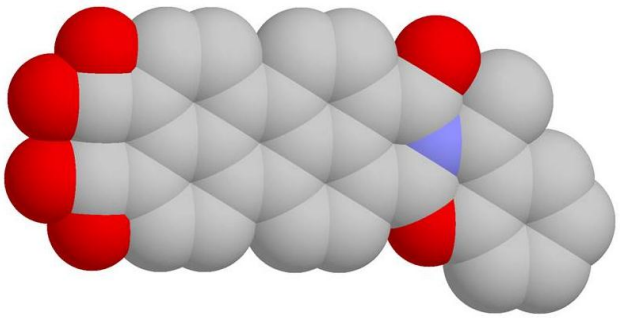

A 2-necked round bottom flask equipped with a thermometer, condenser and magnetic stir bar was added N-((*R*)-(+)-1-phenylethyl)-3,4,9,10-perylenetetracarboxylic-3,4-anhydride-9,10-imide (PMI) (0.387 g, 0.78 mmol) in a mixture of KOH (87.6 mg, 1.56 mmol) and isopropanol (80 mL). The solution was stirred for 30 min at room temperature. The homogeneous mixture formed was then stirred at reflux for 18 h. The crude mixture was then cooled to room temperature and poured into CH_2Cl_2, added aq. NH_4Cl solution (pH 7) and the organic phase was extracted. After drying the organic phase over Na_2SO_4, the solution was concentrated to dryness giving a crude product of carboxylic acid chiral perylene dye. The product was dried in vacuum oven overnight at 100 ^oC.

Yield: 80% (321 mg); **Color:** brown; **mp:** >300 ^oC.

FT-IR (KBr, cm^{-1}): ν = 3450, 3096, 2925, 2852, 1769, 1732, 1699, 1657, 1594, 1318, 810, 739.

UV-Vis ($CHCl_3$) λ_{max}, nm (ε_{max}, $M^{-1}cm^{-1}$): 457 (73300), 487 (155800), 523 (179000).

Anal. calcd for ($C_{32}H_{19}NO_6$), (513.51): C, 74.85; H, 3.73; N, 2.73. **Found:** C, 74.17; H, 3.64; N, 2.69.

3.7 General Synthesis Reaction Mechanism of Perylene Dyes

Step: 1

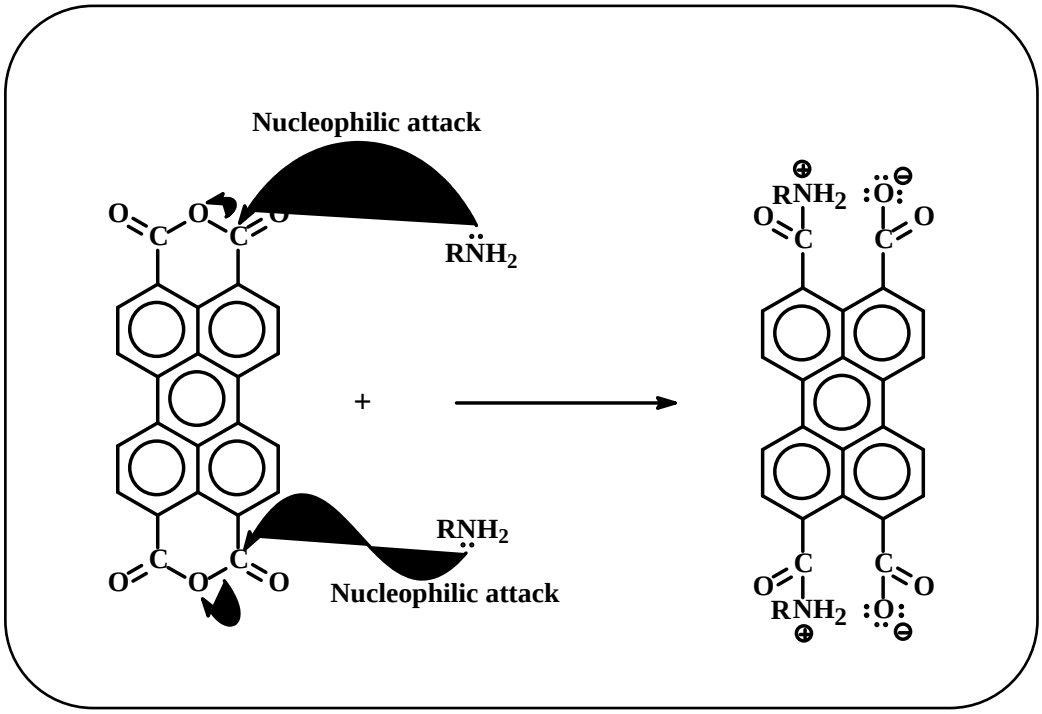

Step: 2

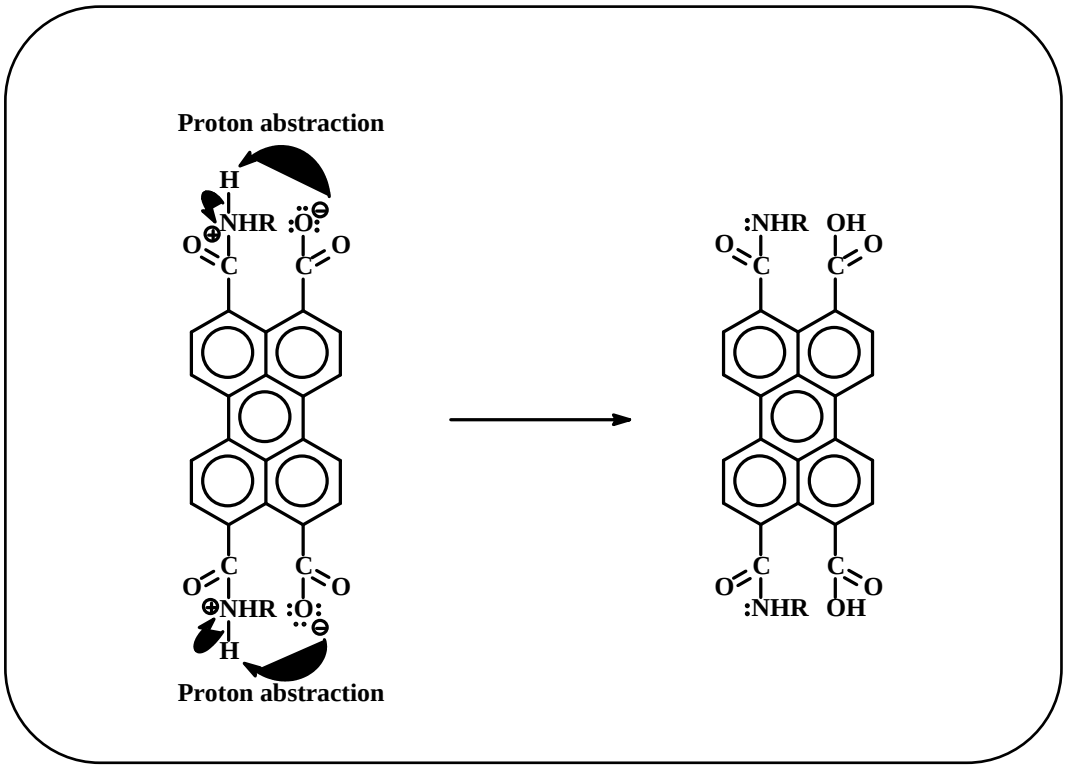

Step: 3

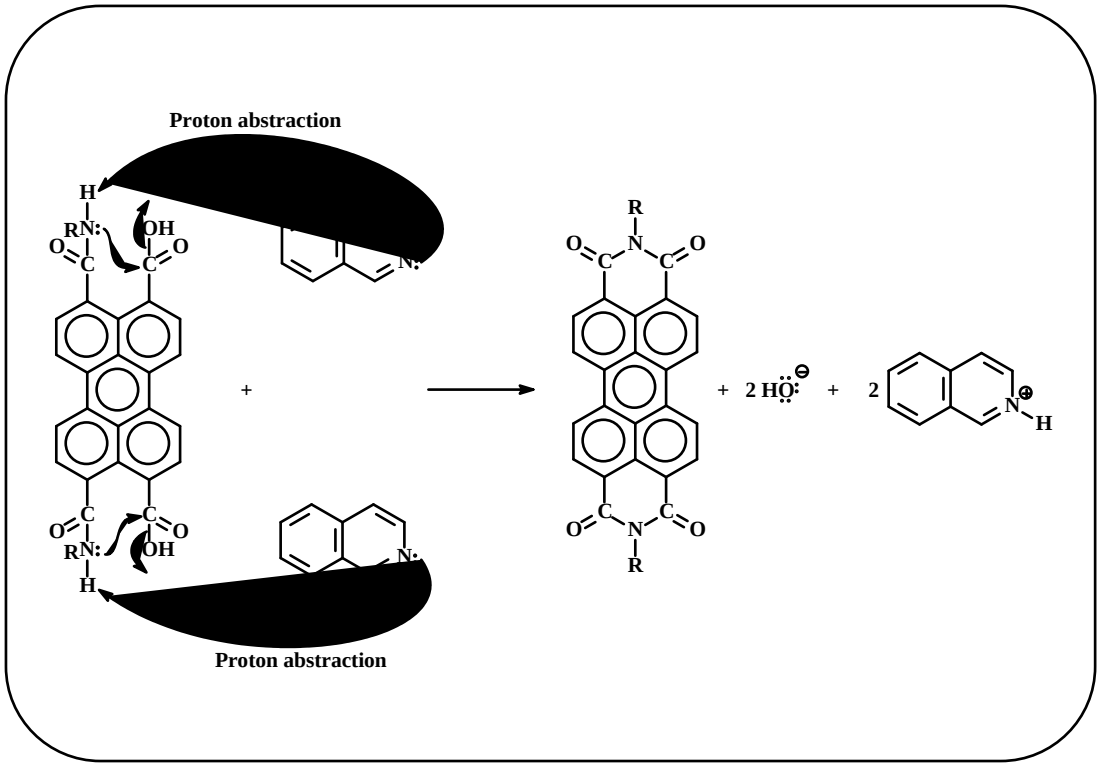

Step: 4

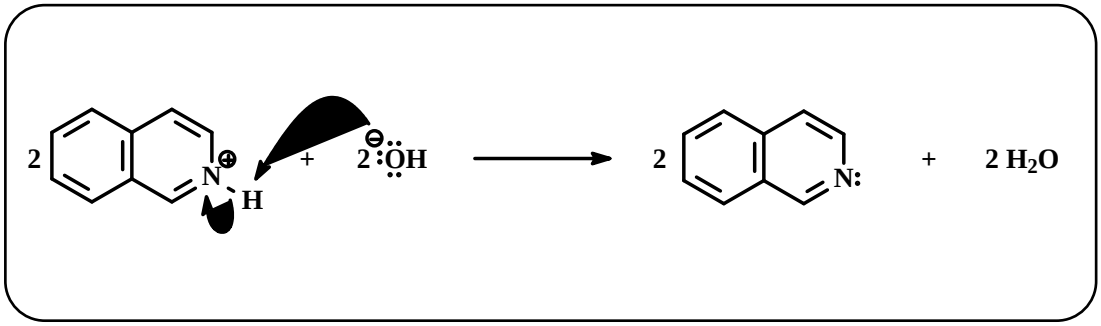

Chapter 4

DATA AND CALCULATIONS

4.1 Calculations of Maximum Extinction Co-efficients (ε_{max})

The linear relationship from Beer-Lambert's law gives following equation to calculate $\varepsilon_{max.}$

$$\boldsymbol{\varepsilon_{max} = \frac{A}{cl}}$$

Where, $\boldsymbol{\varepsilon_{max}}$**:** Maximum extinction co-efficient in $L \cdot mol^{-1} \cdot cm^{-1}$ at λ_{max}

***A*:** Absorbance

***c*:** Concentration in mol L^{-1}

***l*:** Path length in cm

ε_{max} Calculation of PMI:

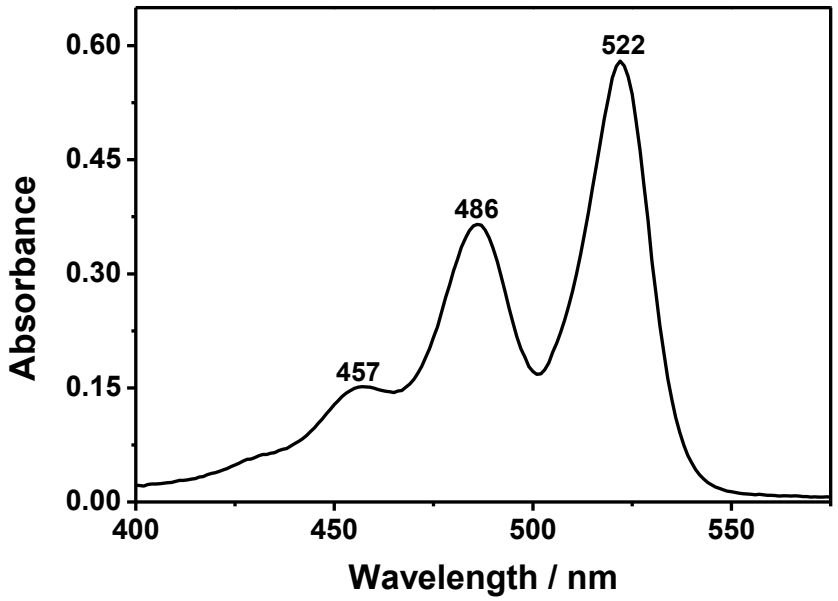

Figure 4.1: Absorption Spectrum of PMI in Chloroform at 1×10^{-5} M Concentration

According to the absorption spectrum of PMI (Figure 4.1) the absorption is 0.58 for the concentration of 1×10^{-5} M at the wavelength, λ_{max} = 522 nm.

$$\Rightarrow \boldsymbol{\varepsilon_{max}} = \frac{\mathbf{0.58}}{\mathbf{1\times10^{-5}\ M \times 1\ cm}} = \mathbf{58000\ L \cdot mol^{-1} \cdot cm^{-1}}$$

$$\Rightarrow \boldsymbol{\varepsilon_{max}}\ \textbf{of PMI} = \mathbf{58000\ L \cdot mol^{-1} \cdot cm^{-1}}$$

The molar absorptivities of the synthesized compounds were calculated in the similar method and listed below (Table 4.1).

Table 4.1: Molar absorptivity data of PDI, PMI and CPMI

Compound	Concentration	Absorbance	λ_{max}	ε_{max} ($M^{-1}cm^{-1}$)
PDI	1×10^{-5} M	0.80	527 nm	80000
PMI	1×10^{-5} M	0.58	522 nm	58000
CPMI	1×10^{-5} M	1.79	523 nm	179000

4.2 Calculations of Half-width of the Selected Absorption ($\Delta\bar{\nu}_{1/2}$)

The half-width of the selected maximum absorption is the full width at half maximum and can be calculated from the following equation.

$$\Delta\bar{\nu}_{1/2} = \bar{\nu}_{I} - \bar{\nu}_{II}$$

Where, $\bar{\nu}_{I}$, $\bar{\nu}_{II}$: The frequencies from the absorption spectrum in cm^{-1}

$\Delta\bar{\nu}_{1/2}$: Half-width of the selected maximum absorption in cm^{-1}

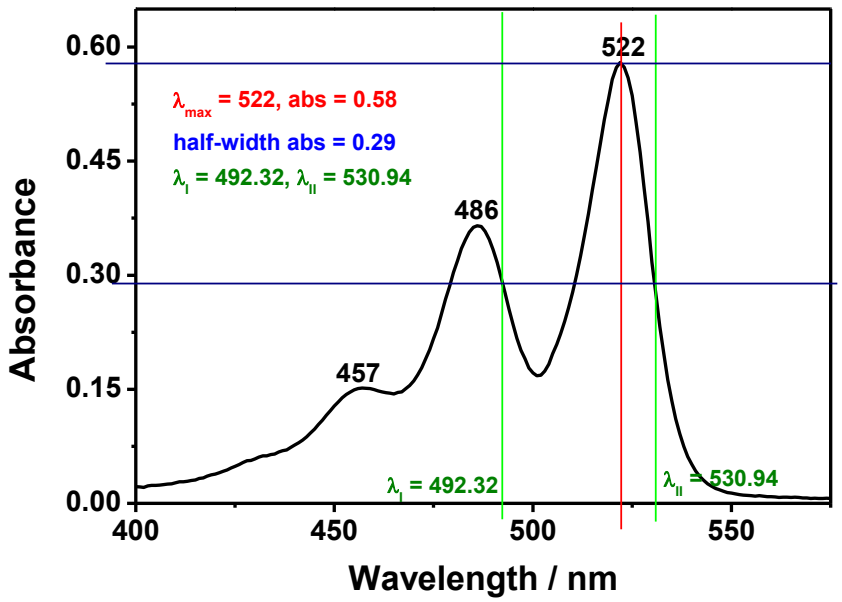

Figure 4.2: Absorption spectrum of PMI in chloroform and half-width representation

From the Figure 4.2,

λ_I = 492.32 nm

⇨ $\lambda_I = 492.32 \text{ nm} \times \frac{10^{-9} \text{ m}}{1 \text{ nm}} \times \frac{1 \text{ cm}}{10^{-2} \text{ m}} = 4.9232 \times 10^{-5} \text{ cm}$

⇨ $\bar{\nu}_I = \frac{1}{4.9232 \times 10^{-5} \text{ cm}} = 20311.99 \text{ cm}^{-1}$

λ_{II} = 530.94 nm

⇨ $\lambda_{II} = 530.94 \text{ nm} \times \frac{10^{-9} \text{ m}}{1 \text{ nm}} \times \frac{1 \text{ cm}}{10^{-2} \text{ m}} = 5.3094 \times 10^{-5} \text{ cm}$

⇨ $\bar{\nu}_{II} = \frac{1}{5.3094 \times 10^{-5} \text{ cm}} = 18834.52 \text{ cm}^{-1}$

$\Delta\bar{\nu}_{1/2} = \bar{\nu}_{I} - \bar{\nu}_{II} = 20311.99 \text{ cm}^{-1} - 18834.52 \text{ cm}^{-1} = 1477.47 \text{ cm}^{-1}$

⇨ **$\Delta\bar{\nu}_{1/2}$ = 1477.47 cm^{-1}**

It is required to estimate the half-widths of the compounds in order to calculate the theoretical radiative lifetimes of the compounds. In the similar manner shown above, the half-widths were calculated and presented below in Table 4.2.

Table 4.2: Half-widths of the selected absorptions of compounds PDI, PMI and CPMI measured in chlororform

Compound	**λ_I (nm)**	**λ_{II} (nm)**	**$\Delta\bar{\nu}_{1/2}$ (cm^{-1})**
PDI	496	536	1476.05
PMI	492	530	1477.47
CPMI	493	530	1453.57

4.3 Calculations of Theoretical Radiative Lifetimes (τ_0)

The theoretical radiative lifetime of a molecule refers to the lifetime of an excited molecule theoretically measured in the absence of nonradiative transitions.

$$\boldsymbol{\tau_0 = \frac{3.5 \times 10^8}{\bar{\nu}_{max}^2 \times \varepsilon_{max} \times \Delta\bar{\nu}_{1/2}}}$$

Where, $\boldsymbol{\tau_0}$**:** Theoretical radiative lifetime in ns

$\boldsymbol{\bar{\nu}_{max}}$**:** Mean frequency of the maximum absorption band in cm^{-1}

$\boldsymbol{\varepsilon_{max}}$**:** The maximum extinction coefficient in $L \cdot mol^{-1} \cdot cm^{-1}$ at the maximum absorption wavelength, λ_{max}

$\boldsymbol{\Delta\bar{\nu}_{1/2}}$**:** Half-width of the selected absorption in units of cm^{-1}

Theoretical Radiative Lifetime of PMI:

With the help of calculated molar absorptivity and half-width of selected absorptions of PMI,

From the Figure 4.1 and 4.2, $\boldsymbol{\lambda_{max}}$ **= 522 nm**

$\lambda_{max} = 522 \text{ nm} \times \frac{10^{-9} \text{ m}}{1 \text{ nm}} \times \frac{1 \text{ cm}}{10^{-2} \text{ m}} = 5.22 \times 10^{-5} \text{ cm}$

⇨ $\bar{\nu}_{max} = \frac{1}{5.22 \times 10^{-5} \text{ cm}} = 19157.09 \text{ cm}^{-1}$

⇨ $\bar{\nu}_{max}^2 = (19157.09 \text{ cm}^{-1})^2 = 3.67 \times 10^8 \text{ cm}^{-2}$

Now, the theoretical radiative lifetime can be calculated from the above mentioned equation,

$$\boldsymbol{\tau_0} = \frac{\mathbf{3.5 \times 10^8}}{\bar{\nu}^2_{\mathbf{max}} \times \boldsymbol{\varepsilon}_{\mathbf{max}} \times \Delta\bar{\nu}_{\mathbf{1/2}}} = \frac{3.5 \times 10^8}{(19157.09)^2 \times 58000 \times 1477.47}$$

⇨ $\tau_0 = 1.11 \times 10^{-8}$ s

⇨ $\boldsymbol{\tau_0 = 11.1\ ns}$

With similar method of calculation, theoretical radiative lifetimes were calculated for the other synthesized compounds in chlororform and the data was presented below.

Table 4.3: Theoretical radiative lifetimes of compounds PDI, PMI and CPMI measured in chloroform

Compound	$\boldsymbol{\lambda_{max}}$ **(nm)**	$\boldsymbol{\varepsilon_{max}}$ **(M^{-1}·cm^{-1})**	$\bar{\nu}^2_{max}$ **(cm^{-2})**	$\Delta\bar{\nu}_{1/2}$ **(cm^{-1})**	$\boldsymbol{\tau_0}$ **(ns)**
PDI	527	80000	3.60×10^8	1476.05	8.23
PMI	522	58000	3.67×10^8	1477.47	11.1
CPMI	523	179000	3.66×10^8	1453.57	3.67

4.4 Calculations of Fluorescence Rate Constants (k_f)

The theoretical fluorescence rate constants for the synthesized perylene derivatives are calculated by the equation given below.

$$\boldsymbol{k_f = \frac{1}{\tau_0}}$$

Where, $\boldsymbol{k_f}$**:** Fluorescence rate constant in s^{-1}

$\boldsymbol{\tau_0}$**:** Theoretical radiative lifetime in s

Fluorescence Rate Constant of PMI:

⇨ $k_f = \frac{1}{11.1 \times 10^{-9}\ s} = 9.0 \times 10^7\ s^{-1}$

⇨ $\boldsymbol{k_f = 9.0 \times 10^7\ s^{-1}}$

The theoretical fluorescence rate constants were estimated in the similar way shown for PMI and the constants were tabulated below (Table 4.4).

Table 4.4: Fluorescence rate constants data of perylene derivatives PDI, PMI and CPMI measured in chloroform

Compound	τ_0 **(ns)**	k_f **(s^{-1})**
PDI	8.23	1.22×10^8
PMI	11.1	9.00×10^7
CPMI	3.67	2.72×10^8

4.5 Calculations of Oscillator Strengths (f)

The oscillator strength is a dimensionless quantity infers the strength of an electronic transition. It can be estimated by the equation below.

$$f = 4.32 \times 10^{-9}\, \Delta\bar{\nu}_{1/2}\, \varepsilon_{max}$$

Where, f: Oscillator strength

$\Delta\bar{\nu}_{1/2}$: Half-width of the selected absorption in units of cm^{-1}

ε_{max}: The maximum extinction coefficient in $L \cdot mol^{-1} \cdot cm^{-1}$ at the maximum absorption wavelength, λ_{max}

Oscillator Strength of PMI:

- $f = 4.32 \times 10^{-9}\, \Delta\bar{\nu}_{1/2}\, \varepsilon_{max}$
- $f = 4.32 \times 10^{-9} \times 1477.47 \times 58000 = 0.37$
- **f = 0.37**

The following table presents the calculated rate constants of radiationless deactivation for PDI, PMI and CPMI.

Table 4.5: Oscillator strengths data of perylene derivatives PDI, PMI and CPMI measured in chloroform

Compound	$\Delta\bar{\nu}_{1/2}$ (cm^{-1})	ε_{max} [a]	f
PDI	1476.05	80000	0.51
PMI	1477.47	58000	0.37
CPMI	1453.57	179000	1.12

[a] ε_{max} data is in the units of $M^{-1}cm^{-1}$

4.6 Calculations of Singlet Energies (E_s)

Singlet energy is the required amount of energy for an electronic transition of a chromophore from ground state to an excited state.

$$E_S = \frac{2.86 \times 10^5}{\lambda_{max}}$$

Where, E_s: Singlet energy in kcal mol^{-1}

λ_{max}: The maximum absorption wavelength in Å

Singlet Energy of PMI:

⇨ $E_S = \frac{2.86 \times 10^5}{\lambda_{max}} = \frac{2.86 \times 10^5}{5220}$ = 54.8 kcal mol^{-1}

⇨ **E_s = 54.8 kcal mol^{-1}**

Similarly, the singlet energies of perylene dyes were calculated and listed in the following table.

Table 4.6: Singlet energies data of perylene dyes PDI, PMI and CPMI measured in chloroform

Compound	λ_{max} (Å)	E_s (kcal mol^{-1})
PDI	5270	54.3
PMI	5220	54.8
CPMI	5230	54.7

4.7 Calculations of Optical Band Gap Energies (E_g)

The optical band gap energy gives important information relating to its HOMO and LUMO energy states to be applicable in solar cells and can be calculated from the following equation.

$$E_g = \frac{1240 \text{ eV nm}}{\lambda}$$

Where, E_g: Band gap energy in eV

λ: Cut-off wavelength of the absorption band in nm

Band Gap Energy of PMI:

The cut-off wavelength of the absorption band can be estimated from the maximum absorption band (0→0 absorption band) by extrapolating it to zero absorbance as shown below (Figure 4.3).

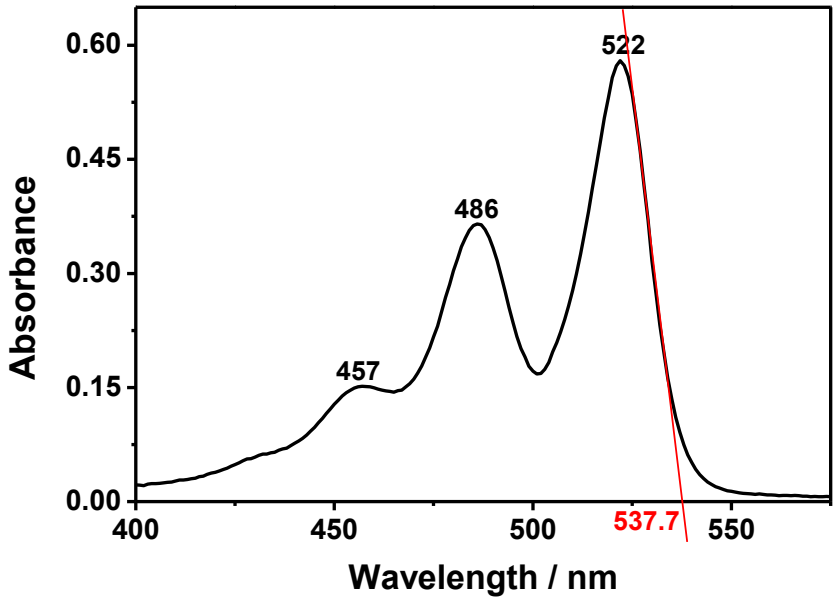

Figure 4.3: Absorption Spectrum of PMI and the cut-off wavelength

$$E_g = \frac{1240 \text{ eV nm}}{\lambda}$$

$$\Rightarrow \quad E_g = \frac{1240 \text{ eV nm}}{\lambda} = \frac{1240 \text{ eV nm}}{537.7} = 2.31 \text{ eV}$$

E_g = 2.31 eV

Similarly, the band gap energies of perylene dyes were calculated and listed in the following table.

Table 4.7: Band gap energies data of perylene dyes PDI, PMI and CPMI measured in chloroform

Compound	**Cut-off λ**	**E_g (eV)**
PDI	542.9	2.28
PMI	537.7	2.31
CPMI	538.9	2.30

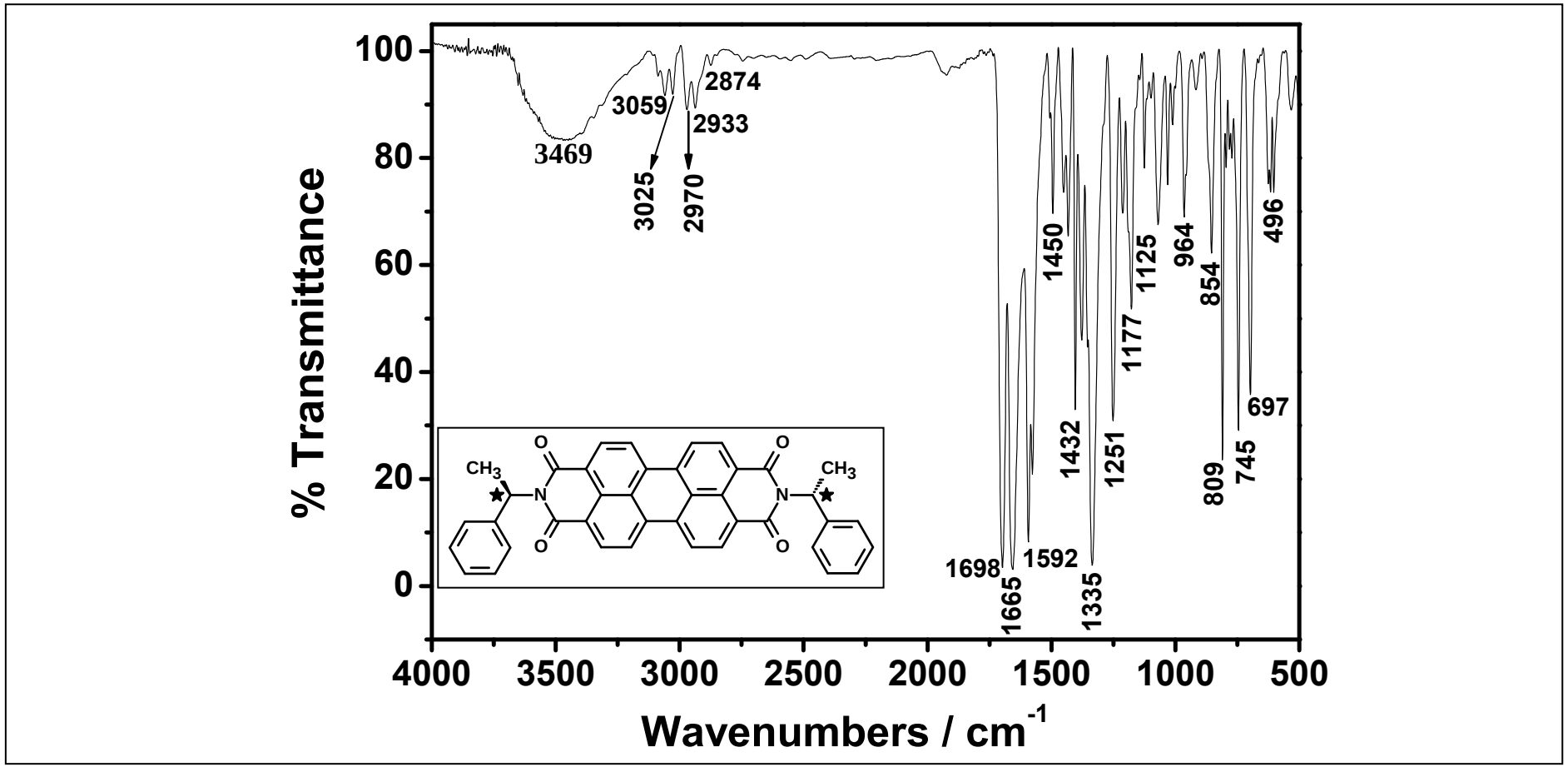

Figure 4.4 FTIR spectrum of PDI

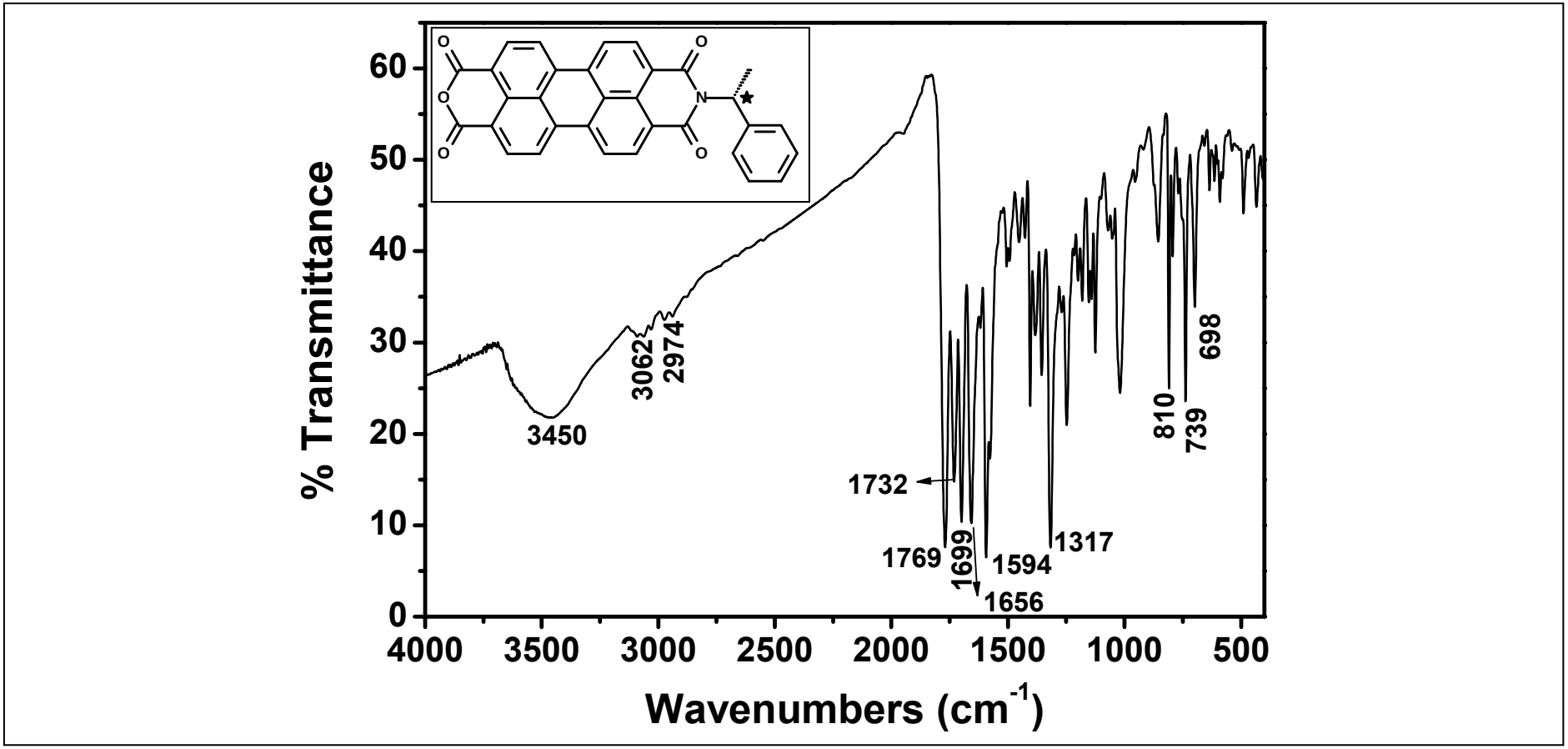

Figure 4.5 FTIR spectrum of PMI

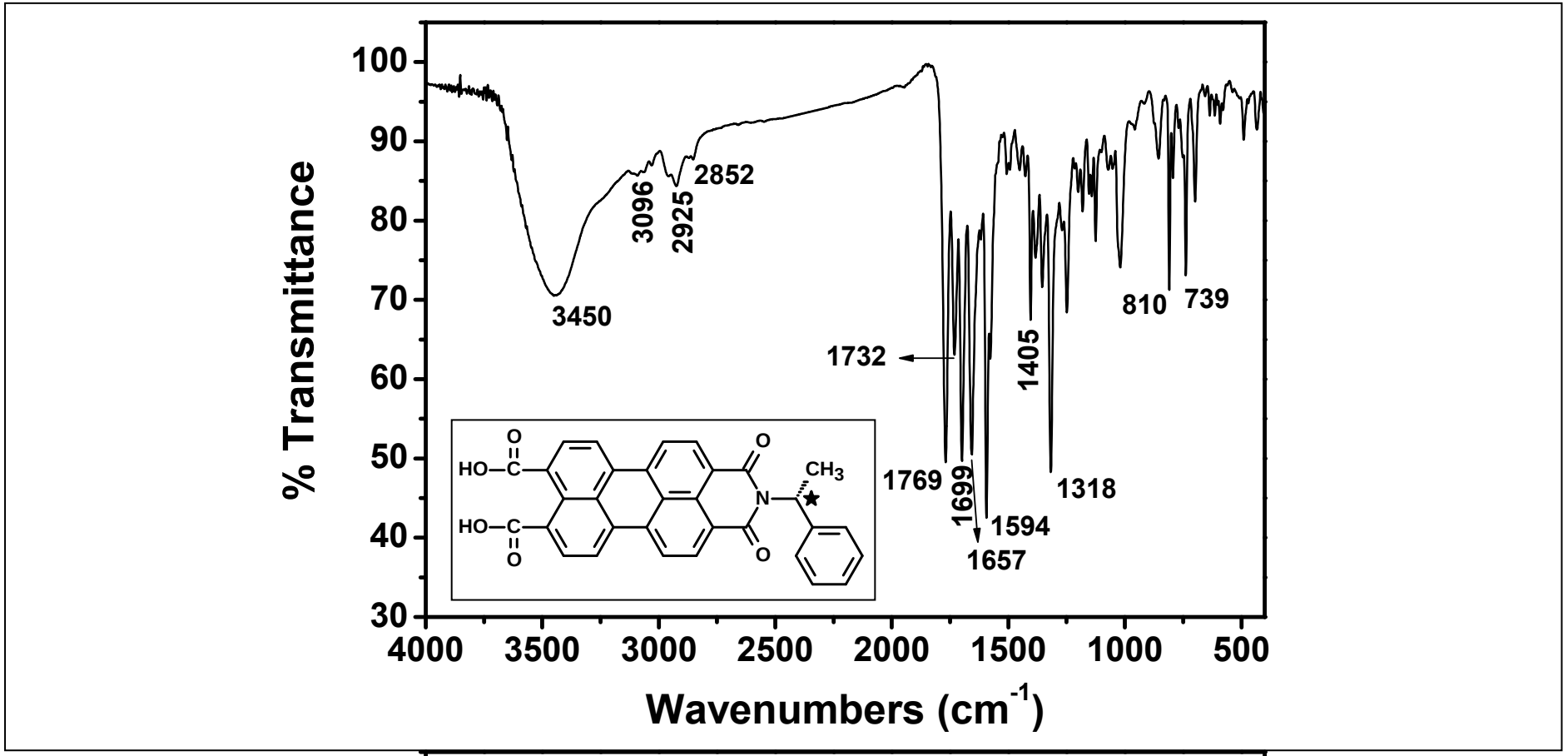

Figure 4.6 FTIR spectrum of CPMI

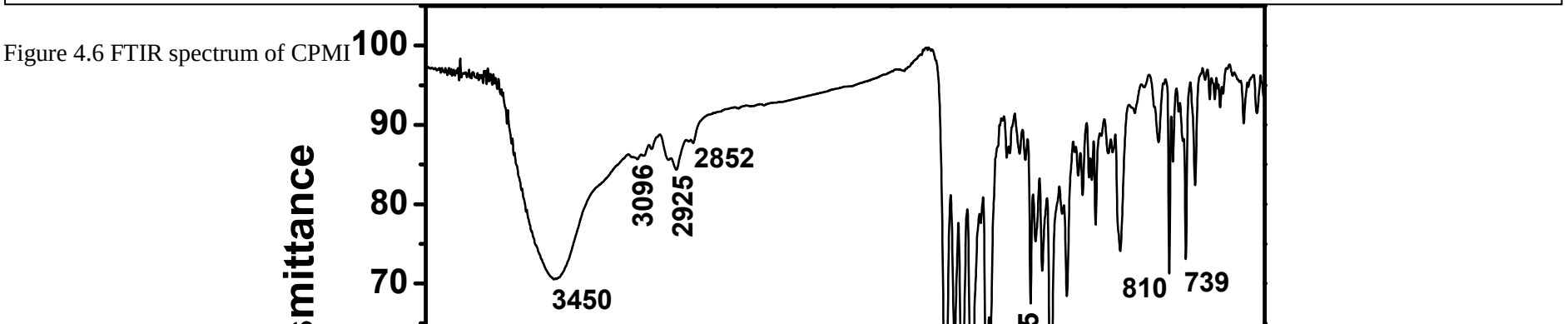

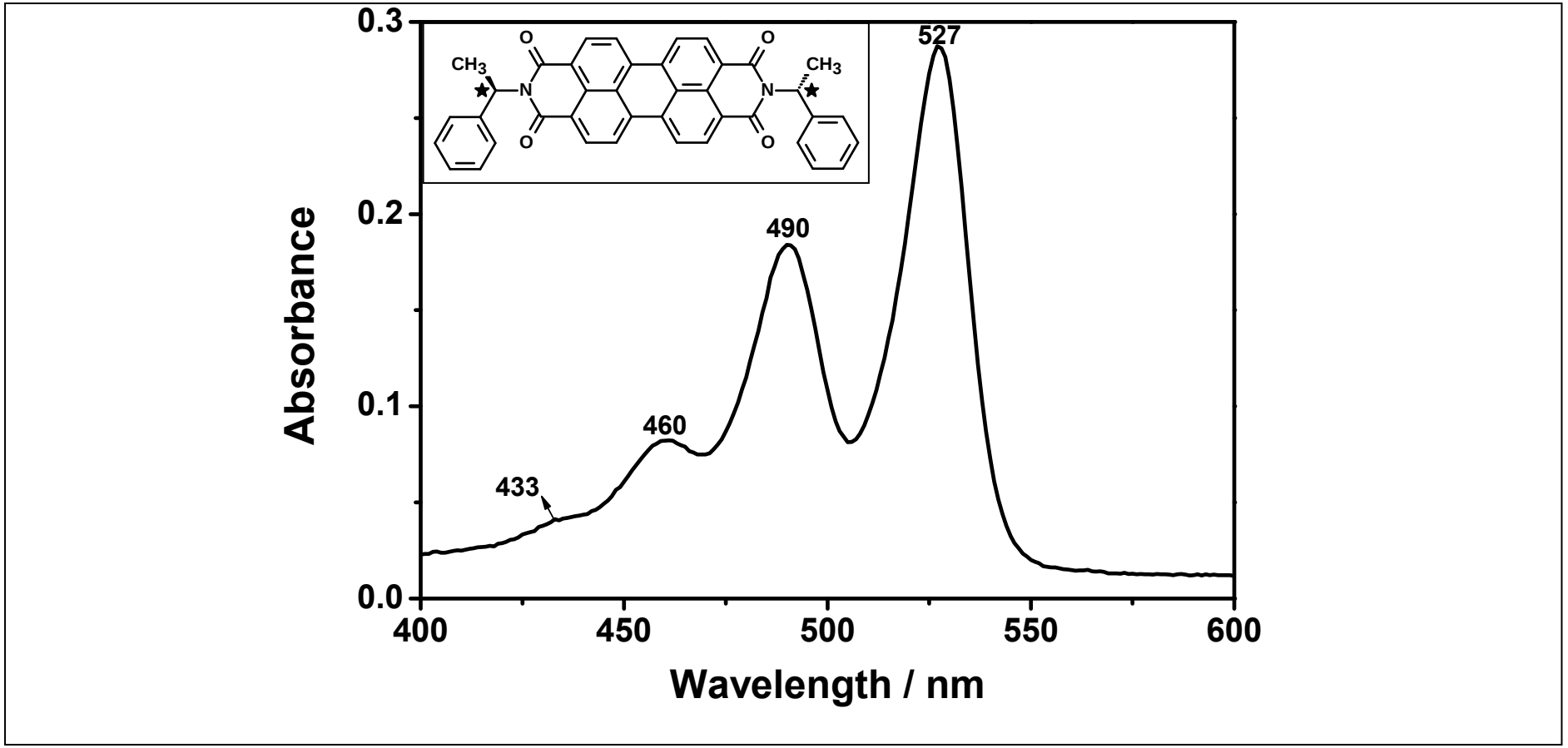

Figure 4.7 UV-vis absorption spectrum of PDI in $CHCl_3$.

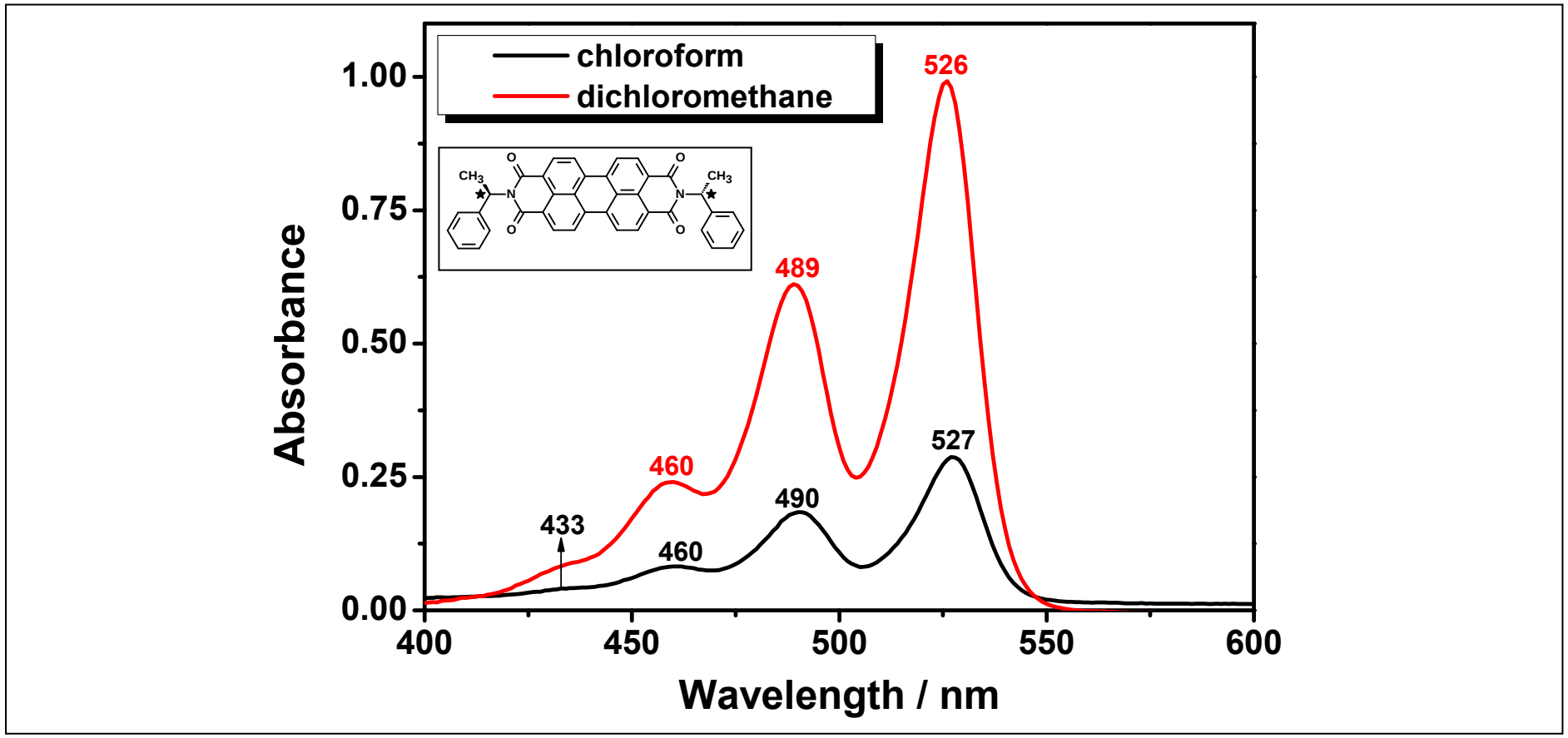

Figure 4.8 UV-vis absorption spectra of PDI in nonpolar solvents.

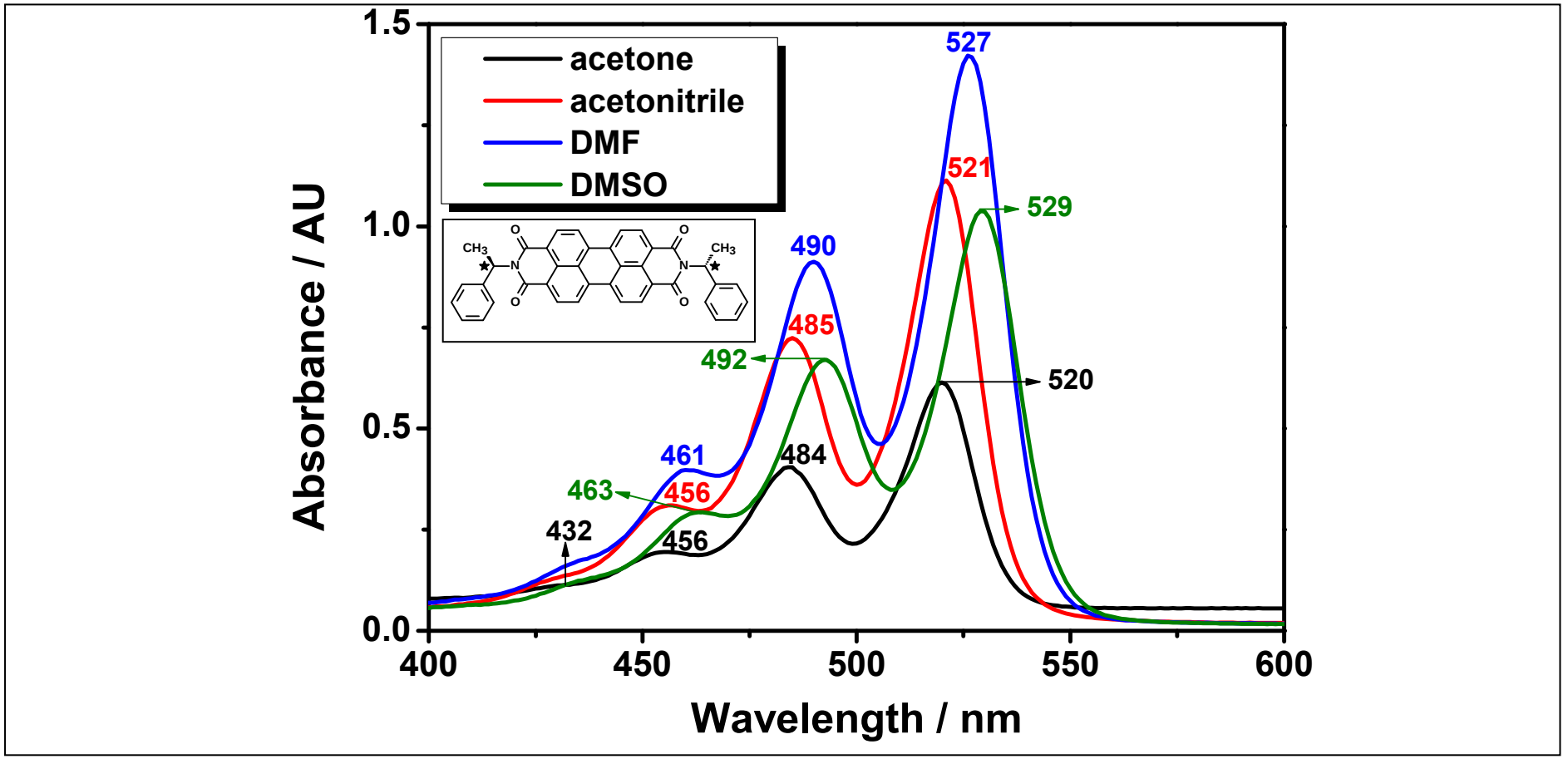

Figure 4.9 UV-vis absorption spectra of PDI in dipolar aprotic solvents.

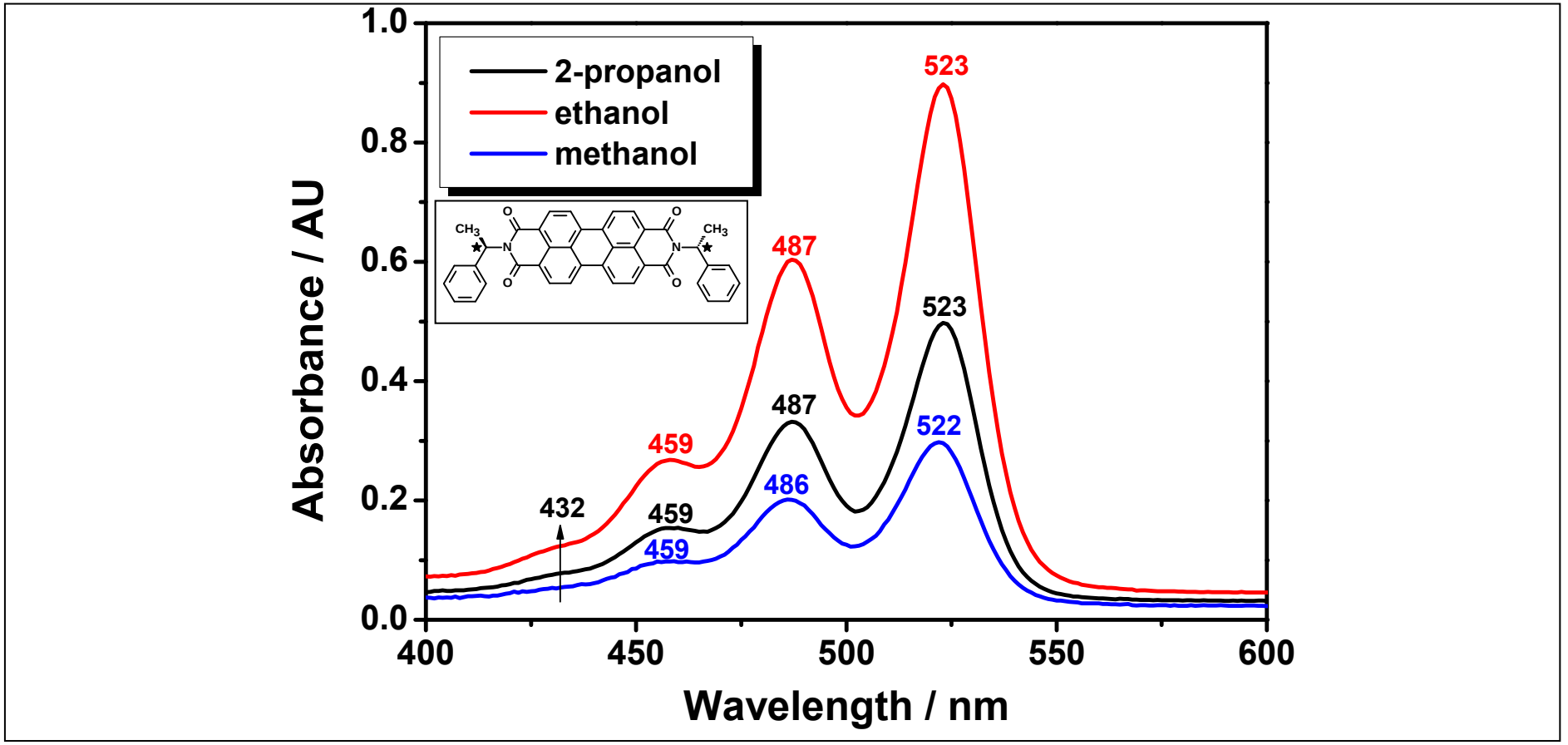

Figure 4.10 UV-vis absorption spectra of PDI in protic solvents.

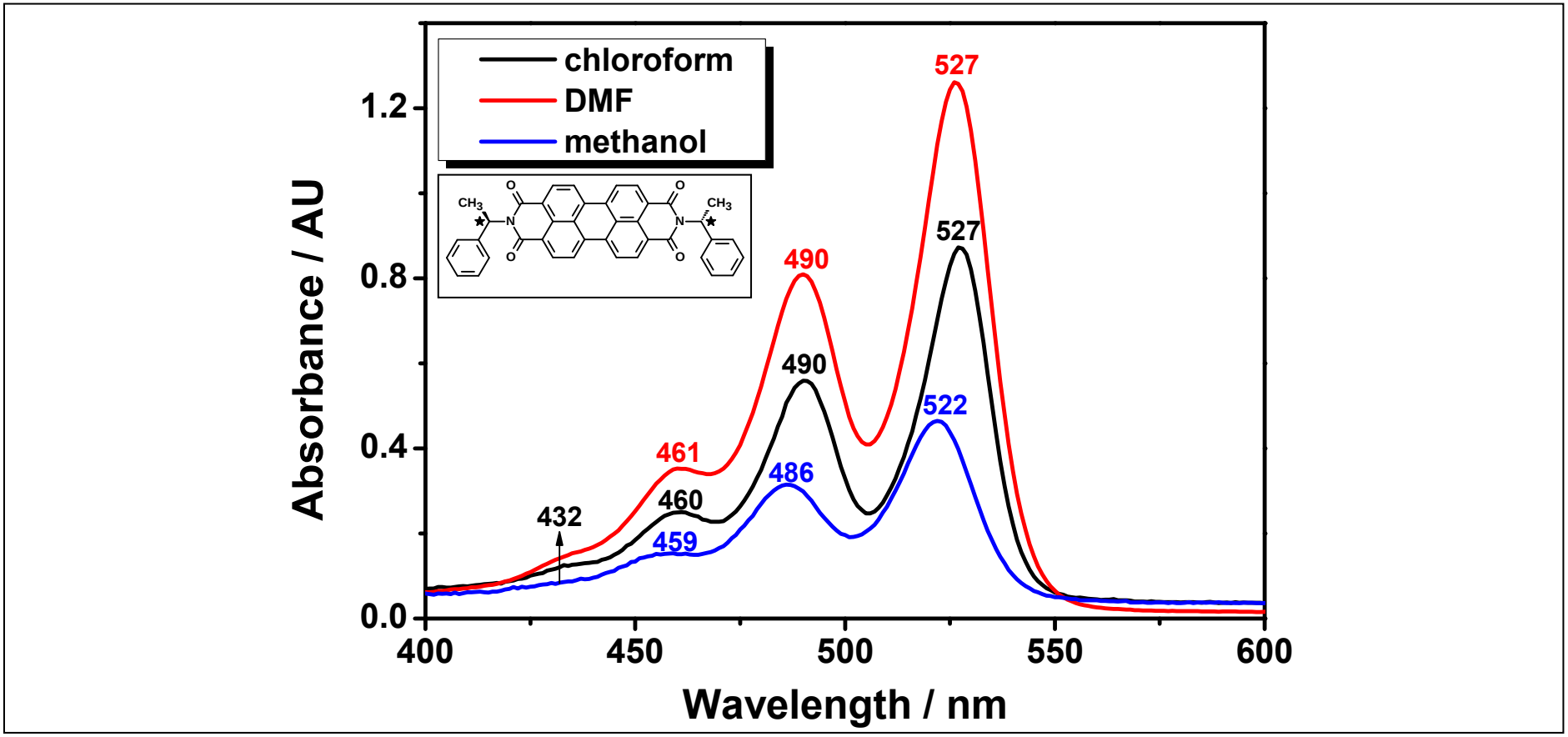

Figure 4.11 Comparison of UV-vis absorption spectra of PDI in nonpolar, dipolar aprotic and protic solvents.

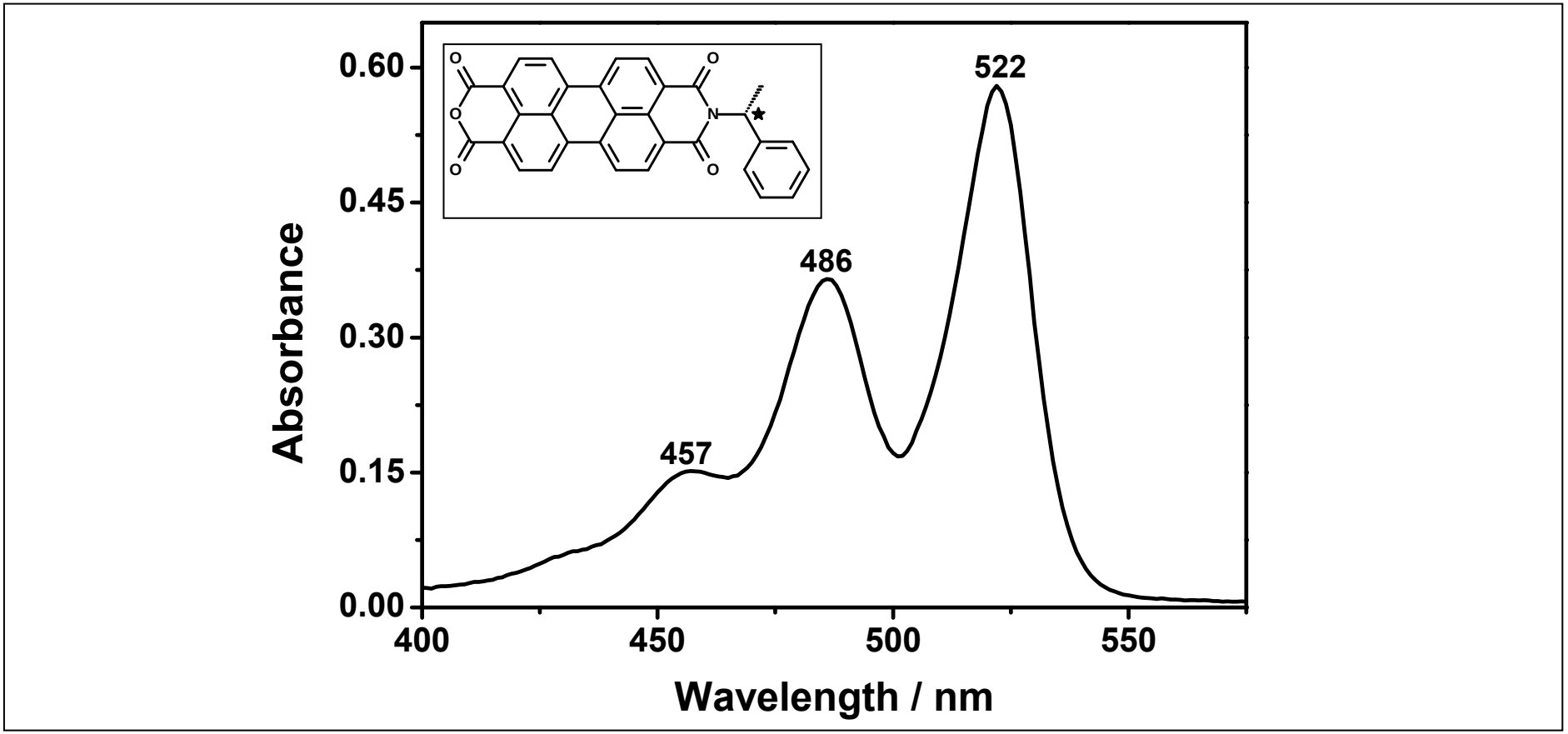

Figure 4.12 UV-vis absorption spectrum of PMI in $CHCl_3$.

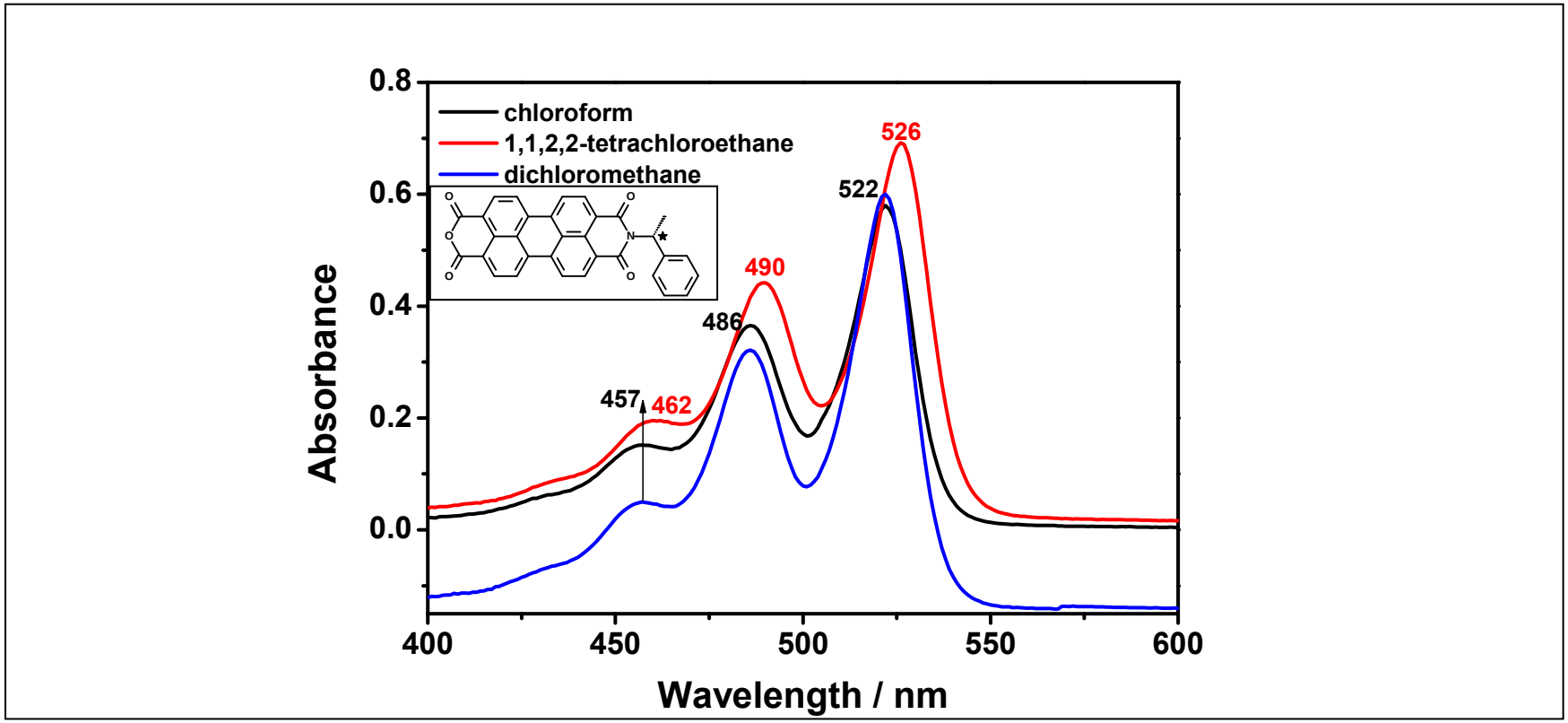

Figure 4.13 UV-vis absorption spectra of PMI in various nonpolar solvents.

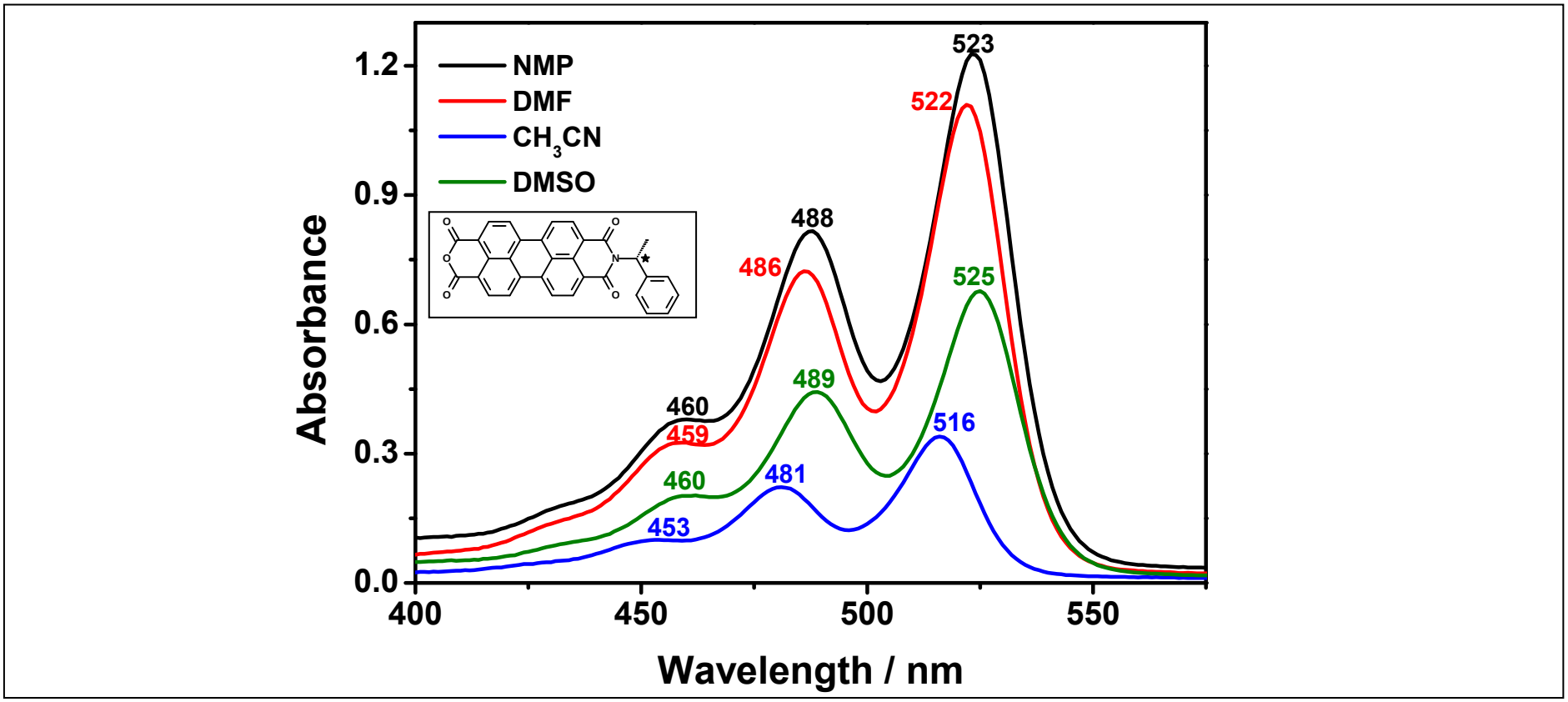

Figure 4.14 UV-vis absorption spectra of PMI in various dipolar aprotic solvents.

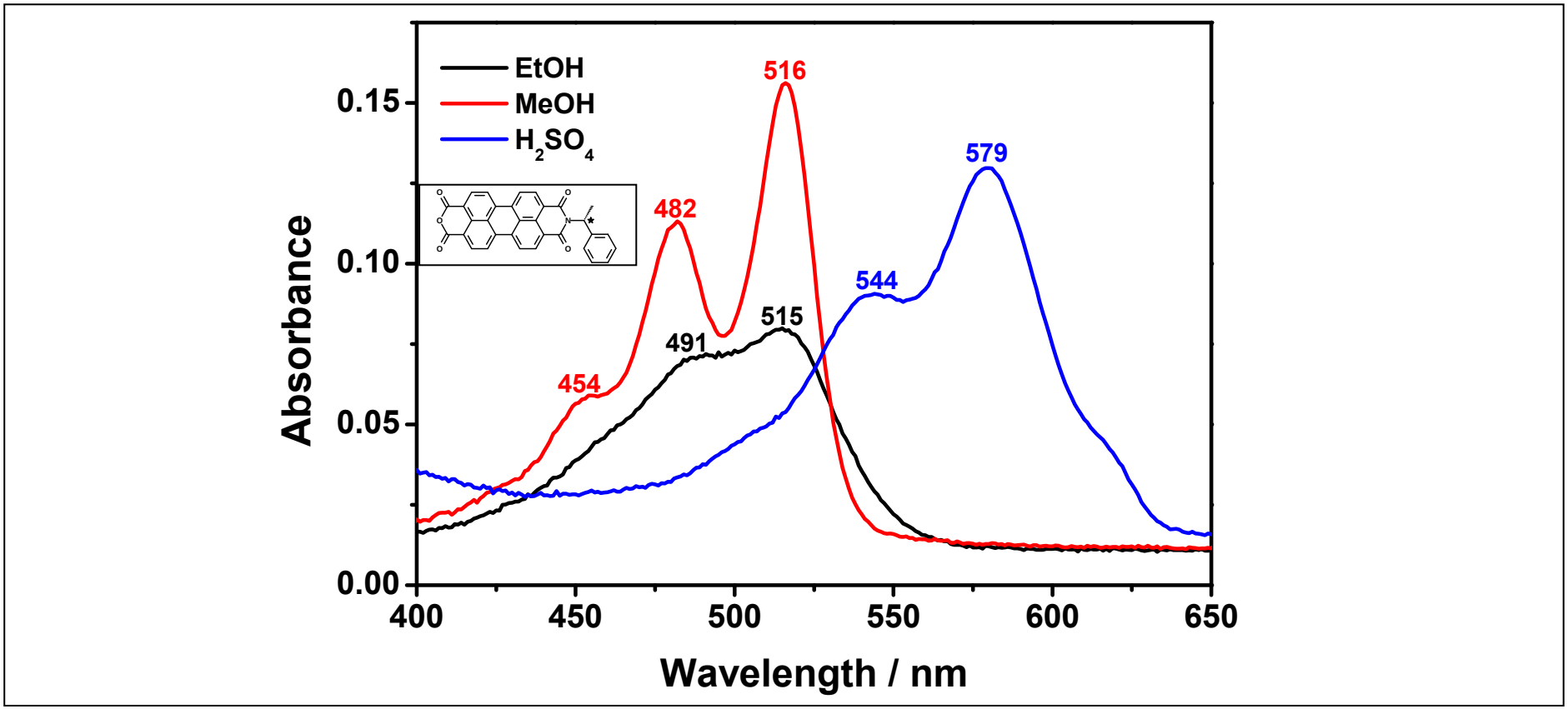

Figure 4.15 UV-vis absorption spectra of PMI in various protic solvents.

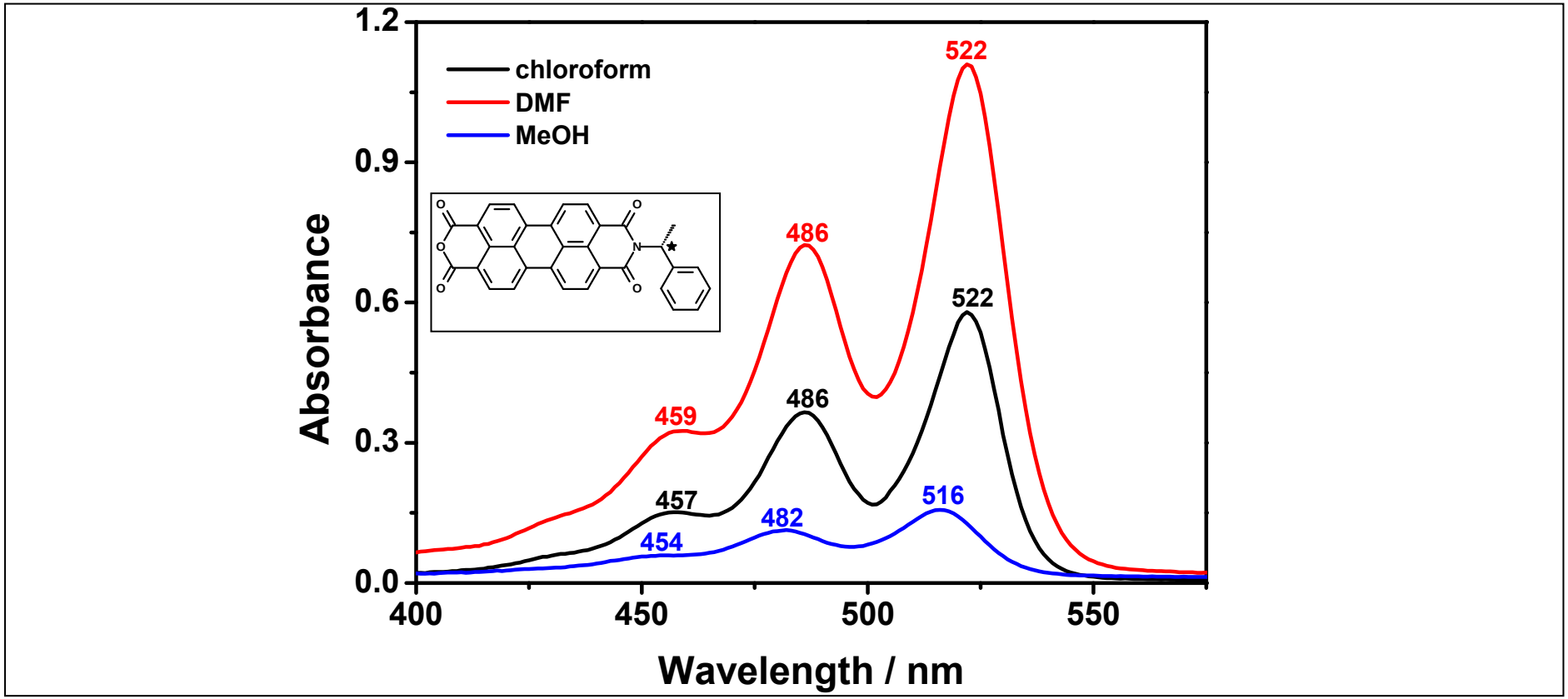

Figure 4.16 Comparison of UV-vis absorption spectra of PMI in nonpolar, dipolar aprotic and protic solvents.

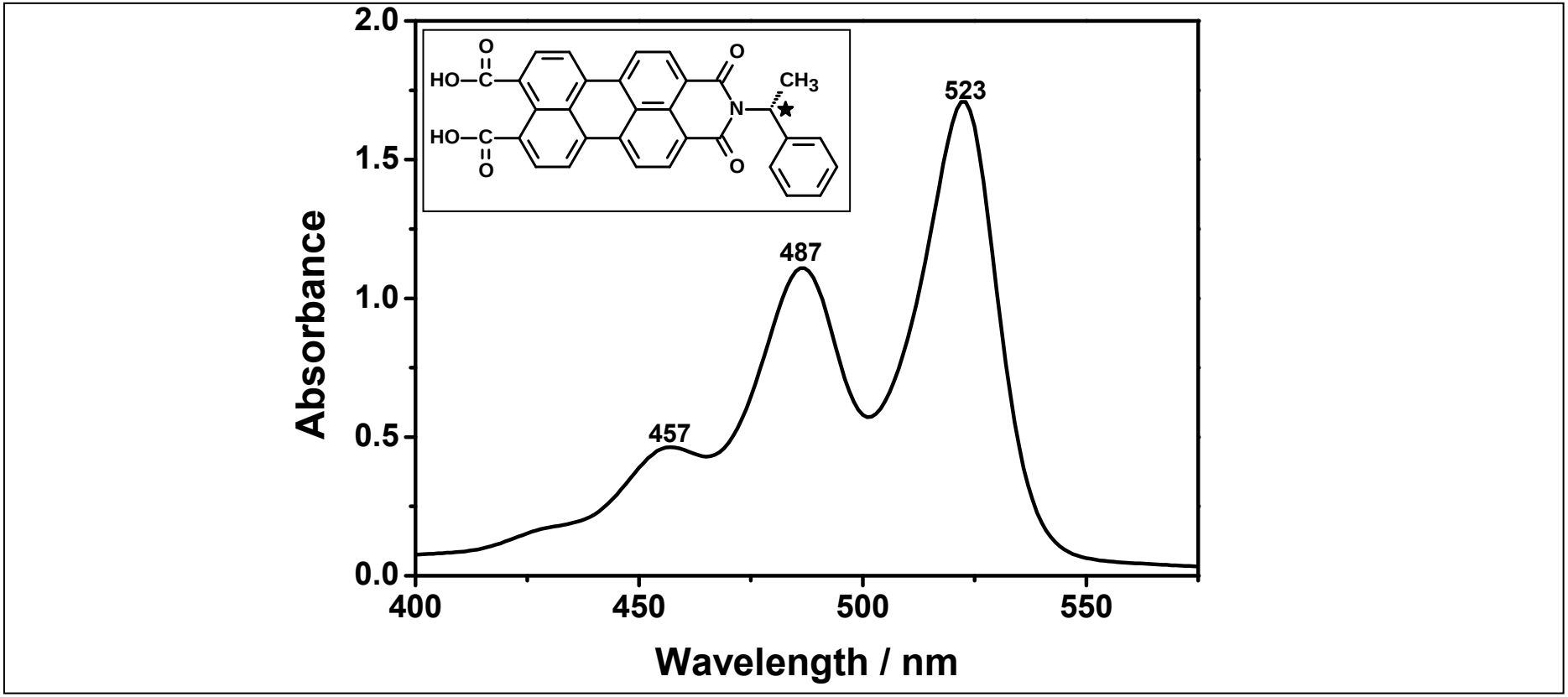

Figure 4.17 UV-vis absorption spectrum of CPMI in $CHCl_3$.

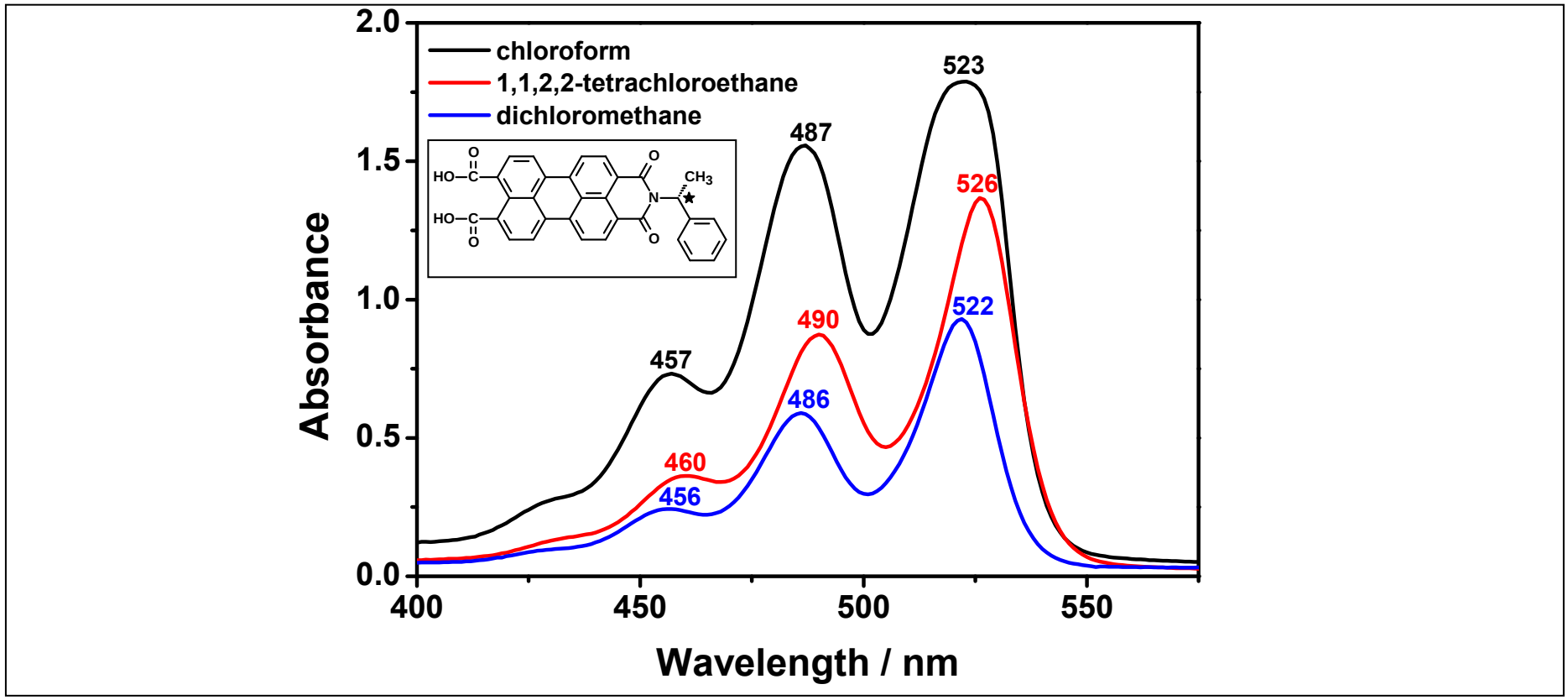

Figure 4.18 UV-vis absorption spectra of CPMI in various nonpolar solvents.

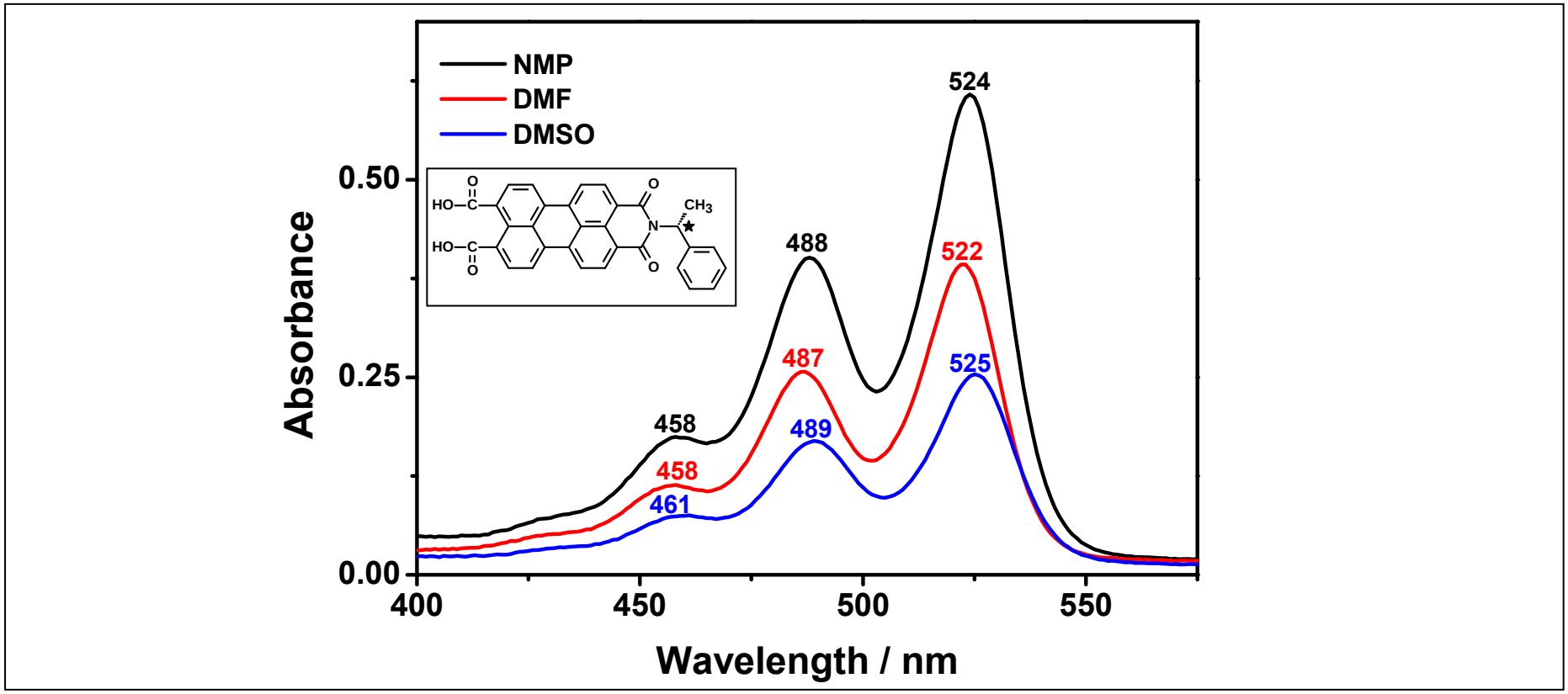

Figure 4.19 UV-vis absorption spectra of CPMI in various dipolar aprotic solvents.

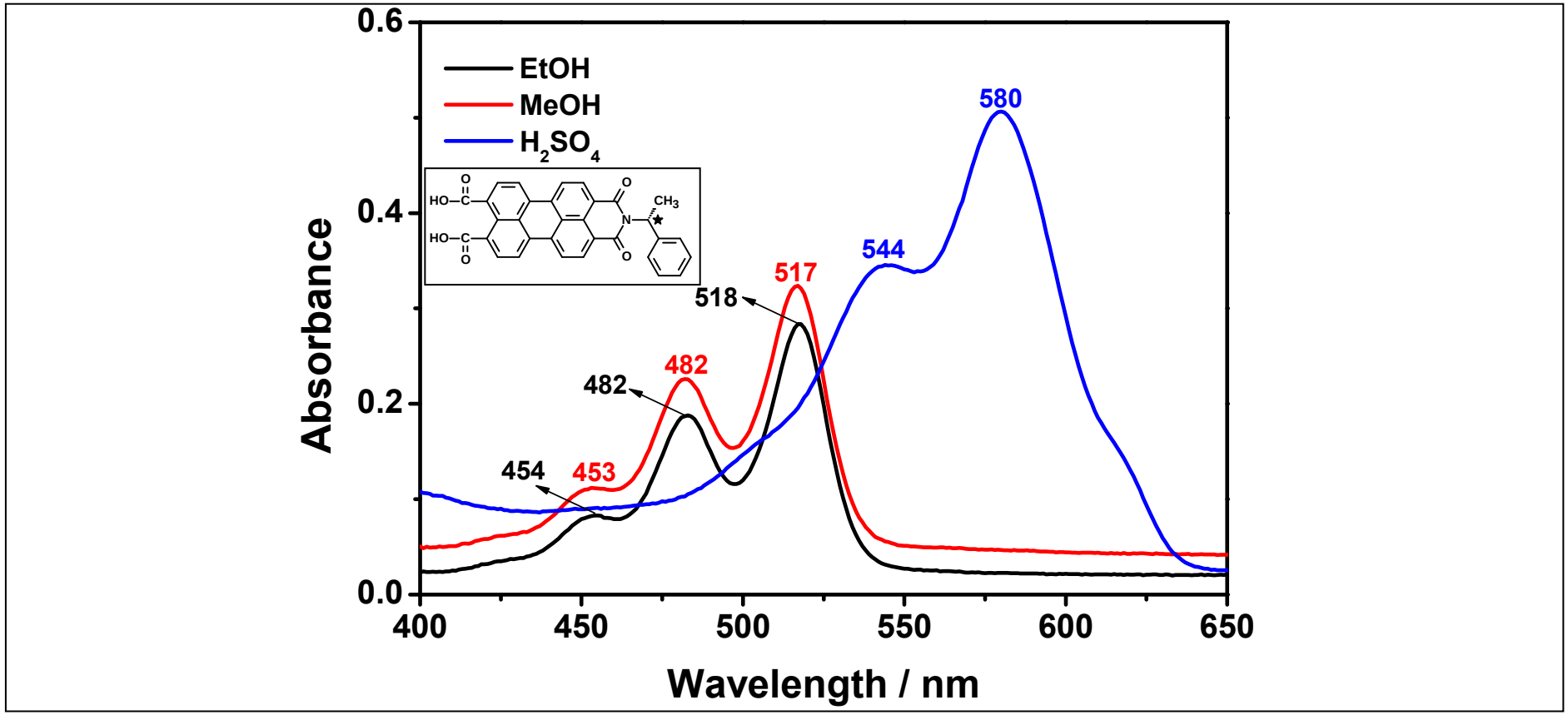

Figure 4.20 UV-vis absorption spectra of CPMI in various protic solvents.

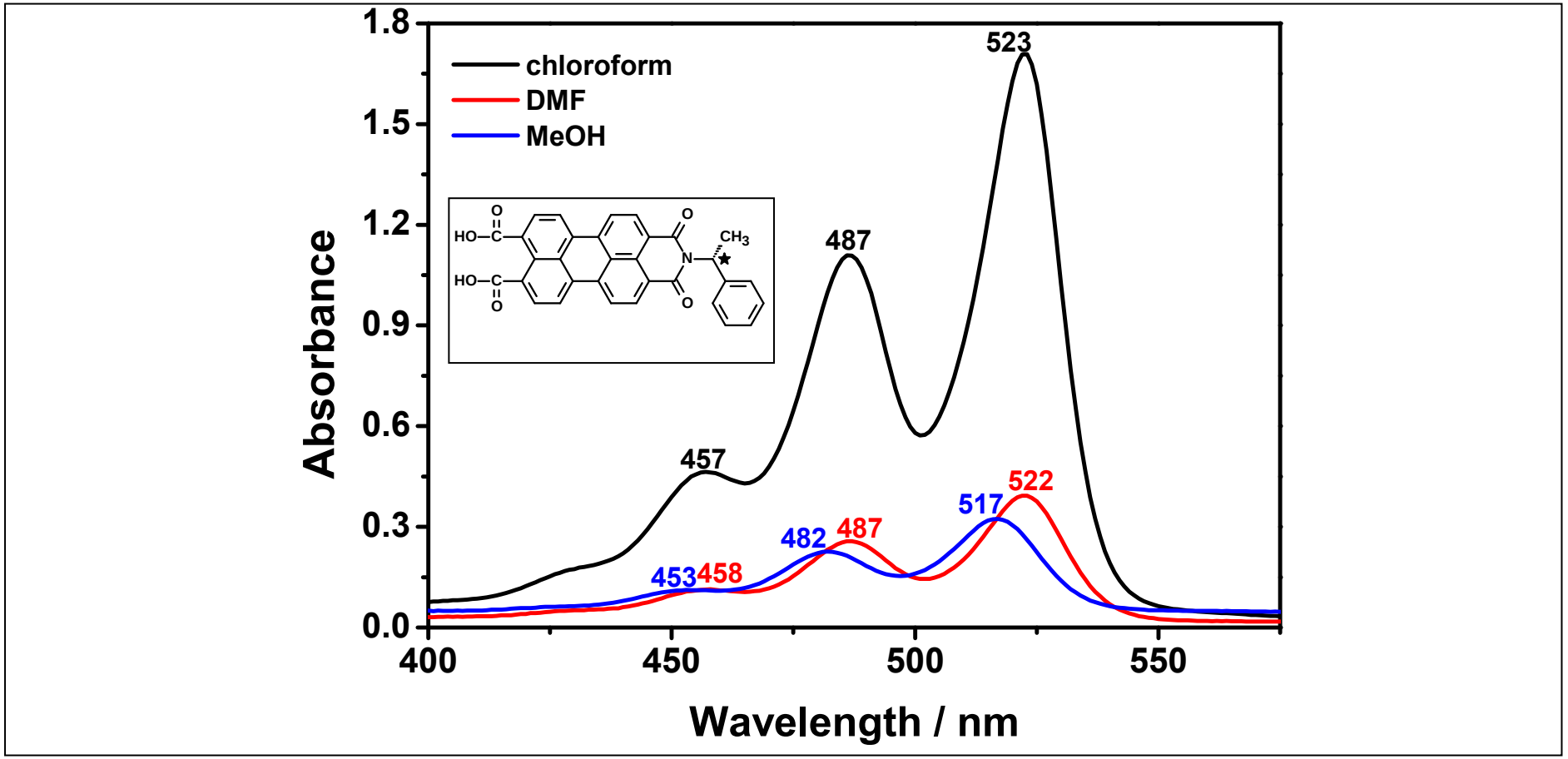

Figure 4.21 Comparison of UV-vis absorption spectra of CPMI in nonpolar, dipolar aprotic and protic solvents.

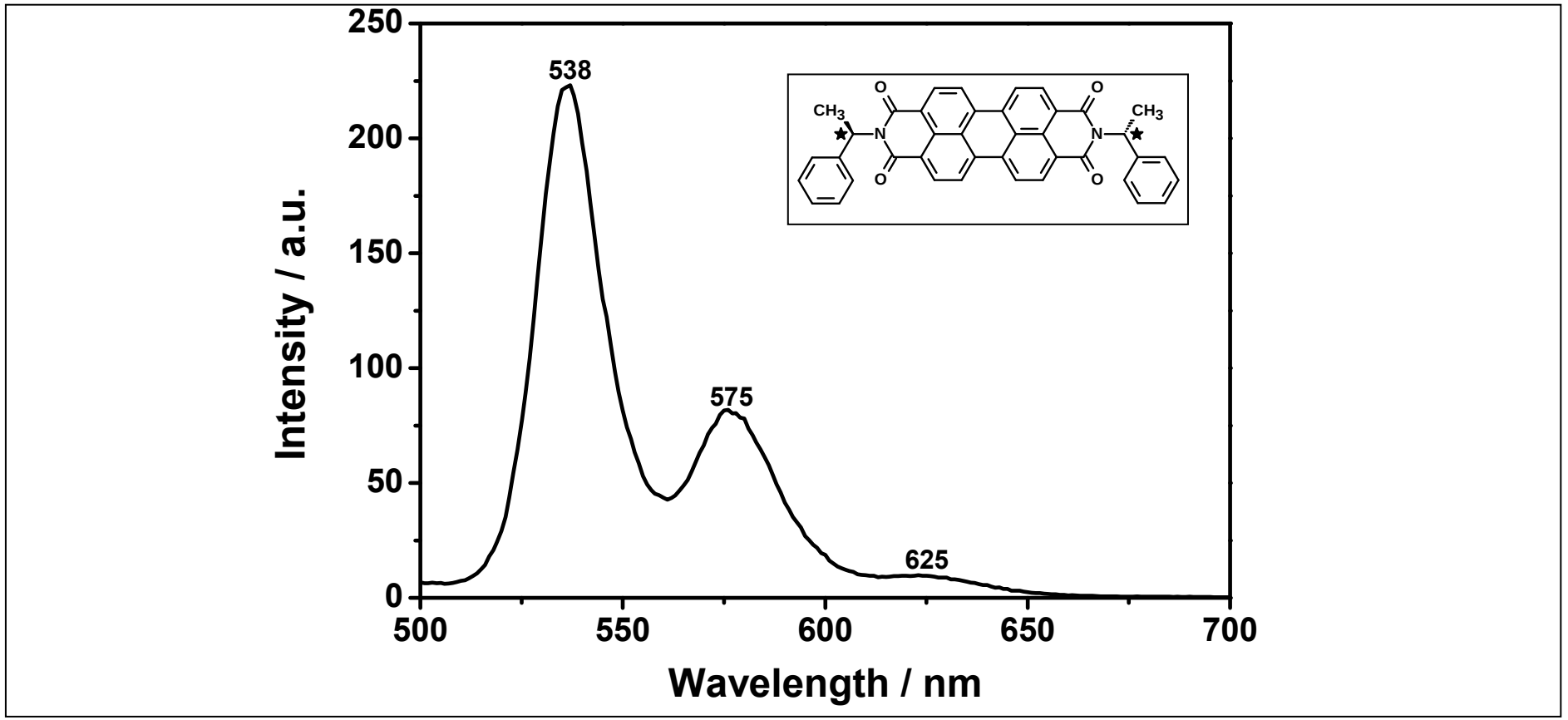

Figure 4.22 Emission (λ_{exc} = 485 nm) spectrum of PDI in $CHCl_3$.

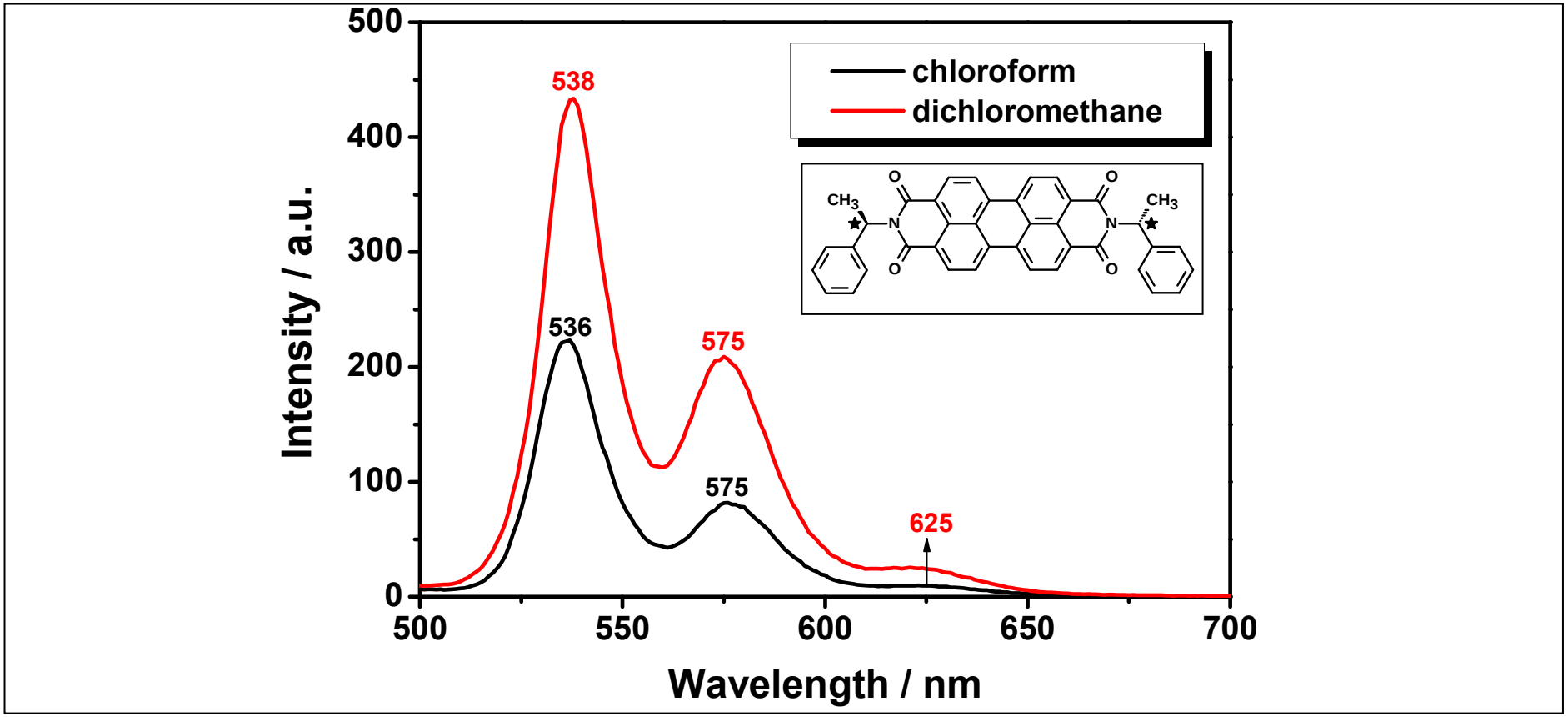

Figure 4.23 Emission (λ_{exc} = 485 nm) spectrum of PDI in various nonpolar solvents.

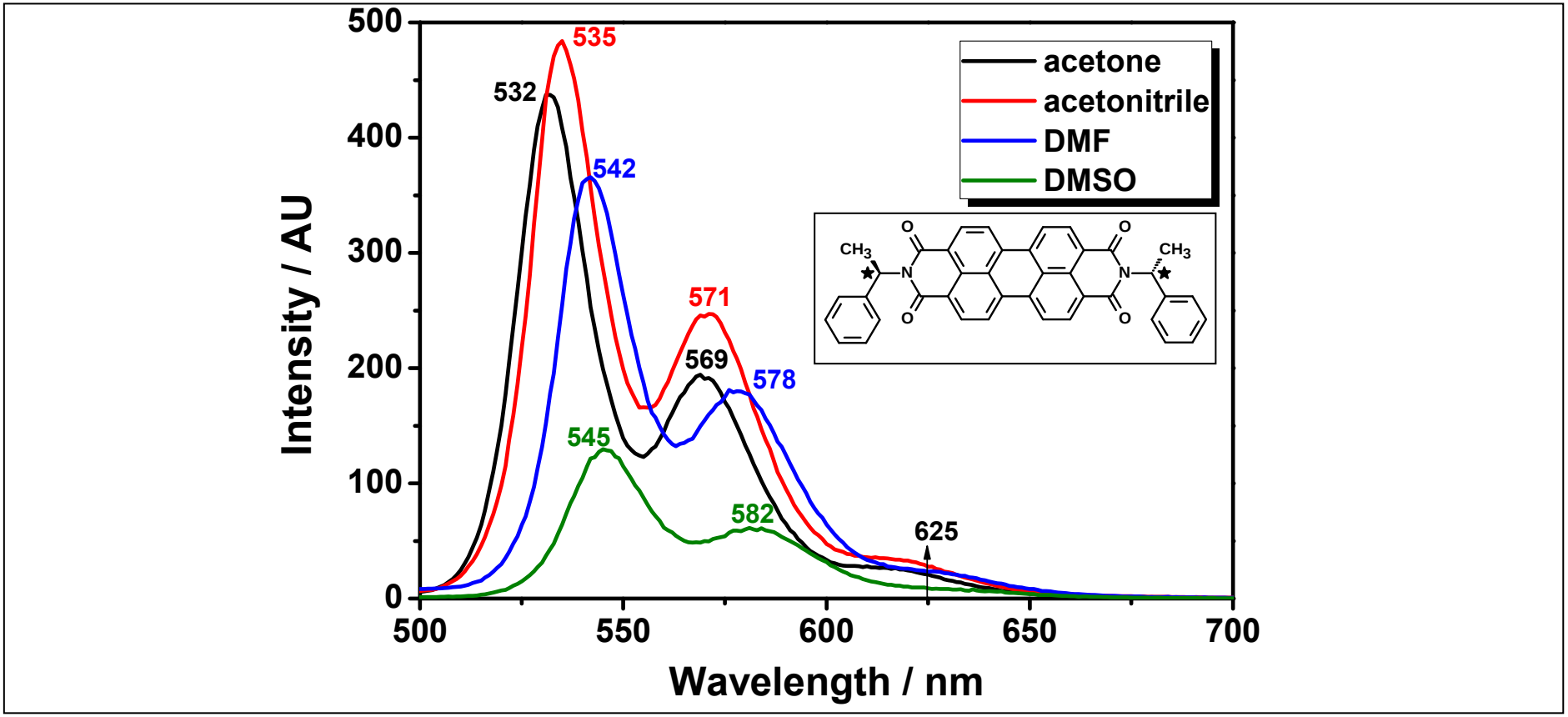

Figure 4.24 Emission (λ_{exc} = 485 nm) spectrum of PDI in various dipolar aprotic solvents.

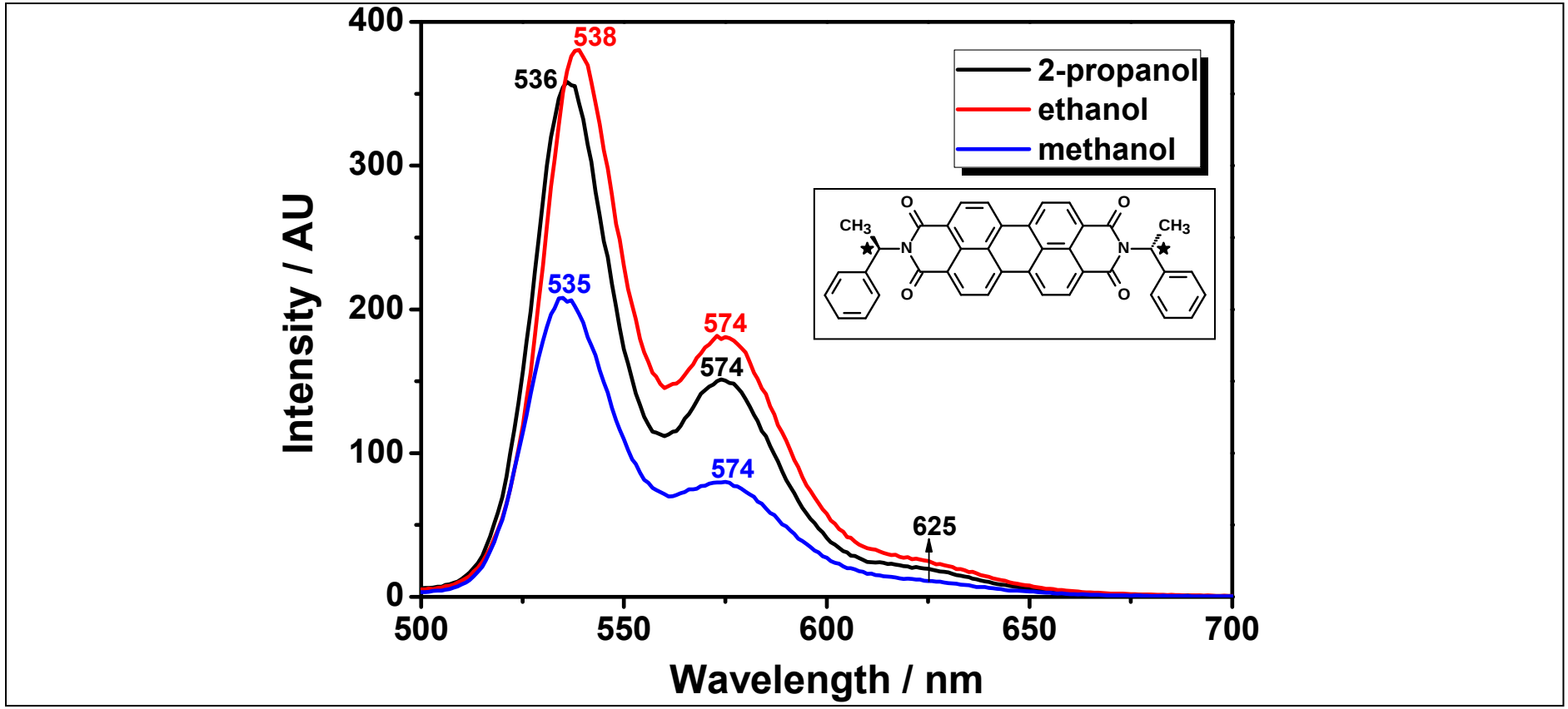

Figure 4.25 Emission (λ_{exc} = 485 nm) spectrum of PDI in various protic solvents.

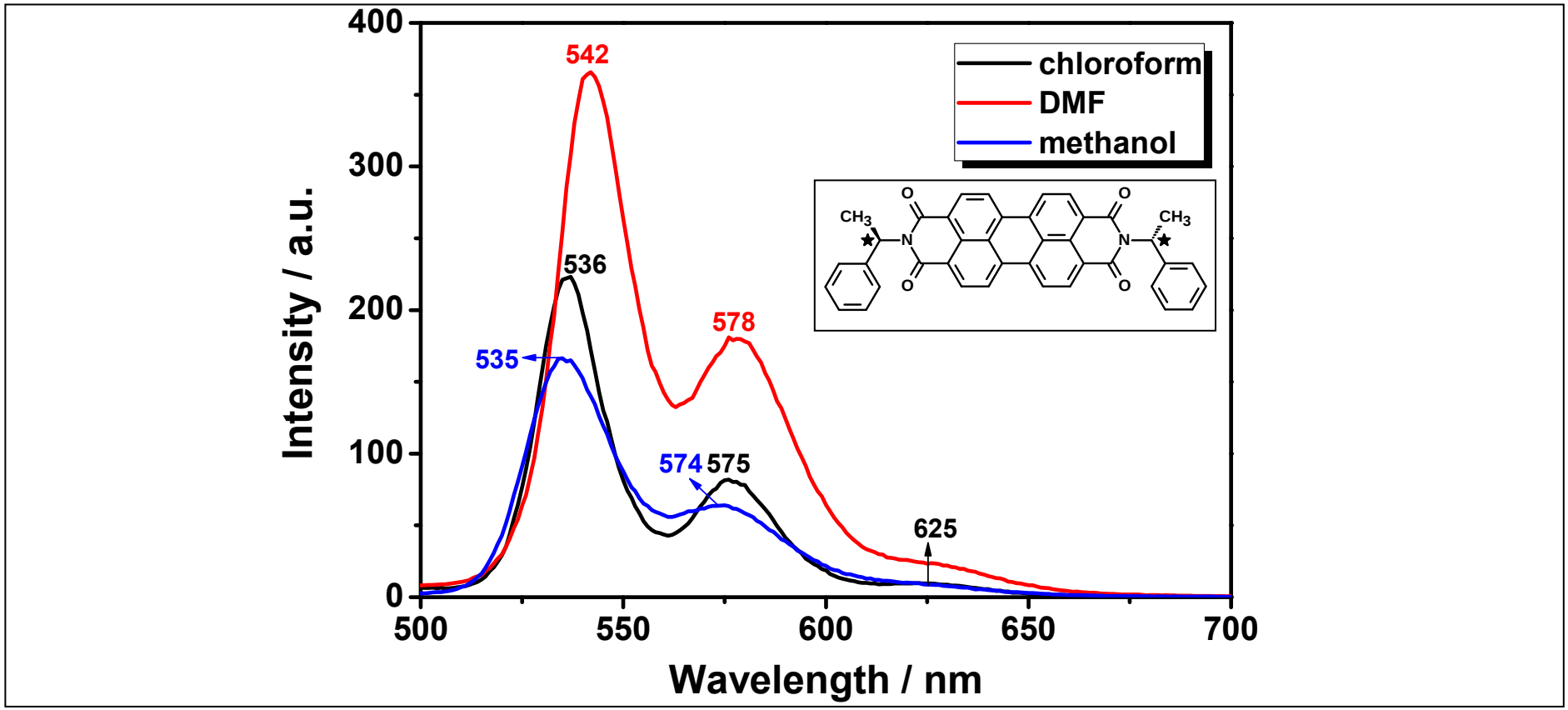

Figure 4.26 Comparison of emission (λ_{exc} = 485 nm) spectra of PDI in nonpolar, dipolar aprotic and protic solvents.

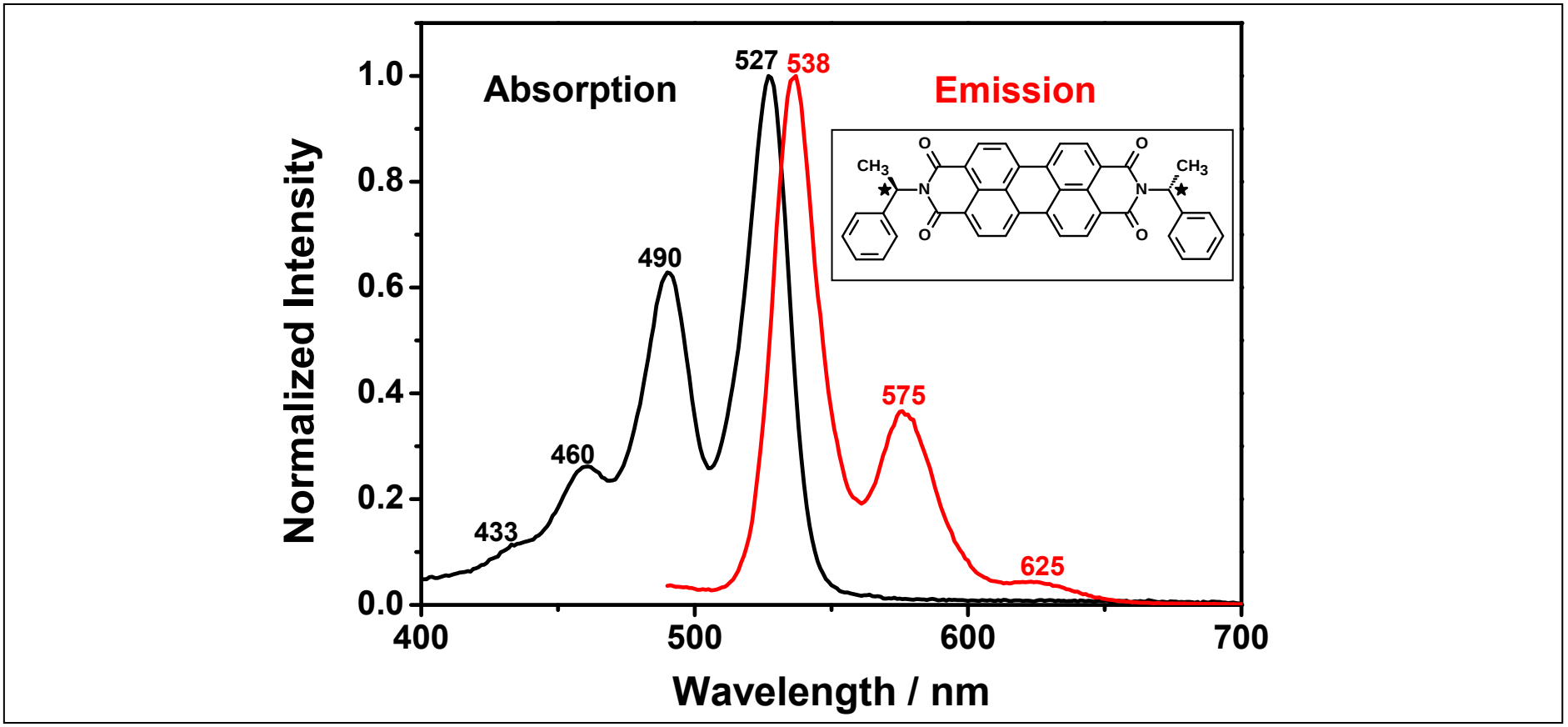

Figure 4.27 Normalized absorption and emission (λ_{exc} = 485 nm) spectra of PDI in $CHCl_3$.

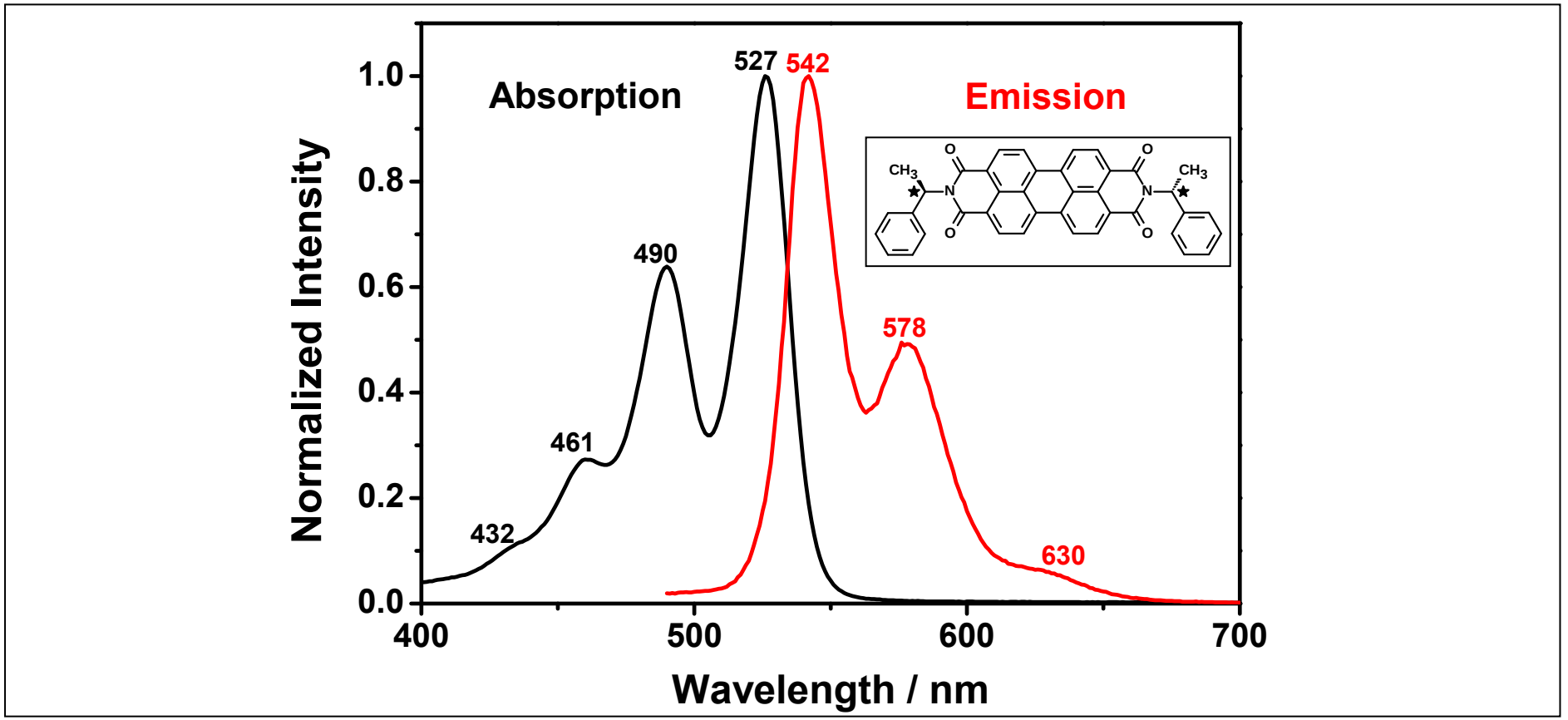

Figure 4.28 Normalized absorption and emission (λ_{exc} = 485 nm) spectra of PDI in DMF.

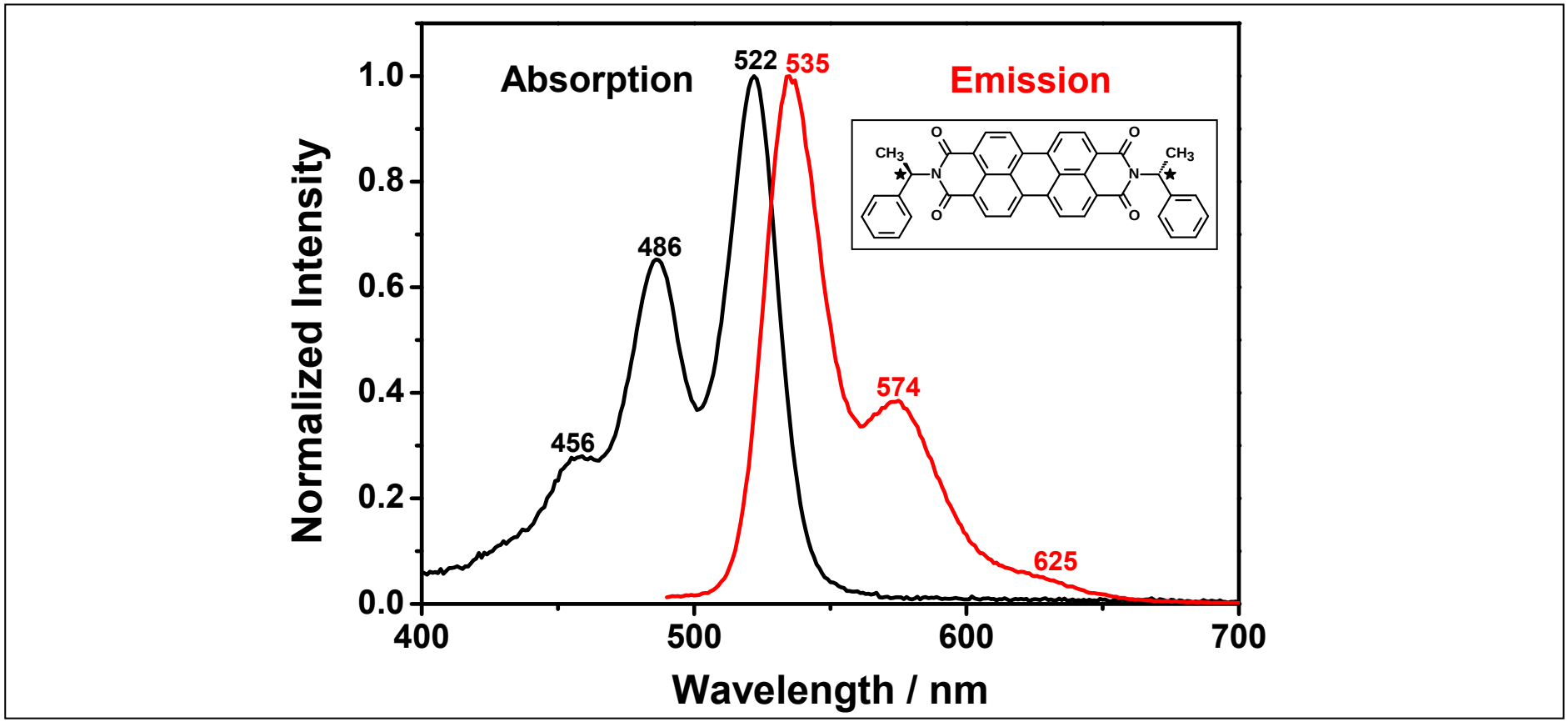

Figure 4.29 Normalized absorption and emission (λ_{exc} = 485 nm) spectra of PDI in methanol.

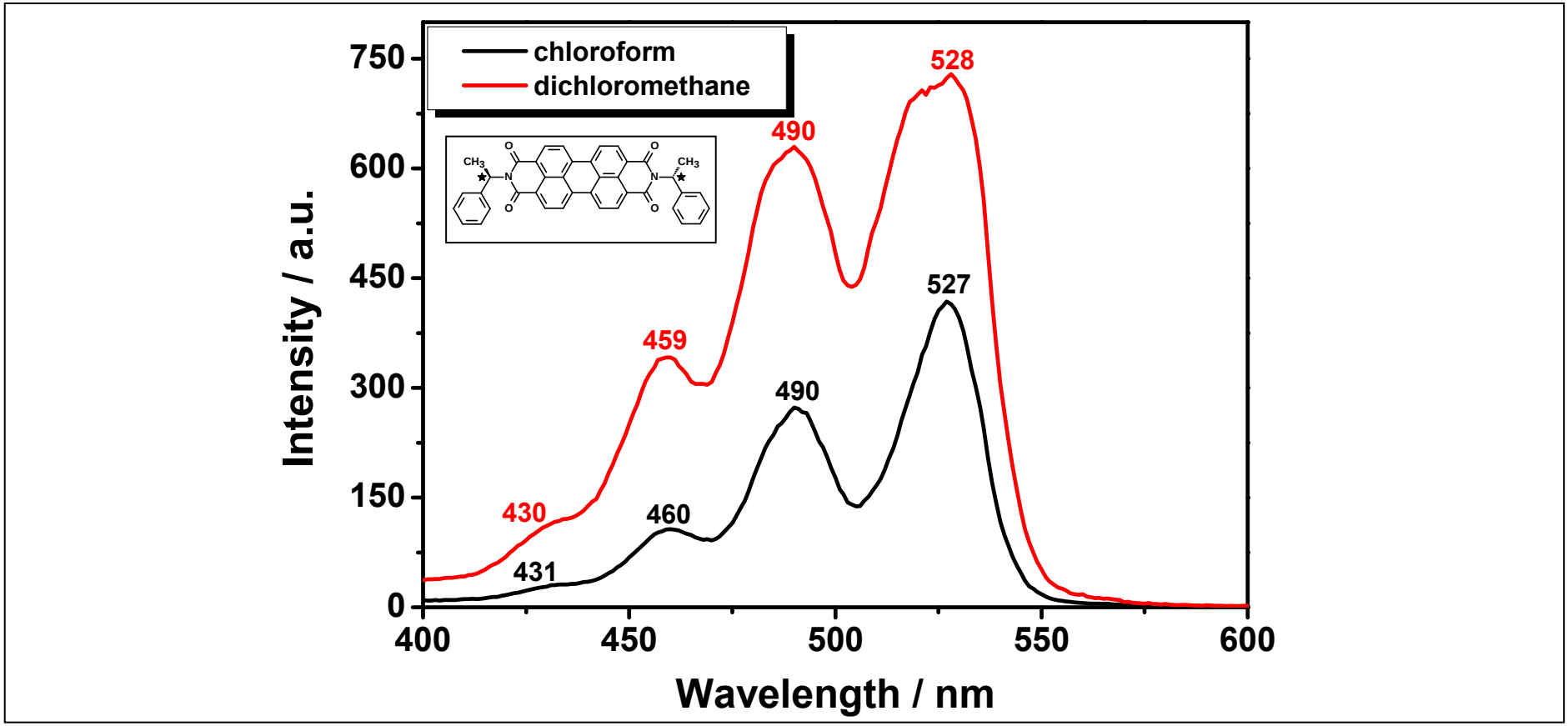

Figure 4.30 Excitation spectra (λ_{em} = 620 nm) of PDI in nonpolar solvents.

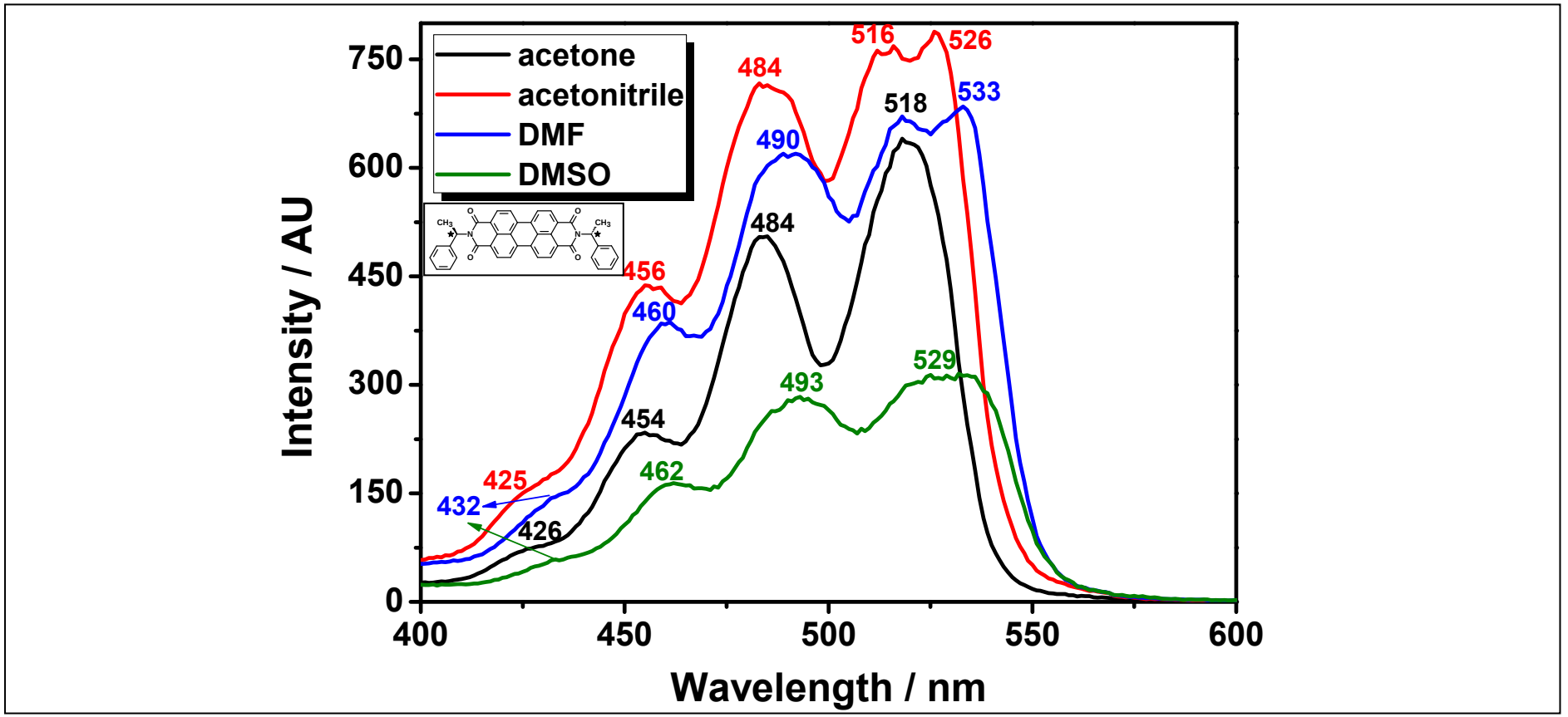

Figure 4.31 Excitation spectra (λ_{em} = 620 nm) of PDI in dipolar aprotic solvents.

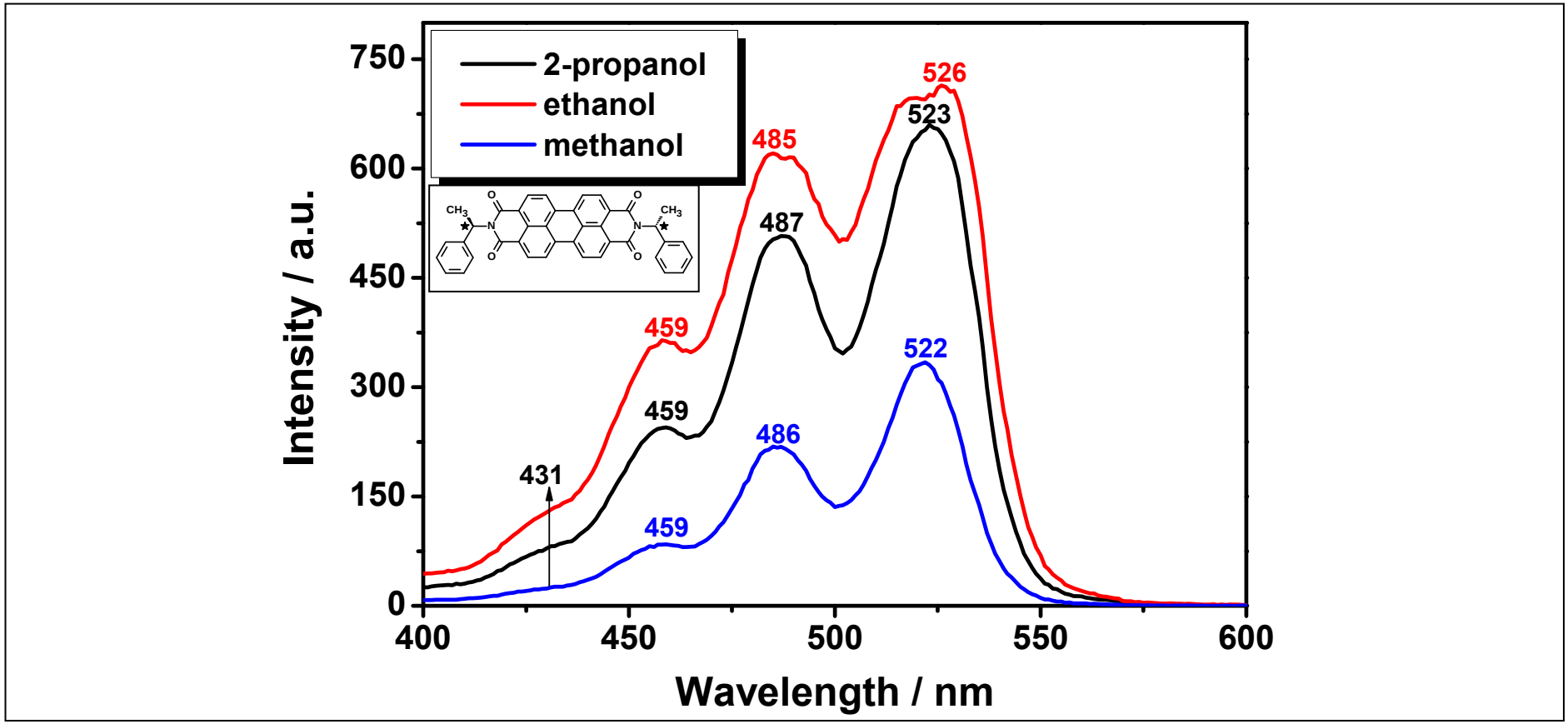

Figure 4.32 Excitation spectra (λ_{em} = 620 nm) of PDI in protic solvents.

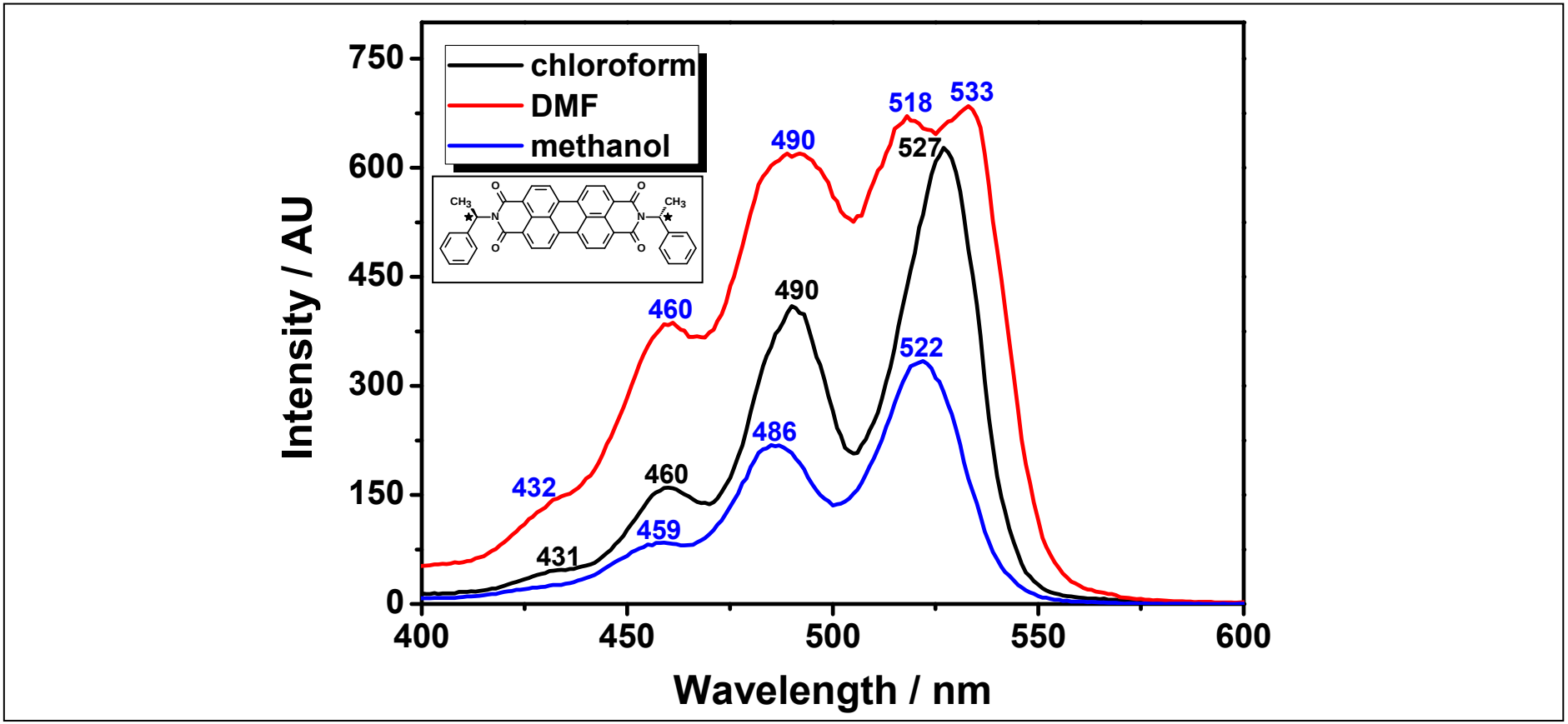

Figure 4.33 Comparison of excitation spectra (λ_{em} = 620 nm) of PDI in nonpolar, dipolar aprotic and protic solvents.

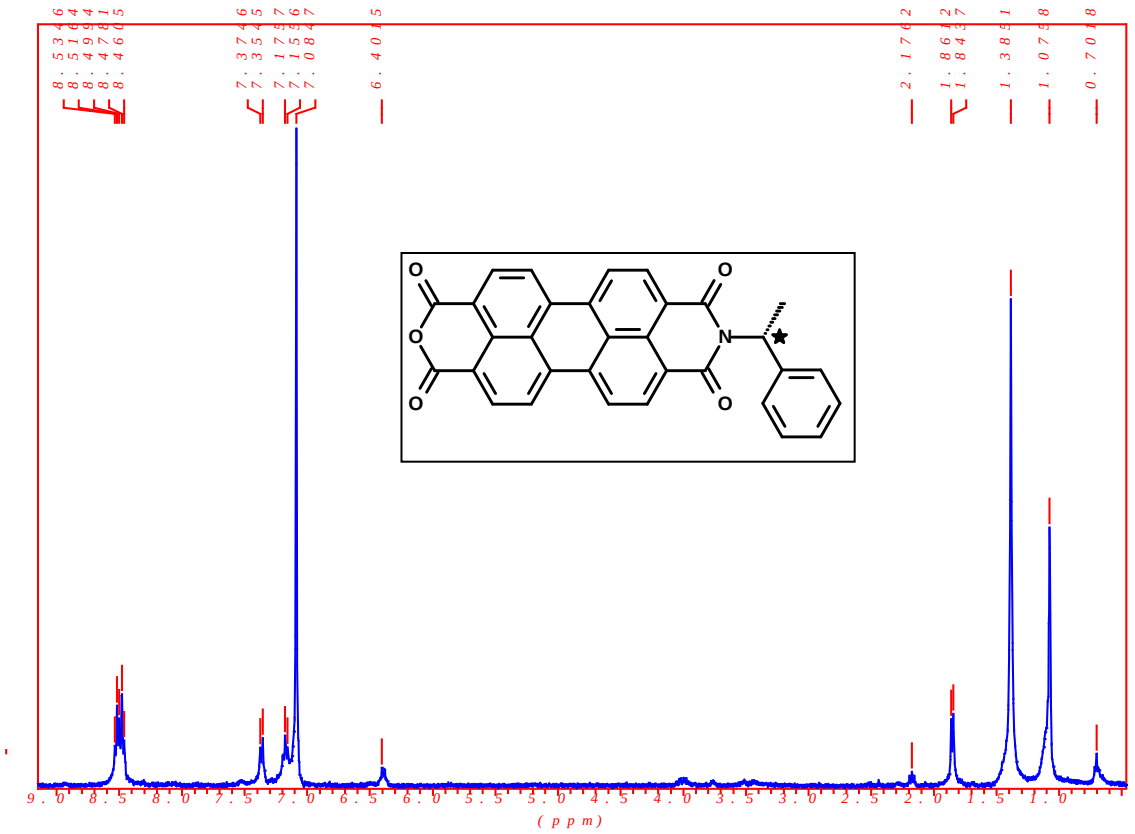

Figure 4.34 ^{1}H NMR spectra of PMI in $CDCl_3$.

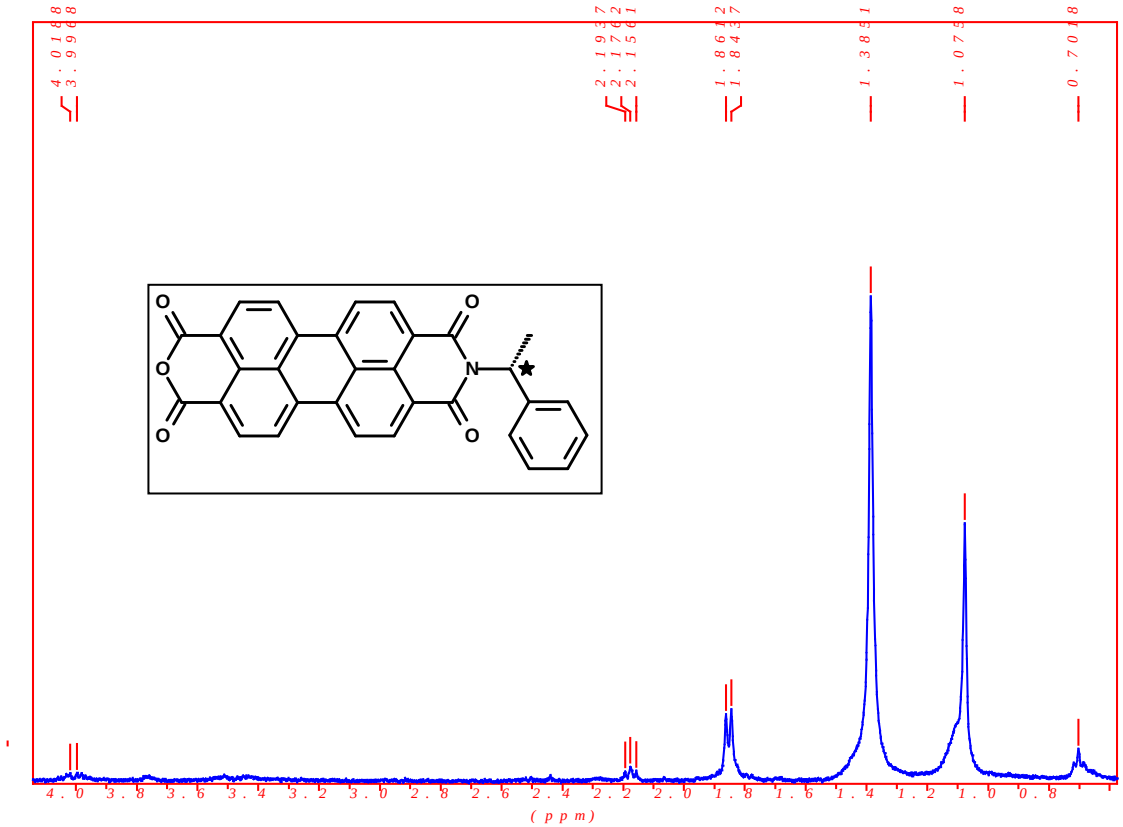

Figure 4.35 ^{1}H NMR spectra of PMI in $CDCl_3$.

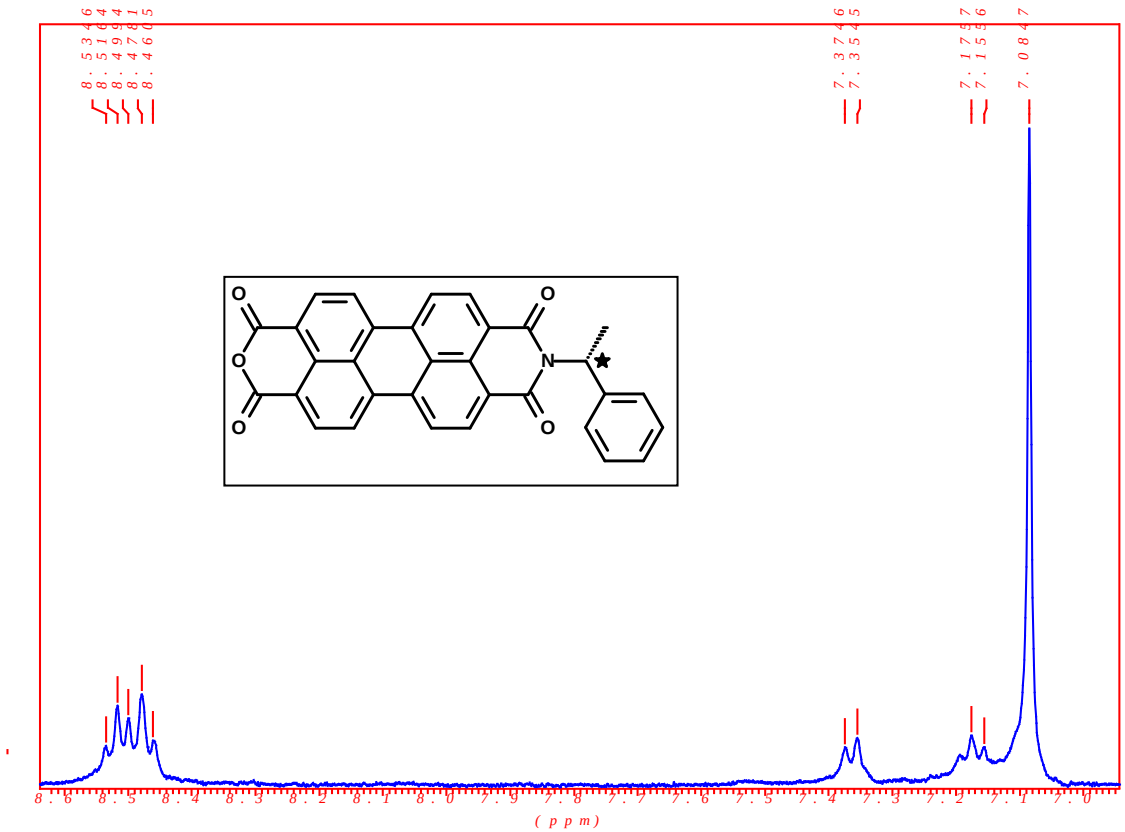

Figure 4.36 ^{1}H NMR spectra of PMI in $CDCl_3$.

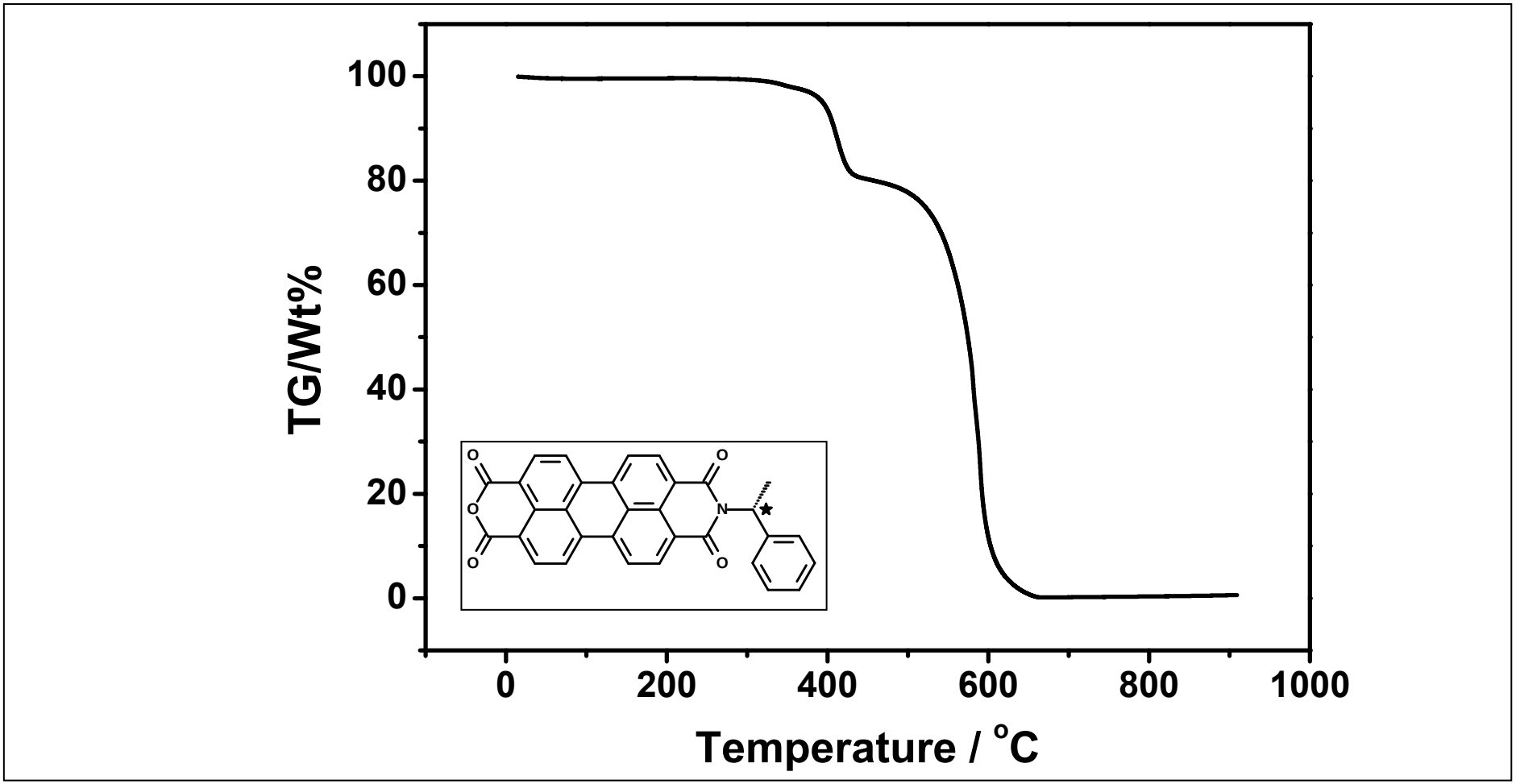

Figure 4.37. TGA thermogram of PMI obtained under oxygen atmosphere at a heating rate of 10 ^{o}C/min.

Chapter 5

RESULTS AND DISCUSSION

5.1 Synthesis of the Designed Perylene Derivatives

The structures of perylene dyes were especially designed to be chiral in order to induce them interesting chiroptical properties besides to the traditional stabilities of the compounds. Three kinds of perylene derivatives were designed, a chiral perylene diimide (PDI), a chiral monoimide (PMI), and a chiral carboxylic acid monoimide (CPMI), and were synthesized successfully in three consecutive steps.

The perylene diimide (PDI) was synthesized in the first step from perylene dianhydride. The synthesized PDI was used in the second step to prepare the PMI and then finally synthesized the CPMI in the third step with the reaction of the second step's product PMI and KOH, respectively.

The yields of three reactions were very high as great care was taken to complete the reaction by means of a continuous monitoring of the reaction progress through thin layer chromatography and FTIR techniques.

5.2 Solubility of the Synthesized Perylene Derivatives

All the perylene dyes synthesized were well soluble in common organic solvents. Appreciable solubility was achieved also in protic solvents such as methanol and ethanol. The solubility properties of the products are tabulated in Table 5.1. One of the interesting properties noticed for all the derivatives in most of the solvents is that the derivatives are very fluorescent. The high solubility combined with fluorescent colors indicates a potential for a wide range of applications in industry.

Table 5.1: Solubility of PDI, PMI and CPMI

	Solubility/Color		
Solvent	**PDI**	**PMI**	**CPMI**
$CHCl_3$	(+ +) F orange	(+ +) F orange	(+ +) F orange
TCE	(+ +) F orange	(+ +) F orange	(+ +) F reddish orange
CH_2Cl_2	(+ +) F orange	(+ +) F orange	(+ +) F orange
NMP	(+ +) F reddish orange	(+ +) F reddish Orange	(+ +) F orange
DMF	(+ +) F reddish orange	(+ +) F orange	(+ +) F orange
CH_3CN	(+ –) F orange	(+ –) F light orange	(– +) F orange
DMSO	(+ +) F reddish orange	(+ +) pink	(+ +) F pink
C_2H_5OH	(– +) deep purple	(– +) pale pink	(+ +) F light orange
CH_3OH	(– +) pink	(– +) F light orange	(– +) F orange
H_2SO_4	(+ +) F deep violet	(+ +) F violet	(+ +) F violet

(+ +): Soluble at RT, (+ –): Partially soluble at RT, (– +): Soluble on heating at 60 ^oC, (– –): insoluble. F: fluorescent.

5.3 Analysis of FTIR Spectra

All the synthesized perylene dye compounds were basically characterized by FTIR spectra for the confirmation of functional groups present in the structures. The spectra completely represented the basic functional groups present in their structure. The peaks observed from the FTIR spectra are described below.

From Figure 4.4, aromatic C–H stretch at 3059 cm^{-1}, aliphatic C–H stretch at 2970 cm^{-1} and 2874 cm^{-1}, imide C=O stretch at 1698 cm^{-1} and 1665 cm^{-1}, conjugated C=C stretch at 1592 cm^{-1}, C–N stretch at 1335 cm^{-1}, aromatic C–H bend at 809 cm^{-1}, 745 and 697 cm^{-1} confirms the structure of PDI.

From Figure 4.5, aromatic C-H at 3062 cm^{-1}, aliphatic C-H stretch at 2974 cm^{-1}, anhydride carbonyl (C=O) stretchings at 1769 and 1732 cm^{-1}, imide carbonyl (N−C=O) stretching at 1699 cm^{-1} and 1656 cm^{-1}, conjugated C=C stretch at 1594 cm^{-1}, C-N stretch at 1317 cm^{-1}, aromatic C–H bend at 810 cm^{-1} and 739 cm^{-1} confirms the structure of PMI.

From Figure 4.6, broad carboxylic O–H stretch at 3450 aromatic cm^{-1}, aromatic C-H at 3096 cm^{-1}, aliphatic C-H stretch at 2925 and 2852 cm^{-1}, carboxylic acid C=O stretchings at 1769 and 1732 cm^{-1}, imide (N−C=O) stretchings at 1699 cm^{-1} and 1657 cm^{-1}, conjugated C=C stretch at 1594 cm^{-1}, C-N stretch at 1318 cm^{-1}, aromatic C–H bend at 810 cm^{-1} and 739 cm^{-1} confirms the structure of CPMI.

5.4 Interpretation of UV-vis Spectra

Figures 4.7 – 4.11 show the absorption spectra of PDI in various solvents. All the absorption spectra recorded for PDI represented three characteristic absorption peaks at 460, 490, and 527 nm (in chloroform) relating to conjugated perylene chromophoric π–π interactions. Table 4.1 suggests the high molar extinction co-efficient (ε_{max} = 80000 $M^{-1}cm^{-1}$) of PDI inferring strong absorption in the visible region. Tables 4.5 and 4.6 also represent the strong possibility for singlet electronic excitation from ground state.

From Figure 4.8, the absorption spectra in nonpolar solvents are similar in peak shapes and the three perylene absorption peaks were noticed.

In dipolar aprotic solvents, the absorption peaks are similar but a red shift of 9 nm is observed when moving from low polar solvent acetone to polar DMSO, attributed to strong polar nature of DMSO and hence stabilization of energy levels of PDI molecules (Figure 4.9).

From Figure 4.10, the absorption spectra in protic solvents are similar with the traditional three peaks and no considerable changes were noticed in the three reported solvents.

The comparison made for UV spectra of PDI in nonpolar, dipolar aprotic and protic solvents show an interesting blue shift in polar protic methanol due to hydrogen bonding (Figure 4.11).

Figures 4.12 – 4.16 show the absorption spectra of PMI in various solvents. All the absorption spectra recorded for PMI represented three characteristic absorption peaks at 457, 486, and 522 nm (in chloroform) relating to conjugated perylene

chromophoric π–π interactions. Table 4.1 suggests the moderate molar extinction coefficient (ε_{max} = 58000 $M^{-1}cm^{-1}$) of PMI inferring strong absorption in the visible region. Tables 4.5 and 4.6 also represent the strong possibility for singlet electronic excitation from ground state. Comparing to PDI, PMI has shown a little hypsochromic shift (5 nm for λ_{max}) in the maximum absorption peaks.

From Figure 4.13, the absorption spectra in nonpolar solvents are similar in peak shapes and the three perylene absorption peaks were noticed. A small red shift (4 nm) was noticed for PMI in 1,1,2,2-tetrachloroethane (TCE) comparing to other nonpolar solvents.

In dipolar aprotic solvents, the absorption peaks are similar but a red shift is observed in high polar DMSO, attributed to strong polar nature of DMSO and hence stabilization of energy levels of PMI molecules as shown in Figure 4.14.

From Figure 4.15, the absorption spectra of PMI in protic solvents are interesting. In low polar ethanol, because of low solubility the absorption peaks are not well resolved and only two peaks were noticed. On the other hand, traditional three peaks were recorded in methanol with a blue shift in λ_{max} of 0→0 transition. Interestingly, the absorptoion peaks in conc.H_2SO_4 solution are completely red shifted (up to 579 nm) comparing to all other absorption spectra which can be explained by possible protonation of PMI molecules.

The comparison made for UV spectra of PMI in nonpolar, dipolar aprotic and protic solvents show an interesting blue shift in polar protic methanol due to hydrogen bonding as predicted (Figure 4.16).

Figures 4.17 – 4.21 show the absorption spectra of CPMI in various solvents. All the absorption spectra recorded for CPMI represented three characteristic absorption

peaks at 457, 487, and 523 nm (in chloroform) relating to conjugated perylene chromophoric π–π interactions. Table 4.1 suggests the high molar extinction co-efficient (ε_{max} = 179000 $M^{-1}cm^{-1}$) of CPMI inferring strong absorption in the visible region. Tables 4.5 and 4.6 also represent the strong possibility for singlet electronic excitation from ground state. Comparing to PDI, PMI; CPMI has shown highest molar absorptivity probably due to the carboxylic acid groups present in the structure.

From Figure 4.18, the absorption spectra in nonpolar solvents are similar in peak shapes and the three perylene absorption peaks were noticed. A small red shift (4 nm) was noticed for CPMI in TCE comparing to other nonpolar solvents.

In dipolar aprotic solvents, the absorption peaks are similar but a red shift is observed in high polar DMSO, attributed to strong polar nature of DMSO and hence stabilization of energy levels of CPMI molecules (Figure 4.19).

From Figure 4.20, the absorption spectra of CPMI in protic solvents are similar in trends with PMI absorption spectra in protic solvents. Unlike the PMI absorption in ethanol, CPMI absorption spectrum was well resolved in ethanol and similar in shapes to absorption spectrum in methanol. The absorptoion peaks of CPMI in conc.H_2SO_4 solution are completely red shifted (up to 580 nm) similar to the PMI absorption peaks which could be due to possible protonation of CPMI molecules.

The comparison made for UV spectra of CPMI in nonpolar, dipolar aprotic and protic solvents show an interesting blue shift in polar protic methanol due to hydrogen bonding (Figure 4.21).

5.5 Interpretation of Emission Spectra

Figures 4.22 – 4.26 show the emission spectra (λ_{exc} = 485 nm) of PDI in various solvents. All the emission spectra recorded for PDI represented three characteristic emission peaks at 538, 575, and 625 nm (in chloroform) relating to conjugated perylene chromophoric π–π interactions.

From Figure 4.23, the emission spectra in nonpolar solvents are similar in peak shapes and the three perylene emission peaks were noticed. A strong fluorescence of similar (*S*)-isomeric PDI was reported in literature. The strong fluorescence is an added advantage to be used in potential photonic applications.

In dipolar aprotic solvents, the emission peaks are similar but a red shift of 13 nm is observed when moving from low polar solvent acetone to polar DMSO, attributed to strong polar nature of DMSO and hence stabilization of energy levels of PDI molecules. Similar red shifts in high polar solvents for perylene diimides were reported in literature (Figure 4.24).

From Figure 4.25, the emission spectra of PDI in protic solvents are similar in peak shapes. Very low blue shifts (3 nm) were noticed for emission spectra in high polar solvent methanol for 0→0 transition due to possible strong hydrogen bonding comparing to other protic solvents.

The comparison made for emission spectra of PDI in nonpolar, dipolar aprotic and protic solvents show an interesting blue shift in polar protic methanol due to hydrogen bonding (Figure 4.26).

Figures 4.27 – 4.29 show comparison of normalized absorption and emission spectra and the Stokes′ shifts in nonpolar ($CHCl_3$), dipolar aprotic (DMF), and protic

(methanol) solvents, respectively. The absorption and emission spectra in all three kinds of solvents were mirror images to each other and a Stokes′ shifts of 11 nm, 15 nm, 13 nm were noticed in nonpolar, dipolar aprotic and protic solvents, respectively. The comparisons suggest the loss of energy of PDI molecules mostly via radiation path way by releasing a photon.

5.6 Interpretation of Exitation Spectra

Figures 4.30 – 4.33 explore the excitation spectra of PDI in various solvents. In general, excitation spectra resemble UV-vis spectra. An emission wavelength of 620 nm is selected to record the excitation spectra.

Figure 4.30 shows the excitation spectra of PDI taken in nonpolar solvents. The peaks are broader and similar to their UV spectra.

The similar results were noticed in dipolar aprotic solvents protic solvents. Resembling the absorption spectra, red shifts and blue shifts were also noticed in high polar DMSO and methanol, respectively (Figures 4.31 – 4.32).

The comparison made in Figure 4.33 for the excitation spectra of PDI in three kinds of solvents result in similar trends like their absorption spectra.

5.7 Interpretation of NMR Spectra of PMI

Figures 4.34 – 4.36 show the ^{1}H NMR spectra of PMI recorded in $CDCl_3$.

NMR analysis of N-((*R*)-(+)-1-phenylethyl)-3,4,9,10-perylenetetracarboxylic-3,4-anhydride-9,10-imide (PMI)

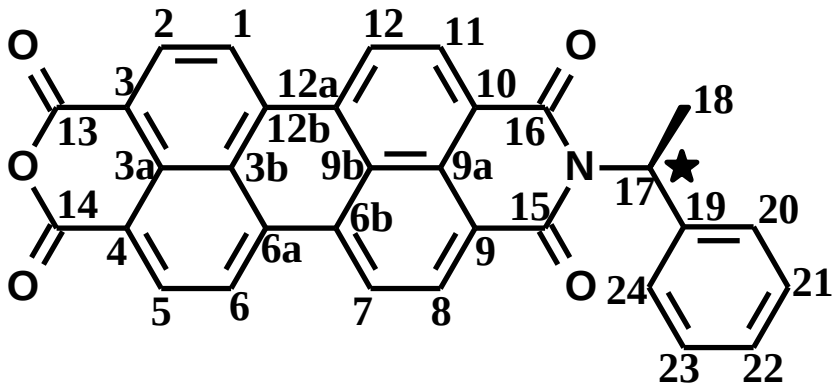

^{1}H NMR (400 MHz, $CDCl_3$, ppm): 8.53 – 8.46 (multiplet, 8Ar-H (C – 1,2,5-8, 11,12)), 7.37 – 7.15 (multiplet, 5Ar-H (C – 20-24)), 6.41-6.37 (q, CH, H-C(17), 1.23 (br d, CH_3, H-C(18) (Figures 4.34 – 4.36).

5.8 Thermal Stability of PMI

Figure 4.37 shows TGA thermogram of PMI obtained under oxygen atmosphere at a heating rate of 10 ^{o}C/min.

The TGA thermogram infers that the decomposition initializes at 400 ^{o}C. Weight loss of 17% was noticed from 400 – 450 ^{o}C. Then a very rapid weight loss of 80% occurred up to 900 ^{o}C. The initial decomposition temperature 400 ^{o}C suggests the high thermal stability of PMI.

Chapter 6

CONCLUSION

- A chiral perylene diimide (PDI), chiral perylene monoimide (PMI) and chiral dicarboxylic acid perylene monoimide (CPMI) were designed and synthesized. The perylene derivatives synthesized in high yields by traditional polycondensation and Tröster methods of preparation.
- The three chiral perylene derivatives were well soluble in common organic solvents.
- The FTIR spectra and elemental analyzes confirm the basic functional groups present in the structures and confirm the purity of the samples, respectively.
- The UV-vis absorption spectra recorded in various category of solvents (nonpolar, dipolar aprotic, and protic) suggest high absorption ability of the compounds. Particularly, CPMI has shown very high molar absorptivity of 179000 $M^{-1}cm^{-1}$.
- The absorption spectra of all perylene derivatives exhibited three traditional perylene chromophoric absorption peaks.
- The emission spectra recorded for PDI have shown the characteristic three emission peaks in all kinds of solvents.
- The excitation spectra measured for PDI in various solvents resembled their absorption spectra and exhibited three characteristic peaks.

- The initial decomposition temperature of 400 ^{o}C for PMI has proved the high thermal stability.

References

Asir S. and etal (2010). The synthesis of novel, unsymmetrically substituted, chiral naphthalene and perylene diimides: Photophysical, electrochemical, chiroptical and intramolecular charge transfer properties. Dyes and Pigments. 84. 1–13.

Andrea P. and etal. (2010). Association phenomena of a chiral perylene derivative in solution and in poly(ethylene) dispersion. Reactive & Functional Polymers 70 (2010) 951–960.

Aleshinloye O.A (2009), Ms Thesis, Eastern Mediterranean University.

Belser P. and etal. (1999). Molecular architecture in the field of photonic devices. *Coordination Chemistry Reviews.* 190–192, 155–169.

Chen Li. and etal. (2009). Rainbow Perylene Monoimide: Easy Control of Optical Properties. Chem. Eur. J. 15, 878 – 884.

Chiba Y. and etal. (2006). Dye-Sensitized Solar Cells with Conversion Efficiency of 11.1%. Japanese Journal of Applied Physics Vol. 45, No. 25, pp. L638–L640.

Cornell C.and etal. (2004). Lesson and Lab Activity with Photovoltaic Cells. Copyright CCMR Educational Programs.

Edvinsson T. and etal. (2007). Intramolecular charge - transfer tuning of Perylene: Spectroscopic features and performance in dye - sensitized solar cells', Journal of physical chemistry C.Vol.111, no.42, pp.15137-15140.

Erin K T. and etal. (2005). Chiral imides as potential chiroptical switches: synthesis and optical properties. Tetrahedron Letters 46, 587–590.

Frank Wurthner, (2004), The Royal Society of Chemistry, Chem.Commun., 1564-1579.

Hassan L.M. and etal. (2012). Fluorescent cellulose nanocrystals via supramolecular assembly of terpyridine-modified cellulose nanocrystals and terpyridine-modified perylene. Materials Science and Engineering B .177. 350– 358.

Hari M. and etal. (2012). Band-gap tuning and nonlinear optical characterization of Ag:TiO2 nanocomposites. JOURNAL OF APPLIED PHYSICS 112, 074307.

Icil H. and etal. (1997). Fluoresence quenching between strong n-electrone donor-acceptors of carbazolocarbazole and tetranitrofluorenone leading to electron transfer. Journal of Luminescence .75. 353-359.

Icil H. and etal. (2008). Highly soluble perylene diimide and oligomeric diimide dyes combining perylene and hexa(ethylene glycol) units: Synthesis,

characterization, optical and electrochemical propertie. Dyes and Pigments .79. 224–235.

Icil, H and etal, (2001), Spectrosc.Lett., 34(3). 355-363.

Imahori H. and etal. (2009). Porphyrin-modified electrodes for solar energy conversion *J. Porphyrins Phthalocyanines* Vol. 13, Issue 10.

Jose R. and etal. (2009). Electron transport in electrospun TiO_2 nanofiber dye-sensitized solar cells. Applied Physics Letters. 95, 012101.

Kanaparthi K.R. and etal. (2012). Metal-free organic dyes for dye-sensitized solar cells: recent advances. Tetrahedron .68. 8383-8393.

Langhals. and etal. (1995).A two- step Synthesis of Quaterrylenetetracarboxylic Bisimides - Novel NIR Fluorescent Dyes. Tetrahedron letters, Vol, 36, No.36, pp.6423-6424.

Lang Y.Y. and etal. (2008). Chinese Chem. Let., 19, 1260-1263.

Regan B O. and etal. (1991). A low-cost, high-efficiency solar cell based on dyed-sensitized colloidal TiO_2 films', Nature,Vol.353, no.6346,pp.737-740.

Sharma D.G. and etal. (2012). Effect of Deoxycholic Acid on the Performance of Liquid Electrolyte Dye-Sensitized Solar Cells Using a PeryleneMonoimide Derivative.

International Journal of Photoenergy Volume. 2012, 7 pages.